



**NTNU – Trondheim**  
Norwegian University of  
Science and Technology

# Analysis of accidental iceberg impacts with LNG tank carriers

**Knut Aaberge Dahl**

Marine Technology

Submission date: June 2012

Supervisor: Jørgen Amdahl, IMT

Norwegian University of Science and Technology  
Department of Marine Technology



## Abstract

In this report different critical collision scenarios between spherical type LNG carriers and icebergs are discussed. The most critical scenario, a bow shoulder collision, is chosen when simulations of collision scenarios are performed.

A review of ALE-modelling in LS-DYNA is carried out. By using this modelling approach the surrounding water can be included in the ship-iceberg collisions.

A detailed FE model of the bow shoulder of a 125 000 dwt. spherical type LNG tanker is modelled. In addition, a global model of the ship including coarse geometry and correct properties is created. Boundary conditions and other relevant parameters for the FE models are discussed, and correct mass and centre of gravity is ensured.

Two different FE models of icebergs are created. The icebergs are irregular box shaped with smoothed corners, and the smallest iceberg is modelled with side lengths of 15 m and has a mass of 2500 tons while the large iceberg is modelled with side lengths of 30 m and has a mass of 19 000 tons.

Three different collision approaches have been performed for two different impact angles,  $5.71^\circ$  and  $30^\circ$ . For the local bow shoulder model both a prescribed displacement analysis and an initial velocity analysis has been performed. From the simulations it seems like the prescribed displacement analysis yields over-conservative results for long duration simulations. Based on the global analyses it also seems like the local initial velocity analysis over-estimates the indentations and energy absorption.

Accelerations in spots which is not directly impacted by the impact have also been investigated. No extreme values in these spots are found.



## Scope of work

MASTER THESIS 2012

for

Stud. Techn. Knut Aaberge Dahl

### **Analysis of accidental iceberg impacts with LNG tank carriers**

*Analyse av ulykkesstøt fra små isfjell mot LNG skip*

The global demand for Liquefied Natural Gas (LNG) is increasing. A significant part of LNG will have to be transported at sea. The expected increase of exploitation of gas fields in Northern regions, such as Western Russia, will precipitate the development of arctic LNG shipping. LNG ships carry huge amount of energy and it is vital that these ships possess adequate resistance to collision with other ships and icebergs. A potentially severe risk is associated collision with small icebergs (berg bits/growlers). Large icebergs are very likely to be observed by radars installed aboard the ship or by airborne radars, but smaller icebergs may avoid detection. This implies that rare (accidental) events cannot be disregarded and must be considered in the design.

The cargo containment system may vary for the different LNG vessels. The Moss-Kværner spherical containment system was developed in the early 1970's and became highly successful. The spherical tank is supported at the tank's "equator" by a skirt fabricated of a high tensile steel skin. This introduces flexibility between the spherical tank and the ship structure, thus minimizing interaction between the hull deformation and the tank deformation. Recently the Gas Transport/Technigas (GTT) cargo containment system (CCS) – the membrane tank - has become popular. The membrane tank consists of a cryogenic liner directly supported by the ship inner hull. The primary and secondary insulation system consists of 0.7 mm nickel–steel alloy carried by prefabricated plywood boxes filled with expanded perlite. The membrane containment system is considered favorable because it has larger cargo capacity for the same ships size, which e.g. gives a Suez toll advantage.

It has been maintained that the support of membrane tank directly on the inner hull as well as the smaller space between the cargo tank and the side shell make these concepts more vulnerable to collisions with ships and icebergs than e.g carriers with spherical tanks. Further, in some Korean numerical studies very large accelerations have been reported (up to 2000g). The findings are not discussed in detail, but the magnitude of the accelerations have caused some concern that iceberg collisions may cause failure in the cargo containment system far away from the contact area, in addition the local hull damage. If this should be correct, it represents a significant drawback of membrane tanks.

For accidental iceberg collisions use of ship classification design rules may yield overly conservative design. The rules are typically based upon elastic or plastic bending failure modes of stiffeners and plates implying small deformations. For accidental/abnormal iceberg impacts some degree of damage to the structure (side shell/frames) may be accepted, but the integrity of the cargo tank should not be impaired, causing gas leakage to the environment and possible ignition. In the Accidental Limit State the resistance may be assessed by non-linear methods of analysis; the structure may undergo yielding, buckling

and large permanent deformations on member and sub-structure level. This can only be assessed accurately if both the ship and the ice are modeled, and the interaction between the two structures is accounted for.

A PhD-student at department of marine technology – Zhenhui Liu - approaches the ship-iceberg collision problem numerically by using the Tsai-Wu based ice material model by an Explicit FE code. In the study, the Tsai-Wu material model turned out to be a promising candidate for calculating the ice impact loads.

The purpose of the work is to study the behavior and resistance of Arctic LNG carriers with the membrane tank system subjected to accidental impacts from ships and icebergs.

The work is proposed carried out in the following steps:

1. Establish a finite element model of an LNG fore ship side structure (Moss-Rosenberg type). The finite element model for the ship and the ice shall be sufficiently fine to capture the governing deformation mechanisms, but still meet requirements with respect to acceptable CPU consumption. The kinematical/boundary conditions adopted for the study shall be discussed with respect to physical relevance.
2. Establish a finite element model for ice-fluid/structure interaction analysis. The model shall be very simple, e.g. box-shaped, and shall be used to familiarize with this type of analysis before proceeding to advanced analysis of realistic hull model.
3. Briefly review the basic theory behind the fluid-structure interaction applied in LS DYNA, and document the assumptions and limitations imposed by the selected method.
4. Determine relevant impact scenarios for: among others impact geometry, speed of the two vessels and in case of iceberg, size and shape of iceberg
5. Conduct external mechanics analysis of the collision scenarios for various iceberg global shapes. For given impact scenarios (speed, direction, iceberg mass etc) calculate the demand for energy dissipation and the damage on the basis of the results from the internal mechanics analysis.
6. Perform internal mechanics analysis of iceberg-ship impacts, i.e. the iceberg is pushed into the finite-element model of the ship side structure. The contact location and the iceberg shape may be varied. Identify the force-deformation relationship and the associated energy dissipation of the side structure and the iceberg.
7. Establish a complete global model of the ship, iceberg and the surrounding water for integrated analysis. Use the Moss-Rosenberg tank for this analysis. The side model established in pt.1 shall be integrated into a hull model of the entire ship. Considerations shall be given to how the hull girder horizontal and vertical bending moment as well as shear forces can be accounted for. Conduct integrated analysis for the same scenarios as investigated in pt.5 and 6. Identify force-deformation relationships and energy dissipation in ship and iceberg.
8. Compare the results from the integrated analysis with those of the simplified approach( external and internal mechanics). Comment upon the the accuracy of the

simplified approach. What is the best estimate of an equivalent added mass for the impact?

9. Compare the resistance of the two LNG tankers with respect to critical impact energy causing failure of the membrane tanks.
10. Conclusions and recommendations for further work.

Literature studies of specific topics relevant to the thesis work may be included.

The work scope may prove to be larger than initially anticipated. Subject to approval from the supervisors, topics may be deleted from the list above or reduced in extent.

In the thesis the candidate shall present his personal contribution to the resolution of problems within the scope of the thesis work.

Theories and conclusions should be based on mathematical derivations and/or logic reasoning identifying the various steps in the deduction.

The candidate should utilise the existing possibilities for obtaining relevant literature.

**Thesis format** The thesis should be organised in a rational manner to give a clear exposition of results, assessments, and conclusions. The text should be brief and to the point, with a clear language. Telegraphic language should be avoided.

The thesis shall contain the following elements: A text defining the scope, preface, list of contents, summary, main body of thesis, conclusions with recommendations for further work, list of symbols and acronyms, references and (optional) appendices. All figures, tables and equations shall be numerated.

The supervisors may require that the candidate, in an early stage of the work, presents a written plan for the completion of the work. The plan should include a budget for the use of computer and laboratory resources which will be charged to the department. Overruns shall be reported to the supervisors.

The original contribution of the candidate and material taken from other sources shall be clearly defined. Work from other sources shall be properly referenced using an acknowledged referencing system.

The report shall be submitted in two copies:

- Signed by the candidate
- The text defining the scope included
- In bound volume(s)
- Drawings and/or computer prints which cannot be bound should be organised in a separate folder
- The report shall also be submitted in pdf format along with essential input files for computer analysis, spreadsheets, Matlab files etc. in digital format

**Ownership** NTNU has according to the present rules the ownership of the thesis. Any use of the thesis has to be approved by NTNU (or external partner when this applies).

The department has the right to use the thesis as if the work was carried out by a NTNU employee, if nothing else has been agreed in advance.

**Thesis supervisors**

Prof. Jørgen Amdahl

Prof. Soren Ehlers

Ph.D student Martin Storheim

Deadline: June 10 2012

Trondheim, January 13, 2012

Jørgen Amdahl



## Preface

This report is the result of the Master thesis work for stud. techn. Knut Aaberge Dahl at the Norwegian University of Science and Technology, NTNU, spring 2012. The work has been carried out as a continuation of the Project thesis work carried out in fall 2011. In the Project thesis basic theory for the problems was reviewed, and this theory is therefore not given in this Master thesis.

Before the thesis work started I had no knowledge about any of the modelling software used. The first challenge met in the work was to establish an ALE-model of the water surrounding the colliding objects in LS-PrePost. After a lot of different unsuccessful tests on this subject it was concluded that no further time could be spent on solving the problems, and the subject was postponed for further work. The results obtained from this work was not directly usable for the rest of the thesis, but the knowledge in use of LS-PrePost and LS-DYNA was improved.

During the modelling work in the FE modelling software MSc. Patran I really experienced great progress. Simple challenges which in the beginning could take hours to perform, could at the end of the modelling process be solved in a few minutes. During the process I have also learned a lot more about the finite element method, on how to create a good mesh which yields accurate results and on what factors that will influence the results.

The analysis of the global ship model collision with the large iceberg includes approximately 1 750 000 elements, and such analysis demands large computer resources. The simulations has been performed on 4 dedicated workstations where a total number of 40 CPU's was available. The analysis results have been obtained after 80-400 hours at 6-8 CPU's, and a total of 10 000 - 14 000 CPU hours has been used during the collision analyses.

The work has been challenging regarding both modelling, collision setup and result comparisons, but the overview of a collision scenario obtained from such thesis has been a large motivation for me during the work. First of all I would like to thank my supervisor Professor Jørgen Amdahl and my co-supervisor Ph.D. Candidate Martin Storheim for all their help during the thesis work. Without their guidance and motivating discussions, it had been really difficult to obtain satisfying results from the thesis work. Especially Martin Storheim has been to great help during the modelling work and by always being available for questions and giving me suggestions for solutions. I would also like to thank my co-supervisor Professor Sören Ehlers for suggestions to the outline of the thesis, and my co-master students for sharing their experiences.

Trondheim, June 10th, 2012



Knut Aaberge Dahl



## Summary

The number of collisions between ships and icebergs are increasing in correlation with the increase of the number of ships sailing in Arctic areas. Due to the exploitation of gas fields in Arctic areas, the LNG shipping in these areas is expected to increase. The consequences of an iceberg impact can be critical for ship structure, the crew and the cargo, and it is important to be able to predict the result of such a scenario.

Different relevant impact scenarios have been discussed, and it has been concluded that the most critical scenario for a spherical type LNG carrier is an impact at the bow shoulder where the distance between the outer hull and the cargo tanks is at its shortest. Based on this study, a bow shoulder impact has been chosen as the scenario investigated in the thesis.

To investigate the influence of the surrounding water, an ALE-model representing this was therefore supposed to be modelled in LS-DYNA. After several unsuccessful tests this work was postponed to further work, but a detailed description of the ALE-modelling and the different options tested has been carried out.

A detailed FE model of the bow shoulder section of an ice strengthened spherical type LNG carrier has been carried out. The mesh in this section has been modelled sufficiently fine to capture the governing deformation mechanisms and the total number of elements in the model are therefore large. This will lead to increased computation time, but this is acceptable based on the accuracy of the results obtained. In addition to the local bow shoulder model, a FE model of a global 125 000 dwt. LNG tanker has been established. The outer shell and coarse geometry has been provided by Ph.D. candidate Martin Storheim, and the detailed bow shoulder model has been included in this global model. The global model is meshed with large rectangular four-node elements, and transitions to the detailed model have been created. Properties have been added to the global model in terms of getting a model which represents the real ship to the best extent possible.

The steel material model used is developed by Hagbart Alsos and includes a RTCL fracture criterion. The ice material model is developed by Zhenhui Liu and is modelled to represent a physical approach to the crushing of the ice. The aluminium material is based on studies performed by Moss Maritime and simple power law calculations.

The added mass and weight of the LNG cargo has been included as increased density in the outer hull below the water line and in the tank shells respectively.

The aim of the simulations has been to investigate similarities and differences in different collision approaches. Three different approaches have therefore been simulated for two different impact angles. For the local model, two simplified approaches have been simulated:

- A prescribed displacement has been applied to the iceberg. This is the most common approach in collision simulations due to lower requirements to computer performance.
- An initial velocity has been given to the iceberg. This approach requires more computer resources, but will probably yield less conservative results.

Pinned boundary conditions have been applied to the bow shoulder model for all the local analyses. In addition to the local analyses, a full global analysis has been performed for the two different impact angles. In these simulations no boundary conditions have been applied to any of the colliding bodies, and initial velocity is given to the ship structure. The mass of the iceberg is approximately 2500 tons and for the global analyses no velocity of the iceberg has been assumed.

The results obtained from these simulations have shown that both of the local simulations tends to over-estimate the indentations. The prescribed displacement analyses yields over-conservative results for long duration simulations, but at large impact angles the results obtained are reasonable for longer simulated time than for small impact angles. The initial velocity method yields more reasonable results, and this approach is therefore better to apply when the damage from a collision scenario is estimated by simplified methods.

To investigate the effect of the iceberg size, two simulations including an iceberg of approximately 19 000 tons have been carried out. These simulations have shown that the damage in such collision is significantly larger than for the small iceberg. It has also been seen that there is less difference between the simplified approach and the full analysis for the large iceberg than for the small iceberg approaches. This is remarkable, since the boundary conditions have been assumed to give larger contribution to the result for the large iceberg.

Unreasonable large accelerations have been found in collision simulations described in different papers. To investigate this in the simulations performed in this thesis, the accelerations and motions have been observed in different spots which is not directly impacted by the collision. No extreme values of either accelerations or motions have been found, and it is concluded that this is not a problem for the collision scenario simulated in this thesis.

## Samandrag

Talet på kollisjonar mellom skip og isfjell aukar i takt med auken av skipstrafikk i Arktiske område. Som ei følgje av at ein ønskjer å nytta seg av gassfelt i Arktiske område vil LNG-skipstrafikken i desse områda auka. Konsekvensane av ein kollisjon kan vera kritisk for skipskonstruksjonen, mannskapet og lasta, og det er viktig å kunna forutsjå resultatet av eit kollisjonsscenario.

Ulike aktuelle kollisjonsscenario er diskutert, og det er konkludert med at det mest kritiske av desse for eit LNG-skip med sfærisk tankdesign er ein kollisjon ved baugskulderområdet. Her er avstanden mellom ytre hud og gasstanken kortast, og dette kollisjonstilfellet har difor vorte valt som grunnlag for studiet i denne rapporten.

Effekten av vatnet som omkransar kollisjonen er interessant å undersøka. Ein ALE-modell som representerer dette vatnet skulle difor vorte modellert i LS-DYNA, men etter mange resultatlause forsøk vart dette arbeidet utsatt til vidare arbeid. Ein detaljert rapport om ALE-modellering og dei ulike utførte forsøka er likevel presentert i rapporten.

Ein detaljert elementmodell av baugskulderområdet for ein isforsterka LNG-tankar med sfærisk tankdesign har vorte modellert. Meshet i baugskulderseksjonen er laga fint nok til at kollisjonsmekanismane skal bli fanga og det totalet tal på element i modellen er difor stort. Dette fører til ein auke i analyseringstida, men dette er rekna som akseptabelt på grunn av dei nøyaktige resultatata ein oppnår. I tillegg til den lokale baugskulderseksjonen er det laga ein elementmodell av ein 125 000 dvt. LNG-tankar. Ytre hud og grov geometri i denne modellen har vorte modellert av doktorgradskandidat Martin Storheim, og den detaljerte baugskuldermodellen har vorte inkludert i denne globalmodellen. Globalmodellen er inndelt i store rektangulære fire-nodars element, og overgangar til dei mindre elementa i lokalmodellen har vorte laga for alle flater. Eigenskapane og tjukkeleikane til dei ulike delane av skipet er modellert for å representera eit reelt skip i størst mogleg grad.

Stålmaterialemodellen som er brukt er utvikla av Hagbart Alsos og inkluderer eit RTCL brotkriterie. Ismodellen er utvikla av Zhenhui Liu og er modellert for å representera ei fysisk tilnærming av isknusingen. Aluminiumsmaterialet er basert på studie utført av Moss Maritime og enkle "power law"-berekningar.

Tilleggsmassen til skipet er inkludert som auka tettleik i ytre hud under vasslinja og vekta av LNG-lastar er inkludert som ekstra tettleik i tankskalet.

Målet med simuleringane har vore å undersøka likskapar og ulikskapar i ulike kollisjonstilnærmingar. Tre ulike tilnærmingar har difor vorte simulert for to ulike innfallsvinklar. For globalmodellen har to ulike tilnærmingar vorte simulerte:

- Ei forskyving som er definert på førehand er gitt til isfjellet. Dette er den mest brukte tilnærminga i kollisjonssimuleringar på grunn av lågare krav til dataressursar.
- Ein initiell hastigheit er gitt til isfjellet. Denne tilnærminga krev meir dataressursar, men vil mest sannsynleg gi mindre konservative resultat.

Baugskulderområdet er for alle dei lokale analysane halde fast mot translasjon i alle fridomsgrader. I tillegg til dei lokale analysane er det utført ein globalanalyse for kvar av innfallsvinklane. I desse simuleringane er det ikkje definert grensebetingelsar for verken

skipet eller isfjellet, og den initielle hastigheita er gitt til skipet i desse analysane. Massen av isfjellet er omlag 2500 tonn, og for dei globale analysane er det gått ut frå at isfjellet ikkje har nokon hastigheit.

Resultata som er funne frå desse analysane viser at begge dei lokale simuleringane i større eller mindre grad overestimerar inntrykkingen av skipet. Analysane der isfjellet er gitt ei førehandsdefinert forskyving gir overkonservative resultat for simuleringar med lang varigheit, men ved store innfallsvinklar gir metoden rimelege resultat for lengre simuleringstid enn ved små innfallsvinklar. Metoden med initiell hastigheit gir meir rimelege resultat, og denne tilnærminga er difor betre å bruka når skaden frå eit kollisjonsscenario skal estimerast med forenkla metodar.

For å undersøka effekten av isfjellstørrelsen er to simuleringar med eit isfjell på omlag 19 000 tonn utført. Desse simuleringane viser at skaden frå ein slik kollisjon er markant større enn for det vesle isfjellet. Samtidig viser analysen at det er mindre forskjellar mellom forenkla metode og full analyse for stort isfjell enn for lite isfjell. Dette er oppsiktsvekkande, då det var gått ut frå at grensebetingelsane til lokalmodellen skulle spela ei større rolle på resultata for det store isfjellet.

Urimeleg store akselerasjonar har vorte observerte i kollisjonssimuleringar som er skildra i ulike artiklar. For å undersøka dette problemet i simuleringane i denne oppgåva, har akselerasjonane og rørsleane i ulike punkt som ikkje er direkte i kontakt med kollisjonssområdet vorte observerte. Ingen ekstremverdiar av verken akselerasjonar eller rørsler er funne, og det er konkludert med at dette ikkje er noko problem i kollisjonsscenarioet som er skildra i denne oppgåva.

# Contents

Abstract	i
Scope of work	iii
Preface	vii
Summary	ix
Samandrag	xi
<b>1 Introduction</b>	<b>1</b>
<b>2 Background</b>	<b>2</b>
2.1 Spherical type LNG cargo containment system . . . . .	2
2.2 Previous work . . . . .	2
2.2.1 Simulation of growler impact in water . . . . .	3
2.2.2 LNGC collision response analysis with iceberg considering surround- ing seawater . . . . .	4
2.3 Collision mechanics . . . . .	5
2.4 Relative strength . . . . .	5
<b>3 Impact scenarios</b>	<b>7</b>
3.1 Collision geometry and impact velocity . . . . .	7
3.1.1 Bow collision . . . . .	7
3.1.2 Collision at bow shoulder . . . . .	7
3.1.3 Collision at ship side . . . . .	7
3.1.4 Grounding and bottom impact . . . . .	7
3.1.5 Simulated collision scenario . . . . .	8
3.2 Iceberg shapes . . . . .	8
<b>4 Modelling and analysis software</b>	<b>9</b>
4.1 MSc. Patran . . . . .	9
4.2 LS-DYNA . . . . .	9
4.2.1 Time integration . . . . .	9
4.2.2 Time integration loop . . . . .	10
4.2.3 Time step size . . . . .	10
<b>5 ALE-modelling in LS-DYNA</b>	<b>12</b>
5.1 Limitations . . . . .	12
5.2 Multi-material group . . . . .	13
5.3 Meshing . . . . .	13
5.4 Fluid-structure interaction (FSI) . . . . .	14
5.5 Modelling in practice . . . . .	15
<b>6 FE modelling and meshing</b>	<b>18</b>
6.1 Front tank section . . . . .	18
6.1.1 Geometry modelling . . . . .	18

6.1.2	Meshing . . . . .	21
6.1.3	Time step considerations . . . . .	23
6.1.4	Materials . . . . .	23
6.1.5	Properties . . . . .	25
6.2	Global model . . . . .	26
6.2.1	Geometry modelling . . . . .	27
6.2.2	Meshing . . . . .	27
6.2.3	Time step considerations . . . . .	28
6.2.4	Materials . . . . .	28
6.2.5	Properties . . . . .	29
6.3	Iceberg . . . . .	29
6.3.1	Geometry modelling . . . . .	30
6.3.2	Meshing . . . . .	30
6.3.3	Materials . . . . .	32
6.4	Settings for analyses . . . . .	33
6.4.1	Boundary condtions . . . . .	34
6.4.2	Contact . . . . .	35
6.4.3	Initial velocity . . . . .	35
6.4.4	Prescribed displacement . . . . .	36
6.4.5	Mass and centre of gravity . . . . .	36
6.4.6	Added mass . . . . .	37
6.4.7	Radius of gyration . . . . .	37
<b>7</b>	<b>Analysis setup</b>	<b>39</b>
7.1	Part 1 - front tank vs. iceberg . . . . .	39
7.1.1	Iceberg . . . . .	39
7.1.2	Initial velocity . . . . .	40
7.1.3	Prescribed displacement . . . . .	42
7.1.4	Boundary conditions . . . . .	42
7.2	Part 2 - global model vs. iceberg . . . . .	42
7.2.1	Iceberg . . . . .	43
7.2.2	Initial velocity . . . . .	43
7.2.3	Boundary conditions . . . . .	43
7.3	Part 3 - Large iceberg impact . . . . .	43
<b>8</b>	<b>Results</b>	<b>45</b>
8.1	Pressure-area relationships . . . . .	46
8.2	Contact forces and deformations . . . . .	48
8.2.1	Simplified approach - pinned local model . . . . .	48
8.2.2	Local model compared to global model . . . . .	56
8.2.3	Comparison of both impact angles for the global model . . . . .	64
8.2.4	Large iceberg . . . . .	65
8.3	Energy considerations . . . . .	69
8.3.1	Simplified approach - pinned local model . . . . .	69
8.3.2	Local model compared to global model . . . . .	72
8.3.3	Comparison of both impact angles for global model . . . . .	76
8.3.4	Large iceberg . . . . .	77



8.4	Ice crushing energy . . . . .	78
8.5	Plastic strain . . . . .	81
8.5.1	Local initial velocity analysis . . . . .	81
8.5.2	Prescribed displacement for local model . . . . .	82
8.5.3	Global model . . . . .	84
8.5.4	Observed plastic strains for all analyses . . . . .	84
8.6	Accelerations, velocities and deformations . . . . .	86
8.6.1	Local initial velocity analysis . . . . .	87
8.6.2	Local prescribed displacement analysis . . . . .	89
8.6.3	Global model . . . . .	91
8.6.4	Large iceberg . . . . .	93
8.7	External mechanics . . . . .	95
8.8	Comparison with membrane type LNG carrier . . . . .	96
<b>9</b>	<b>Conclusions and further work</b>	<b>99</b>
9.1	Summary of results . . . . .	99
9.2	Concluding remarks . . . . .	100
9.3	Further work . . . . .	101
	<b>References</b>	<b>103</b>
	<b>Appendices</b>	<b>I</b>
	<b>A Deformations of hull</b>	<b>I</b>
	<b>B Plastic strains</b>	<b>IV</b>
	<b>C MATLAB code for external mechanics calculation</b>	<b>VI</b>
	<b>D Spreadsheet used for weight calculations</b>	<b>X</b>
	<b>E MATLAB codes used for post-processing</b>	<b>XI</b>
	<b>F Input files for LS-DYNA</b>	<b>XXII</b>



## List of Figures

2.1	A cross-section of the spherical type CCS . . . . .	2
2.2	Proximity simulation performed by Gagnon . . . . .	3
2.3	Meshed region for growler impact analysis . . . . .	3
2.4	Collision setup, Lee and Nguyen . . . . .	5
2.5	Relative strength between ship and iceberg . . . . .	6
3.1	Simplified iceberg geometry . . . . .	8
4.1	The time integration loop in LS-DYNA . . . . .	10
5.1	Water pressure gradient in LS-DYNA . . . . .	15
5.2	Steel box on water surface . . . . .	16
5.3	Air "box" with a water "frame" . . . . .	17
6.1	Frames and stiffeners supporting outer shell . . . . .	19
6.2	Stiffeners in front tank area . . . . .	20
6.3	Modelled details in front tank section . . . . .	21
6.4	Cutting of frame stiffener . . . . .	22
6.5	Critical strain for an element exposed to necking . . . . .	24
6.6	Thickness on outer shell . . . . .	26
6.7	Vertical cut of global model at centre line, tanks are not showed . . . . .	27
6.8	Vertical cut of global model at centre line . . . . .	29
6.9	Modelled iceberg . . . . .	30
6.10	Side view of iceberg . . . . .	31
6.11	Cut iceberg for prescribed displacement analyses . . . . .	32
7.1	Iceberg position, front tank analyses . . . . .	40
7.2	Setup of front tank and iceberg for the small impact angle . . . . .	41
7.3	Setup of front tank and iceberg for the large impact angle . . . . .	41
7.4	Setup of global model at small impact angle . . . . .	43
7.5	Setup of global model vs. large iceberg scenario . . . . .	44
8.1	Pressure-area relationships . . . . .	46
8.2	Contour plot of contact pressure at max force for initial velocity, 5.71° . . . . .	47
8.3	Force - indentation relationship, initial velocity and prescribed displacement for local model, 5.71° . . . . .	49
8.4	Horizontal cut for local initial velocity analysis, 5.71° . . . . .	50
8.5	Horizontal cut for local prescribed displacement analysis, 5.71° . . . . .	50
8.6	Force - time, initial velocity and prescribed displacement, 5.71° . . . . .	51
8.7	Ice crushing for local initial velocity and prescribed displacement analyses, 5.71° . . . . .	52
8.8	Force - indentation relationship, initial velocity and prescribed displacement analysis for local model, 30° . . . . .	54
8.9	Horizontal cut for local initial velocity analysis, 30° . . . . .	55
8.10	Horizontal cut for local prescribed displacement analysis, 30° . . . . .	55
8.11	Force - time for local and global model, 5.71° . . . . .	56
8.12	Horizontal cut for local model initial velocity analysis, 5.71° . . . . .	57
8.13	Horizontal cut for global model analysis, 5.71° . . . . .	57
8.14	Max indentation plotted against time for local and global analysis, 5.71° . . . . .	58
8.15	Ice crushing for local and global analysis, 5.71° . . . . .	59

8.16 Relationship between force and max indentation for local and global analysis, 30° . . . . .	60
8.17 Horizontal cut for local initial velocity analysis, 30° . . . . .	62
8.18 Horizontal cut for global analysis, 30° . . . . .	62
8.19 Ice crushing for local and global analysis, 30° . . . . .	63
8.20 Relationship between force and max indentation for both impact angles, global analysis . . . . .	64
8.21 Largest deformation of ship for the two different impact angles, global analysis	65
8.22 Relationship between force and max indentation for local and global analysis, large iceberg at 30° impact angle . . . . .	66
8.23 Horizontal cut for local initial velocity analysis, large iceberg, 30° . . . . .	67
8.24 Horizontal cut for global analysis, large iceberg, 30° . . . . .	67
8.25 Horizontal cut for global analysis, large iceberg at 30° impact angle and t=0.88 s . . . . .	68
8.26 Internal energy for local initial velocity and prescribed displacement analysis, 5.71° . . . . .	70
8.27 Internal iceberg energy for local initial velocity and prescribed displacement analysis, 5.71° . . . . .	71
8.28 Internal energy for local initial velocity and prescribed displacement analysis, 30° . . . . .	72
8.29 Internal energy comparison for local and global model, 5.71° . . . . .	73
8.30 Ice energy comparison for local and global model, 5.71° . . . . .	74
8.31 Internal energy comparison for local and global analysis, 30° . . . . .	75
8.32 Ice energy comparison for local and global analysis, 30° impact angle . . . . .	76
8.33 Comparison of internal energy for both impact angles, global model . . . . .	77
8.34 Internal energy, large iceberg at 30° impact angle . . . . .	78
8.35 Energy ratio for ice crushing, 5.71° impact angle . . . . .	79
8.36 Energy ratio for ice crushing, 30° impact angle . . . . .	80
8.37 Plastic strain at local 5.71° initial velocity impact . . . . .	81
8.38 Plastic strain in outer shell and vertical frames, initial velocity for local analysis, 5.71° . . . . .	82
8.39 Plastic strain in outer shell and vertical frames, prescribed displacement analysis for the local model, 5.71° . . . . .	83
8.40 Plastic strain at 5.71° prescribed displacement impact on local model . . . . .	83
8.41 Plastic strain in outer shell and vertical frames, global model, 5.71° . . . . .	84
8.42 Spots for measuring accelerations . . . . .	86
8.43 Spots for measuring accelerations in tank tower . . . . .	87
8.44 Acceleration curves for the given spots, local initial velocity analysis, 30° . . . . .	88
8.45 Velocity curves for the given spots, local initial velocity analysis, 30° . . . . .	88
8.46 Deformation curves for the given spots, local initial velocity analysis, 30° . . . . .	89
8.47 Acceleration curves for the given spots, local prescribed displacement analysis, 30° . . . . .	90
8.48 Deformation curves for the given spots, local prescribed displacement analysis, 30° . . . . .	91
8.49 Acceleration curves for the given spots, global analysis, 30° . . . . .	92
8.50 Deformation curves for the given spots, global analysis, 30° . . . . .	92
8.51 Acceleration curves for the given spots, global analysis, large iceberg, 30° . . . . .	93

---

8.52	Deformation curves for the given spots, global analysis, large iceberg, 30° .	94
8.53	Comparison of energy values for numerical calculation and simulations . . .	95
8.54	Collision setup for membrane type LNG carrier comparison . . . . .	97
8.55	Internal energy in membrane type LNG carrier . . . . .	97
A.1	Deformation of hull for the global analysis, 5.71° impact angle . . . . .	I
A.2	Deformation of hull for the global analysis, 30 ° impact angle . . . . .	II
A.3	Deformation of hull for the global analysis, colliding with the large iceberg	III
B.1	Plastic strain for global model, 5.71 ° impact angle . . . . .	IV
B.2	Plastic strain for global model, 30 ° impact angle . . . . .	IV
B.3	Plastic strain for global model, large iceberg impact . . . . .	V



## List of Tables

2.1	Lee's collision scenarios . . . . .	4
6.1	Dimensions of modelled ship . . . . .	18
6.2	Steel material properties . . . . .	25
6.3	Aluminium material properties . . . . .	25
6.4	Modified material properties . . . . .	29
6.5	Ice material properties . . . . .	33
6.6	Stability parameters for modelled ship . . . . .	37
6.7	Gyration radius for model . . . . .	38
7.1	Setup parameters for the different analyses . . . . .	39
7.2	Boundary conditions for the analysis . . . . .	42
7.3	Velocity and angle for global model analyses . . . . .	43
8.1	Largest observed plastic strains for the different analyses . . . . .	85

# Nomenclature

## Abbreviations

---

---

ALE	= Arbitrary Lagrangian Eulerian
AMMG	= Arbitrary Lagrangian Eulerian Multi-Material Group
CFD	= Computational fluid dynamics
$CG_x$	= centre of gravity, x-component
$CG_y$	= centre of gravity, y-component
$CG_z$	= centre of gravity, z-component
$CL$	= Centre line
CTYPE	= Coupling Algorithm type
DNV	= Det Norske Veritas
ELFORM	= Element formulation
EOS	= Equation of State
FE	= Finite element
FSI	= Fluid-Structure Interaction
HHI	= Hyundai Heavy Industries
LNG	= Liquefied Natural Gas
LNGC	= Liquefied Natural Gas Carrier
MAT	= Material
MCOUP	= Material Coupling
NORM	= Normals used in fluid modelling in LS-DYNA
NQUAD	= Number of coupling points
$RG_x$	= radius of gyration, x-component
$RG_y$	= radius of gyration, y-component
$RG_z$	= radius of gyration, z-component
SPC	= Single Point Constraint
WL	= Water line



---



---

**Greek symbols**


---



---

$\alpha$	= impact angle [ $^{\circ}$ ]
$\beta$	= constant in calculation for characteristic element length [-]
$\epsilon_0$	= intersection strain [-]
$\epsilon_0$	= initial failure strain [-]
$\epsilon_{cr}$	= critical plastic strain [-]
$\epsilon_{eq}$	= equivalent plastic strain [-]
$\epsilon_f$	= failure strain [-]
$\epsilon_n$	= strain of virtual neck [-]
$\epsilon_{plat}$	= plateau strain [-]
$\epsilon_r$	= strain outside the instability [-]
$\rho$	= material density [ $kg/m^3$ ]
$\sigma_{eq}$	= equivalent stress [MPa]
$\sigma_y$	= initial yield stress [MPa]
$\Delta t$	= time step [s]
$\Delta t_c$	= critical time step [s]
$\Delta t_e$	= critical time step for Belytschko beam elements [s]
$\nu$	= Poisson's ratio [-]

---



---

**Latin symbols**


---



---

$a_0$	= ice material parameter [ $MPa^2$ ]
$a_1$	= ice material parameter [ $MPa$ ]
$a_2$	= ice material parameter [-]
$\mathbf{a}^n$	= nodal acceleration vector
$A$	= area of cross section [ $m^2$ ]
$A$	= added mass [ton]
$A$	= loaded area [ $m^2$ ]
$A_s$	= area of element [ $m^2$ ]
$B$	= breadth [ $m$ ]
$B$	= bulk modulus [ $MPa$ ]
$c$	= sound speed [m/s]
$C_{A,ice}$	= added mass coefficient for the iceberg [-]
$C_{A,ship}$	= added mass coefficient for the ship [-]
$D$	= depth [ $m$ ]
$E$	= Young's modulus [MPa]
$\mathbf{F}^n$	= stress divergence vector
$G$	= shear modulus [ $MPa$ ]
$\mathbf{H}^n$	= hourglass resistance
$I$	= maximum value of moment of inertia [ $m^4$ ]
$K$	= material constant [ $MPa$ ]
$l_e$	= element length [ $m$ ]
$L_i$	= element side lengths [m]
$L_{oa}$	= length over all [ $m$ ]
$L_{pp}$	= length between perpendiculars [ $m$ ]
$L_s$	= characteristic element length [m]

---

$\mathbf{M}$	= diagonal mass matrix
$M$	= mass [ton]
$p$	= pressure [Pa]
$\mathbf{p}^n$	= external and body loads
$p_2$	= larger root of yield function
$p_{cut}$	= cut-off pressure [MPa]
$p_L$	= local pressure [MPa]
$R_x$	= rotational degree of freedom - x [-]
$R_y$	= rotational degree of freedom - y [-]
$R_z$	= rotational degree of freedom - z [-]
$t$	= element thickness [m]
$t$	= material thickness [m]
$T$	= temperature
$T$	= draught [m]
$T_x$	= translational degree of freedom - x [-]
$T_y$	= translational degree of freedom - y [-]
$T_z$	= translational degree of freedom - z [-]
$\mathbf{u}^n$	= nodal displacement vector
$\mathbf{v}^n$	= nodal velocity vector
$V_{el}$	= element volume [m <sup>3</sup> ]
$V_n$	= neck volume [m <sup>3</sup> ]
$V_r$	= volume of remainder of element [m <sup>3</sup> ]
$V_r$	= radial (turning) velocity [m/s]
$V_x$	= x-velocity [m/s]

# 1 Introduction

The expected increase of exploitation of gas fields in the Northern regions such as West Russia demands development of ice strengthened LNG carriers. The increased shipping in the Arctic areas leads to an increased probability for accidental encounters with ice and icebergs. The consequences of such event can be critical for the ship and the crew in addition to the environment due to long distances and challenging climate and environment. It is therefore important to know more about the consequences of an accidental impact between a ship and an iceberg.

Running detailed analyses of collision scenarios demands long modelling time, computation time and large computing resources. Due to these factors, simplified approaches are often chosen. The results obtained from such analyses are assumed to be conservative, and to verify this and in addition reveal possible over-conservatism a comparison of the results from global and simplified analyses is useful. No clear regulations on iceberg collisions are available, but several studies of the problem are developed, both regarding relevant impact scenarios, material models and iceberg shapes. These studies are used as basis for the work presented in this thesis.

According to the problem text, the work carried out can by approval from the supervisors be reduced in extent if the scope is proved to be larger than initially anticipated. In agreement with the supervisor, Professor Jørgen Amdahl, it has been agreed to focus on a comparison study between different simulation approaches for collision analyses. The work has to a large extent been carried out in terms of the problem text, but some details has only been roughly commented while other details has been added to the problem.

The major focus of the thesis has been to establish a detailed local FE model of the front tank and bow shoulder area and a global model including coarse geometry, in addition to two different icebergs. These FE models are used for two different simplified collision analyses and a full global analysis of the problem. The icebergs used in the thesis are modelled as irregular box-shaped icebergs in agreement with the supervisors.

In the project text it is stated that the global analysis shall include the surrounding water in the problem. The ALE-modelling in LS-DYNA has not been successfully modelled, and is therefore not included in the analyses. The modelling problems regarding this is almost solved, but some essential details for getting this physically correct are missing out.

In addition to the comparison of different simulation approaches, an energy comparison with an external mechanics model developed by Liu, [1] has been performed. As a last comparison, an analysis of a membrane type LNG carrier is performed. This tanker is not ice strengthened, and the comparison is therefore not very relevant, but it is interesting to see the effect such ice strengthening will have on the damage. The membrane tank model provided by Stine Aas Myhre, [2], is in addition only including the a ship side, and this collision is therefore simulated as a side collision with lower velocity than for the bow shoulder simulations performed for the spherical Moss Maritime design.

## 2 Background

### 2.1 Spherical type LNG cargo containment system

The spherical tank of the Moss-Rosenberg type is the most recognizable design for LNG tankers. The spherical tanks protrude above the deck and the ships are very characteristic. The hull and tanks are in this design independent. The structural joint equatorial ring acts as the gradient to make use of normal steel possible in the hull. [3]

The tank is only connected to the hull through the transition joint. This joint is made as a transition of three different materials to prevent the mild steel from getting in direct contact with the cold temperatures. The adjacent part to the tank is made of aluminium and the part between the hull steel and the aluminium part is made of stainless steel. The stainless steel will act as a thermal brake due to its low ability to transfer heat. The insulation of the tank is important to maintain the safety against embrittlement. The cold tanks will absorb heat from the hull, and this effect can cause cryogenic embrittlement in the hull steel.

The spherical tank is preferable with respect to sloshing. If the tanks are not completely filled up, the motions of the LNG cargo in a membrane tank will cause large motions for the ship as well. The spherical tank minimizes this problem, since the cargo only will follow the boundary of the tank without transferring motions to the ship structure.

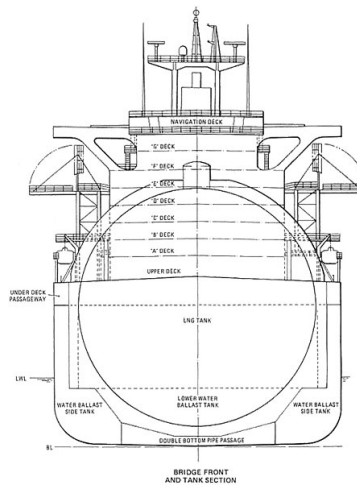


Figure 2.1: A cross-section of the spherical type CCS

### 2.2 Previous work

A couple of technical reports on modelling fluid in LS-DYNA have been studied to get an understanding of the issues regarding this technique. A short summary of the modelling part of these reports will be given in the following sections.

### 2.2.1 Simulation of growler impact in water

R.E. Gagnon [4] has presented results of numerical simulations of growler impact tests. The dimensions of the modelled region and mesh element sizes were determined prior to the simulation by using a set of separate simulations of a model-scale tanker transiting in proximity to a model-scale bergy bit. Figure 2.2 shows the proximity simulation.

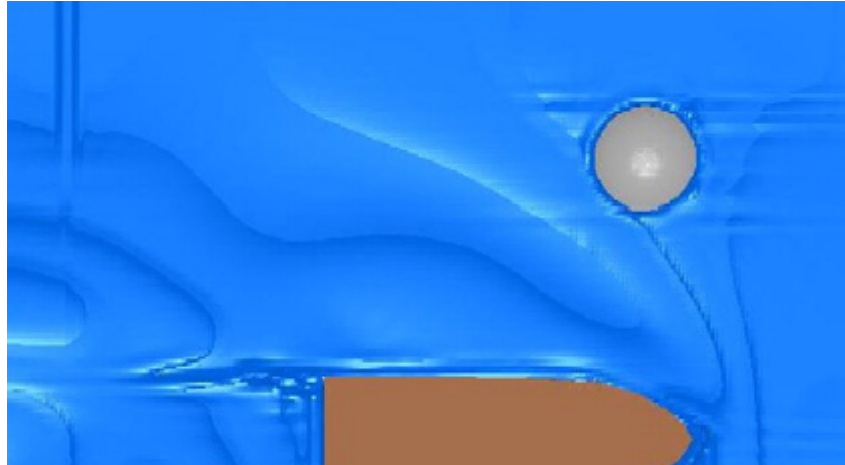


Figure 2.2: Proximity simulation performed by Gagnon

The maximum bergy bit sway due to the hydrodynamic interaction with the tanker was used as the index to compare the results with actual data from physical model tests. The water, bergy bit and air were meshed using solid elements, while the tanker were meshed by shell elements. The meshed region for the analysis is shown in figure 2.3.

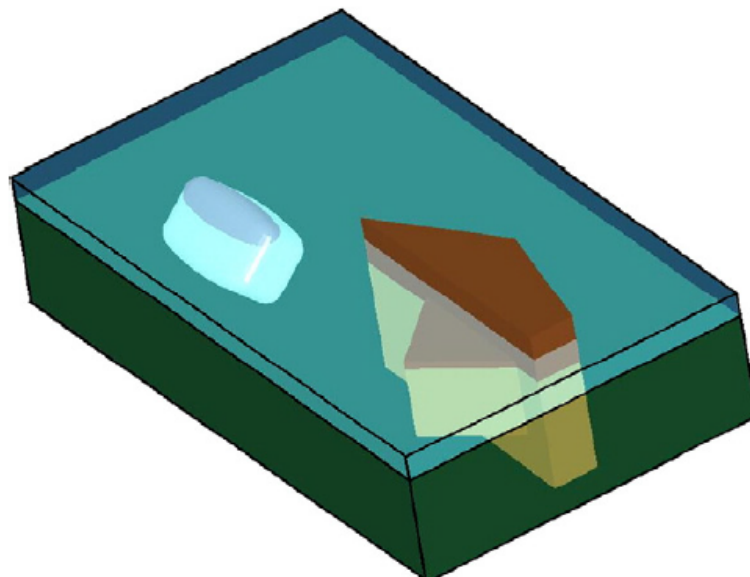


Figure 2.3: Meshed region for growler impact analysis

The growler simulated in the analysis is brick shaped with rounded edges, and has di-

mensions 1.73 m x 0.88 m x 0.98 m and mass 1068 kg. It is rotated by 45° in order to represent an impact of the corner.

To ensure that the water and the other objects behave correctly, gravity must be applied. This is done by applying an acceleration equivalent to the acceleration due to gravity to all elements in the model. This results in the proper hydrostatic pressure gradient developing in the water early in the simulation, which again creates proper buoyant forces on floating objects and enables the formation of waves on the free surface of the water.

To ensure that the water is removed from the volume occupied by the objects (growler and impactor model), the command "initial-volume-fraction" are used. This command works for the shell element-structures. For solid elements, only standard shapes such as spheres, cylinders, bricks etc. can be emptied of water. To ensure that the brick-shaped growler with rounded edges was free of water, a brick shape with squared edges of water was removed.

The impactor was treated as a rigid body, but elastic material would also lead to similar results. The growler was modelled in an ice material which simulates the crushing during impact.

The results of the simulation are not relevant for this thesis and is not reviewed.

### 2.2.2 LNGC collision response analysis with iceberg considering surrounding seawater

Sang-Gab Lee and Hong-Anh Nguyen, [5] has presented results from a collision analysis between a membrane type LNG carrier and an iceberg where the surrounding water also is considered. The collision simulations are carried out by using FSI analysis technique in LS-DYNA. No description of the settings applied in LS-DYNA are included in the paper, but a short summary of the simulation setup and the impact scenarios are given.

Three different scenarios are analysed, and these are shown in table 2.1.

Type	Iceberg		LNGC		
	Current state	Drifting speed	Full speed	Radial speed	Manoeuvring
1	stationary	0	19.5	0	Forward
2	current	2.0	19.5	0	Forward
3	current	2.0	19.5	1.95	Evasive

Table 2.1: Lee’s collision scenarios

The mesh sizes of the shell elements were set to 0.4 m for deformable parts and 0.8 m for rigid parts, while the iceberg and fluid elements was set to 1.0 and 3.0 m respectively. After applying gravity, correct pressure in air and water occurred, and the structures were floated by the buoyancy. An equivalent current load was applied to the iceberg with constant drifting speed to simulate the current flow.

The collision setup is shown in figure 2.4.

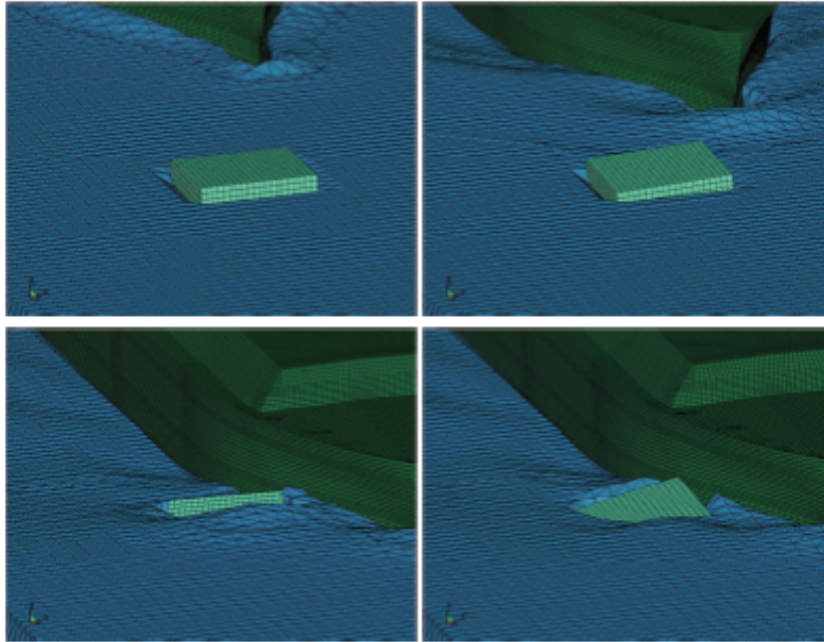


Figure 2.4: Collision setup, Lee and Nguyen

### 2.3 Collision mechanics

During the collision the absorbed energy is limited by the initial kinetic energy of the collision. According to Storheim et al., [6], impacted bodies will behave as rigid bodies in situations where the initial energy is limited. As the energy increases, plasticity effects in the vessel becomes important.

For engineering calculations it is common to decouple the collision event into external and internal mechanics. The external mechanics describes the initial and final kinetic energies which indicates the global system response, while the internal mechanics describes the local deformations and the energy absorbed in the interaction between the colliding bodies. In the external mechanics model developed by Liu, [1], it is assumed that the internal mechanics distributes the energy in deformation for the bodies.

### 2.4 Relative strength

Collision scenarios between deformable bodies can be classified based on the relative amount of energy absorbed in the two bodies, see figure 2.5.

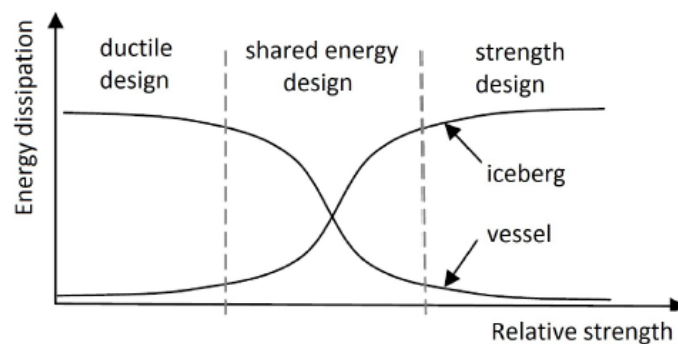


Figure 2.5: Relative strength between ship and iceberg

According to Storheim et al., [6], utilizing ductile strength yields allowance for significantly deformations of the ship structure. All energy is absorbed by the ship, and the iceberg can be treated as rigid.

In a shared energy design, both bodies is absorbing the energy. This leads to deformations in both bodies, and leads to possibilities for an optimized ship structure regarding strength and weight. This design demands a proper ice material model, since this must yield correct results for different levels of deformation.

When strength design are utilized, all energy is absorbed by the iceberg. Small or no deformation of the ship is obtained throughout the collision.



## 3 Impact scenarios

When studying collision scenarios it is important to simulate realistic situations. For the collision scenario between a LNG carrier and an iceberg, a couple of different scenarios can be assumed as realistic.

### 3.1 Collision geometry and impact velocity

Several studies on ship-iceberg collisions are carried out. Two relevant studies are reviewed in section 2.2, and e.g. a report carried out by Hyundai Heavy Industries Co. Ltd. (HHI) et al., [7], describes relevant collision scenarios for a Moss-type LNG tanker. Based on these studies relevant impact scenarios regarding collision geometry and impact can be stated. A couple of different possible collision scenarios and the collision velocity in these are described in the following sections.

#### 3.1.1 Bow collision

For a ship sailing in Arctic areas, a bow collision with an iceberg is a possible scenario. If the size and shape of the iceberg is of a magnitude that prevents it from being visible on the radar, the ship can possibly hit the iceberg at transit speed. Such collision will probably cause large damage to the bow, but this is not critical for the cargo due to the large distance between the bow and the cargo tanks.

#### 3.1.2 Collision at bow shoulder

A more critical collision scenario is an iceberg impact at the bow shoulder. For a spherical LNG cargo containment system, a collision at the bow shoulder is the most critical scenario due to the small distance between the outer hull and the tank shell. Such collision is realistic to occur for a ship in turning, for a drifting iceberg, or a combination of these. The impact velocity will in such scenario be lower than for a bow collision due to the two velocity components of the problem.

#### 3.1.3 Collision at ship side

A collision at the ship side is possible for a drifting iceberg. The velocity in such collision are lower than for both bow collision and bow shoulder collision, and this, combined with larger distance to the cargo tanks, leads to a less critical scenario than the bow shoulder collision.

#### 3.1.4 Grounding and bottom impact

According to a technical report provided by DNV, [8], two different scenarios of grounding and bottom impacts can be considered. In shallow water with grounded icebergs, the ship

can be assumed to be grounded on solid ice. This case will be close to a regular grounding scenario, and is unlikely to happen.

The other possible scenario is a collision where the ship runs over an underwater iceberg. The pressure from the ice will now be caused by the buoyancy of the ice structure, and the pressure will most probably be less than the load assumed for a side collision.

### 3.1.5 Simulated collision scenario

As described in section 3.1.2, the most critical collision scenario is iceberg impact at the bow shoulder. This scenario is therefore chosen for the simulations in this thesis, and different impact angles for this scenario are analysed.

## 3.2 Iceberg shapes

It is difficult to give an exact shape of the iceberg. Icebergs are found in a lot of shapes and sizes, and it is therefore interesting with simulations where the iceberg size and shape is varied.

In the technical report by DNV, different simplified iceberg geometries are proposed. All the proposed icebergs in this report have been determined on the condition that the height above water level is 2 m. The simplified geometries are given in figure 3.1 which is provided by Stine Aas Myhre, [2].

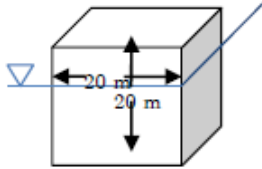
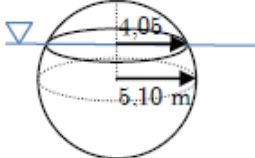
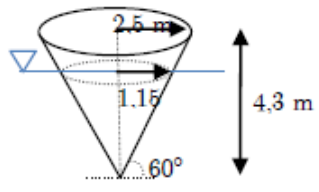
CUBE	SPHERE	CONE
<p>Volume: 8000 m<sup>3</sup> Mass: 7200 tonnes</p> 	<p>Volume: 555 m<sup>3</sup> Mass: 500 tonnes</p> 	<p>Volume: 28 m<sup>3</sup> Mass: 25 tonnes</p> 

Figure 3.1: Simplified iceberg geometry

The sail height of the icebergs is based on the density difference between the ice material and the sea water. As described in section 6.3, the iceberg chosen for the analyses in this thesis is not similar to any of the simplified geometries in the DNV report. A more irregular iceberg shape is chosen based on the assumption that icebergs are not perfectly shaped geometrical figures. Two different icebergs are used in the analysis, but the shape is approximately the same, only the size and mass is varied. Different iceberg shapes should also be investigated, but due to long computation time this has not been done in this thesis.

## 4 Modelling and analysis software

Three different computer programs are used in the modelling part of this thesis. MSc. Patran is used for geometry modelling, LS-PrePost is used for pre- and post-processing and LS-DYNA is used for the analyses.

### 4.1 MSc. Patran

The geometry modelling and meshing are done in the finite element software MSc. Patran 2010.2.3. Patran is a powerful finite element modelling software, with different possibilities of modelling and meshing advanced geometry. Patran does also include tools for e.g. computing mass, radius of gyration and centre of gravity. Based on the FE modelling, input files for analyses in a lot of different FE solvers can be written, and in this thesis input files for LS-DYNA are created.

MSc. Patran are preferable software in this thesis due to its possibilities of modelling advanced geometrical structures, and due to in-house expertise at NTNU.

### 4.2 LS-DYNA

LS DYNA is a computer program using the explicit central difference scheme to integrate the equations of motion. Martin Storheim, [9], has made a short review of the features of the computer program in his master thesis.

#### 4.2.1 Time integration

The semi-discrete equation of motion can be written as:

$$\mathbf{M}\mathbf{a}^n = \mathbf{p}^n - \mathbf{F}^n + \mathbf{H}^n \quad (4.1)$$

Here,  $\mathbf{M}$  is the diagonal mass matrix,  $\mathbf{p}^n$  accounts for external and body loads,  $\mathbf{F}^n$  is the stress divergence vector and  $\mathbf{H}^n$  is the hourglass resistance. When time integration is applied to this equation, we get:

$$\mathbf{a}^n = \mathbf{M}^{-1}(\mathbf{p}^n - \mathbf{F}^n + \mathbf{H}^n) \quad (4.2)$$

$$\mathbf{v}^{n+\frac{1}{2}} = \mathbf{v}^{n-\frac{1}{2}} + \mathbf{a}^n \Delta t^n \quad (4.3)$$

$$\mathbf{u}^{n+1} = \mathbf{u}^n + \mathbf{v}^{n+\frac{1}{2}} \Delta t^{n+\frac{1}{2}} \quad (4.4)$$

$$\Delta t^{n+\frac{1}{2}} = \frac{\Delta t^n + \Delta t^{n+1}}{2} \quad (4.5)$$

$\mathbf{u}$  is the global nodal displacement vector and  $\mathbf{v}$  is the nodal velocity vector. The geometry is updated for each step by adding the displacement increment to the initial geometry.

### 4.2.2 Time integration loop

The time integration is a repeating process, and the loop is given in figure 4.1.

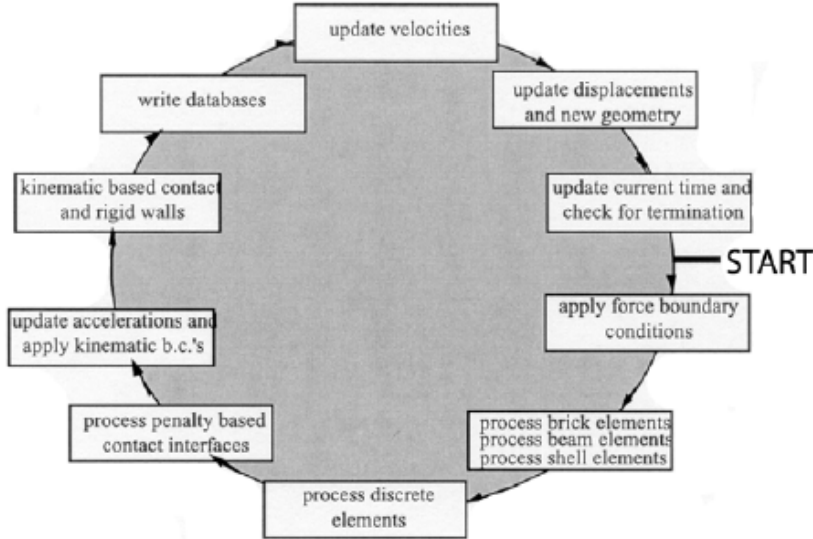


Figure 4.1: The time integration loop in LS-DYNA

### 4.2.3 Time step size

The solution of an explicit dynamic finite element analysis is only conditionally stable. To ensure stability, the time step size must be lower than the critical time step size for the model. The time step need to be smaller than the time a pressure wave is using to pass through the element. If this is not ensured, uncontrolled pressure waves can pass through the model and cause large errors in the result. Another factor considering the time step size is contact between bodies, which also requires small time steps. The time steps will, according to the requirements, be different for different types of element.

For *shell elements* the critical time step is given by eq. 4.6 and eq. 4.7.

$$\Delta t_c = \frac{L_s}{c} \quad (4.6)$$

Where  $L_s$  is the characteristic element length and  $c$  is the sound speed in the material, given by

$$c = \sqrt{\frac{E}{\rho(1 - \nu^2)}} \quad (4.7)$$

The characteristic element length can be defined in three different ways:

- $L_s$  is calculated based on the length of the element size, which is the default option.

- A length based on the diagonals of the element. This gives a larger characteristic length and smaller time steps, and is thus conservative.
- A non-conservative option where the length are chosen to obtain large time steps. This is frequently used when small triangular shell elements are needed.

For the default option the time step can be obtained by using the characteristic length given in eq. 4.8

$$L_s = \frac{(1 - \beta)A_s}{\max(L_1, L_2, L_3, (1 - \beta)L_4)} \quad (4.8)$$

where  $\beta = 0$  for quadrilateral elements and  $\beta = 1$  for triangular shell elements,  $A_s$  is the area and  $L_i$  is the length of the element sides.

For Belytschko *beam elements*, two different equations defining the time step size are needed, where the minimum value is used in the analysis. For beams representing the ship's hull girder, the bending related time step is often ten times smaller than the one related to longitudinal sound of speed due to the large dimensions involved. The time step related to longitudinal sound of speed is given in eq. 4.9 while the bending related step size is given in eq. 4.10.

$$\Delta t_e = \frac{L}{c} \quad (4.9)$$

$$\Delta t_e = \frac{0.5L}{c\sqrt{3I[\frac{3}{12I+AL^2} + \frac{1}{AL^2}]}} \quad (4.10)$$

where  $c = \frac{E}{\rho}$ ,  $L$  is the element length,  $I$  is the maximum value of the moment of inertia and  $A$  is the maximum value of the area of the cross section.

To reduce computational costs without decreasing the stability and accuracy of the model significantly, LS-DYNA uses a process called *subcycling* or *mixed time integration*. The elements are sorted into different groups where the time step is an even multiple of the critical step size. In this way, the smallest time step during the analysis only need to be applied to the smallest elements. The elements in the different groups are assumed to behave linearly between the smaller time steps.

## 5 ALE-modelling in LS-DYNA

A review of guidelines for ALE modelling in LS-DYNA, [10], is presented in the following sections. The software LS-DYNA is further described in section 4.2.

When fluid behaviour is modelled in LS-DYNA, a Lagrangian approach is often not suitable due to very large deformations of the material and mesh. In a Lagrangian approach, the deformation of the mesh exactly follows the deformation of the material, and this method is therefore not well suited for such problems. When the elements get very large deformations, the time step will be small which contributes to errors in the results.

In an Eulerian approach, the mesh is fixed in space, and the fluid material is allowed to freely move within the elements. In such approach, each element will contain a mixture of fluid and void at a given point in time, and this content will vary throughout the simulation. The fluid is allowed to flow from one element into an adjacent element, and to simulate the change of materials in each element the term “multi-material” is used. This term is further described in section 5.2.

Another possible approach is the Arbitrary Lagrangian Eulerian approach. In this approach the mesh is directed to move in a prescribed manner. The Eulerian approach is a special case of the ALE method, where the prescribed mesh velocity is zero. In the ALE approach, the material and the mesh does not need to move exactly together. Material advection is still required, but the amount of transported material in each time step is in general less than in the Eulerian approach if the mesh is directed to move in the same direction as the material. An advantage of ALE is that, especially for coarser meshes, the less material that is advected per time step, the more accurate simulation. In addition, since the mesh can approximately follow along with the fluid materials, fewer elements are needed compared to the Eulerian approach, which again leads to an advantage.

When fluid-structure interaction is considered, the Eulerian or ALE parts interact with the Lagrangian parts. This requires some sort of coupling between the different parts. Three different approaches to ALE-to-Lagrangian coupling exist, and they are further described in section 5.4.

### 5.1 Limitations

The ALE solver is developed with the intent of simulating short duration problems with high pressure and velocity gradients, and is not well suited for problems driven by low pressure gradients or long duration problems lasting longer than a few seconds.

In the case of ALE, the time step size is limited by the penalty stiffness of the ALE-Lagrange coupling. Tuning of the coupling stiffness is often necessary to achieve proper fluid-structure interaction. If the coupling is too soft, leakage may be excessive, and if it is too stiff, the time step will drop and the computation time will increase.

The solver is based on conservation laws with the material behaviour uncoupled from the system of governing equations. This is the main deviation from the traditional CFD-type Navier Stoke solvers, where the material behaviour variables may be explicitly integrated into the equations. The solver does not account for boundary layer effects, e.g. drag, and

it cannot handle turbulence-dominated processes. Effects of fluid viscosity are included solely in the material model as dynamic viscosity.

## 5.2 Multi-material group

When two or more fluids, where empty space counts as one fluid, are to be modelled using the ALE approach, the recommended element formulation is the multi-material ALE formulation, given as `ELFORM = 11` in `*SECTION_SOLID` in LS-DYNA. As the ALE materials flow through the ALE mesh, the material boundaries do not coincide with the mesh lines. The material interfaces are internally reconstructed each time step based on the volume fractions of the materials within the elements. Each material which is wanted to be tracked individually must be assigned to a unique multi-material group, AMMG, defined in the `*ALE_MULTI-MATERIAL_GROUP` option in LS-DYNA. Materials not sharing the same properties cannot be included in the same AMMG. If e.g. water and air is modelled, two AMMGs must be applied. The air can be modelled as an ideal gas with non-zero density, and the material `*MAT_NULL` and an equation of state, given by `*EOS_IDEAL_GAS`, should be assigned.

The motion of the ALE mesh must also be defined. This is controlled by the `*ALE_REFERENCE_SYSTEM` option command in LS-DYNA. Without such command, the ALE mesh will remain stationary, and the problem becomes the Eulerian approach. When these commands are used, the motion of the mesh can be prescribed in either a very specific manner or it can be made to approximately follow the mass-weighted average velocity of the ALE materials. The latter option is the most common, and is introduced by setting `PRTYPE=4` in `*ALE_REFERENCE_SYSTEM_GROUP`.

Since the ALE method allows materials to flow between elements and the user has directly control over the mesh motion, element distortion is generally not a problem. Hourglass deformation, which is the case if the element distortion is large, is therefore less of an issue in an ALE formulation than in Lagrangian formulations. The hourglass forces needed to restrict hourglass deformation are much reduced or eliminated using an ALE formulation. For material modelled as ALE, hourglass formulation 1 and a much reduced hourglass coefficient, i.e.  $1E-6$  or less, is recommended to prevent application of inappropriate hourglass forces.

## 5.3 Meshing

The initial ALE mesh should be created by hexagon elements with reasonable aspect ratios. Tetrahedrons, pentahedrons and other degenerate element shapes should be avoided as they will lead to reduced accuracy or even numerical instability during the advection. Controls in the `*ALE_REFERENCE_SYSTEM` option may affect the element shapes as the analysis progresses, and if unreasonable element shapes occur, the commands may be adjusted to maintain reasonable element shapes.

An initial ALE mesh may be constructed using one of the following two approaches:

- The initial mesh of the ALE domain may be constructed to only include one material in the initial configuration. There is no mixing of materials in the cells, and there are no partly filled cells. Mesh lines follow the outer contour of each AMMG.
- A regular, orthogonal ALE mesh is constructed with no restriction that the mesh lines follow the outer contour of each AMMG. This will possibly lead to elements containing more than one AMMG, and for these mixed elements the initial volume fractions of AMMGs must be prescribed by the `*INITIAL_VOLUME_FRACTION` command.

## 5.4 Fluid-structure interaction (FSI)

In LS-DYNA, fluids are normally modelled by ALE hexahedrons and structures are modelled by Lagrangian shells or solids. In such a model, the Lagrangian mesh does usually not share nodes with the ALE mesh. The coupling between the two surfaces are described by a coupling algorithm defined by the command `*CONSTRAINED_LAGRANGE_IN_SOLID`. This coupling serves to generate forces that resist penetration of the ALE material through the Lagrangian parts. Coupling is a complex aspect of ALE modelling, and some of the parameters used in the command are presented in the following.

The slave side parameters identify the Lagrangian parts. The master side parameters identify the ALE mesh which interacts with the slave side. The master side identifies mesh and not material. These two parameters define what codes the computer will search for interaction, but they are not specifying which ALE materials flowing through the ALE domain which are to be coupled to the Lagrangian structure. A separate parameter, `MCOUP`, identifies the specific ALE materials which will interact with the slave side.

`MCOUP` defines the AMMGs which are coupled with the Lagrangian materials. In situations where more than one AMMG is modelled, but one of the AMMGs dominates the forces imparted to the Lagrangian structure, e.g. water and air, `MCOUP` is set to 1.

The parameter `NQUAD` determines the number of coupling points distributed over each Lagrangian slave segment. If `NQUAD` is set to default (=2), there will be 2 x 2 coupling points on each slave segment. Throughout the analysis, the coupling algorithm will look for penetration of any ALE material across each of the coupling points. If penetration at a coupling point is found, coupling forces are applied to counteract penetration. In situations where the Lagrangian elements is of same size or smaller than the ALE elements, `NQUAD = 2` will generally give sufficient results. If the Lagrangian mesh is coarser than the ALE mesh, `NQUAD` may need to be raised to 3 or higher.

`CTYPE` identifies the coupling algorithm employed. In most applications, penalty-based coupling is more robust than the constraint-based coupling, and the `CTYPE` parameter should normally be set to 4.

When the slave side of the coupling is set to the Lagrangian part of the interaction, it is important that the shell normals must point toward the AMMGs. All the normals can be reversed by setting the parameter `NORM` to 1, but it is important that all the normals are pointing in the same direction if this option is used.



Leakage is an undesirable condition where the coupling does not prevent unreasonable penetration of the ALE material through the Lagrangian surface. A small amount of leakage is to be expected for penalty-based coupling and can be tolerated, but in case of excessive leakage the following modifications can be applied to the coupling input:

- Increase the number of coupling points, NQUAD. Increase in NQUAD will increase the CPU-time, and the CPU-time must therefore also be considered.
- When coupling to a shell surface, assign one AMMG ID to the ALE material on one side and another AMMG ID to the ALE material on the other side of the shell surface, even if the same ALE material are present on both sides.
- Use a separate `*CONSTRAINED_LAGRANGE_IN_SOLID` command for each AMMG. This will require use of a negative MCOUP value, and a `*SET_MULTI-MATERIAL_GROUP` list command for each `*CONSTRAINED_LAGRANGE_IN_SOLID` command.

## 5.5 Modelling in practice

In practice it has been difficult to obtain knowledge about the ALE modelling in LS-DYNA. Only a couple of papers describing the problem have been found, and none of these are describing the modelling technique used. The ALE modelling process has therefore been characterized by testing of different solutions. By following small examples given in the LSTC guideline, [10], a stable pressure gradient, with initial pressure  $1.013\text{E}+05$  Pa in the air, was successfully modelled, see figure 5.1

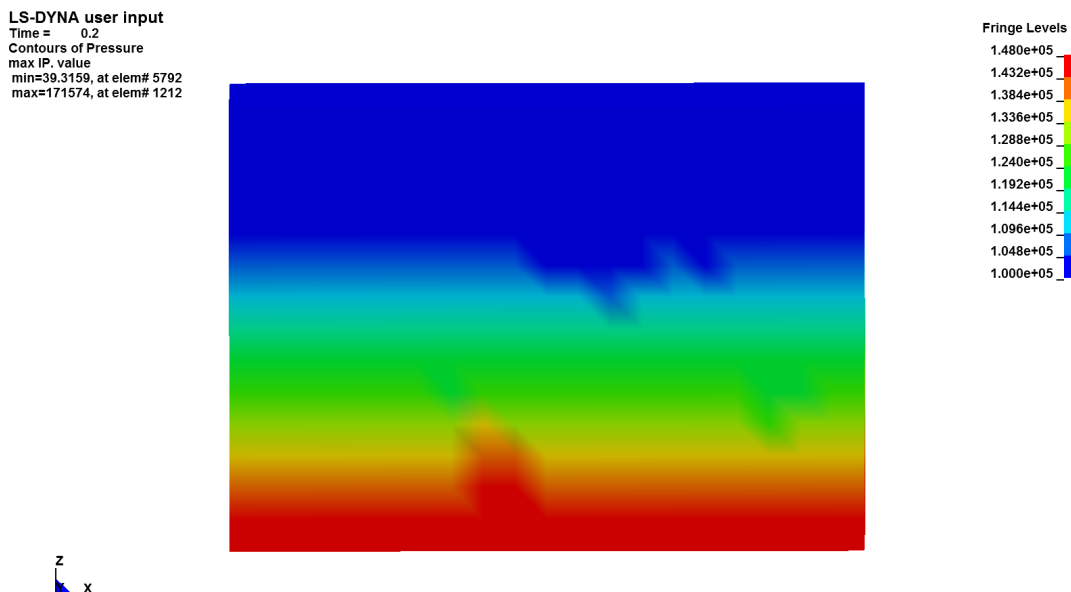


Figure 5.1: Water pressure gradient in LS-DYNA

This water "box" is modelled using the following parameters:

- **\*BOUNDARY\_SPC\_SET**: The boundaries along the X-faced edges are fixed in Y-direction. The Y-faced edges in X-direction, the corners in X- and Y-direction and the bottom in X- Y- and Z-direction.
- **\*ALE\_MULTI-MATERIAL\_GROUP**: The model includes both air and water. Two AMMG commands has therefore been used, one for each of the materials.
- **\*EOS\_LINEAR\_POLYNOMIAL**: An equation of state for each of the fluids are included. The equation of state is a relation between state variables, e.g. pressure and volume, and is useful when the relationship between different fluids are described.
- **\*HOURLASS**: The hourglass command is used to control the zero energy modes, which will appear in one-point integration in solid elements. Hourglass modes are further described in the LS-DYNA theory manual, [11].
- **\*INITIAL\_HYDROSTATIC\_ALE**: The initial pressure is stated in this command. In this command both the gravitational acceleration and the initial air pressure are defined.
- **\*CONTROL\_ALE**: In addition to the time step and termination control, a control for the ALE formulation is needed.

Based on the reviewed articles, see section 2.2, floating bodies will automatically get correct buoyancy based on the pressure gradient in the water. By inserting a small box on the water surface, it should automatically stabilize in the water, but after the analysis the box still was located on top of the water, and there had been no change in the draught of the box, see figure 5.2.

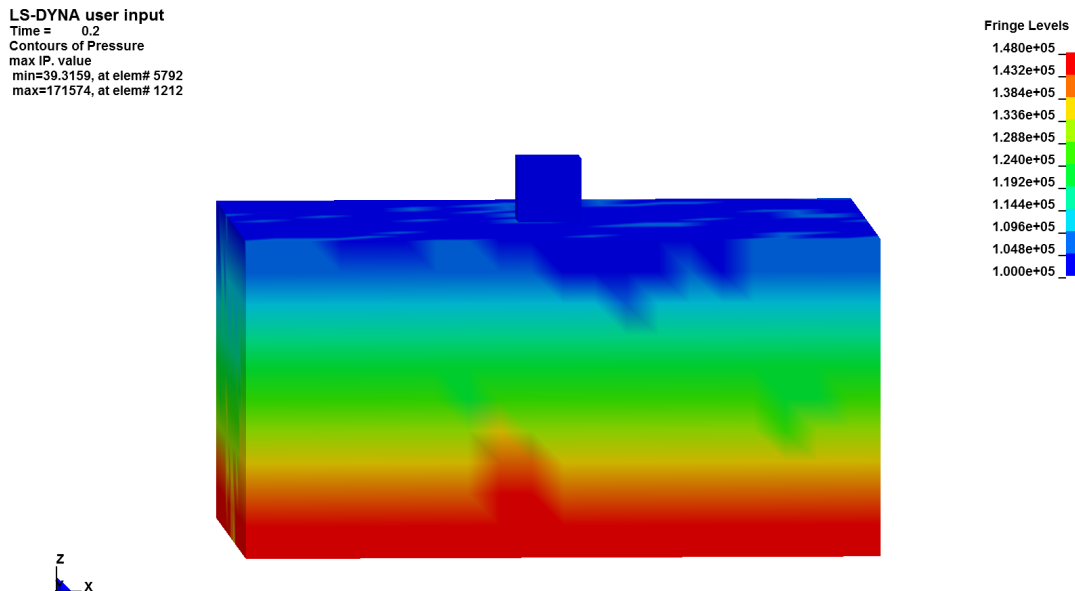


Figure 5.2: Steel box on water surface

The command **\*INITIAL\_VOLUME\_FRACTION** has not been used in this test. It was assumed that the box did not share any elements with the water, and the volume fraction

was therefore not necessary. This assumption can possibly cause the problem, but after discussing the problem with the supervisors it was concluded that the focus from this date had to be on modelling the ship and iceberg.

Before the paper with guidelines for ALE-modelling was received, a lot of test analyses on water combined with air were performed. LS-DYNA has a lot of analysis options, but to familiarise with these is time consuming, and it requires experience to understand what options that must be used for a given analysis.

The main target of the first tests was to start with a "frame" of water with an air "box" inside, see figure 5.3. The aim was to achieve results with water flow into the air, and after a couple of different attempts, the initial air box was filled with water, but the total water level was not reduced.

These tests were performed before the volume fraction command was familiarised, and this command can possibly solve this problem. It is important to define the initial air fraction if this is not done implicit when the material of the different parts are applied. It seems like the difference in density between water and air causes the water to replace the air, but the air vanishes throughout the analysis. If an initial fraction of air is defined, this problem may be avoided.

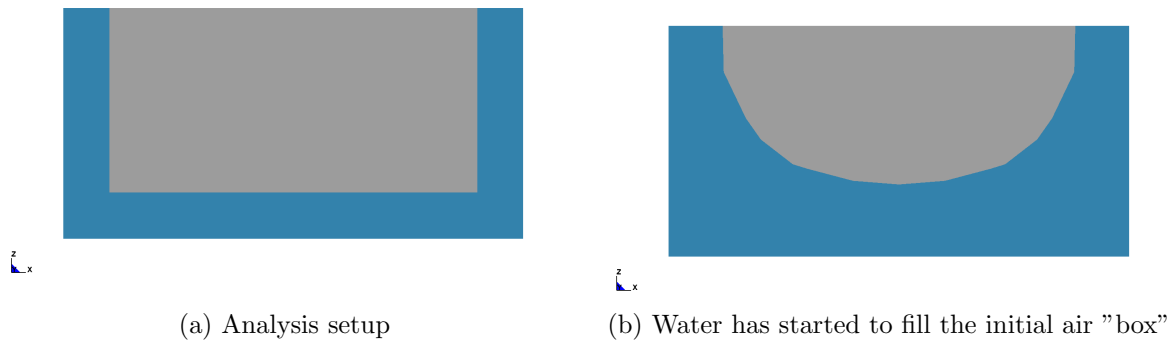


Figure 5.3: Air "box" with a water "frame"

Due to the problems with the fluid-structure interaction, the surrounding water is not included in the collision simulations between ship and iceberg presented in section 7. The issues could probably be solved if more time is spent on solution testing, but to obtain results from the collision scenarios the ALE modelling had to be postponed for further work.

## 6 FE modelling and meshing

A model of the outer shell including coarse geometry is used as basis for the modelling in this thesis. This model can, by using minor simplifications, be mirrored, and only half of the hull is modelled. Detailed geometry has only been modelled in the front tank section, since this is the most critical section for the collision scenario considered in this thesis. For the rest of the ship, the detail level is limited to coarse geometry.

To the best extent, the model is created to represent a real ship. Scantlings and drawings of a generic ice reinforced spherical LNG tanker with 170000  $m^3$  cargo capacity is provided by Ph.D. candidate Martin Storheim and Moss Maritime AS, and all details are modelled in terms of these drawings. The vessel is designed to ARC 7 ice class with additional accidental ice impact reinforcement. Some details were excluded from the detailed model of the front tank. Small brackets, manholes and detailed geometry of corners etc. are excluded since these details will have limited impact on the results.

The main dimensions of the modelled ship are given in table 6.1.

Ship dimensions	
Length over all, $L_{oa}$	300 m
Length between perpendiculars, $L_{pp}$	283.5 m
Breadth, $B$	52 m
Depth, $D$	27.5 m
Draught, $T$	11 m
Dead weight	125 000 tons

Table 6.1: Dimensions of modelled ship

### 6.1 Front tank section

The front tank section is modelled in detail in purpose of getting a result which represents the physics of the collision in a satisfying extent. A sufficiently fine model to capture the governing deformation mechanisms is important to obtain realistic results.

#### 6.1.1 Geometry modelling

Stiffeners on the outer hull is modelled by dividing the outer shell in smaller surfaces and extruding the intersection curves between the surfaces to the given stiffener web height. The web height varies from 500 mm in the ice belt to 445 mm on the keel plating. The stiffeners are modelled as T-stiffeners with flange length 150 mm. The outer shell has such stiffeners each 700 mm and larger transverse frames at approx. 4200 - 4250 mm. The frames are also stiffened by both horizontal and vertical stiffeners. The frames and stiffeners supporting the outer hull are shown in figure 6.1.

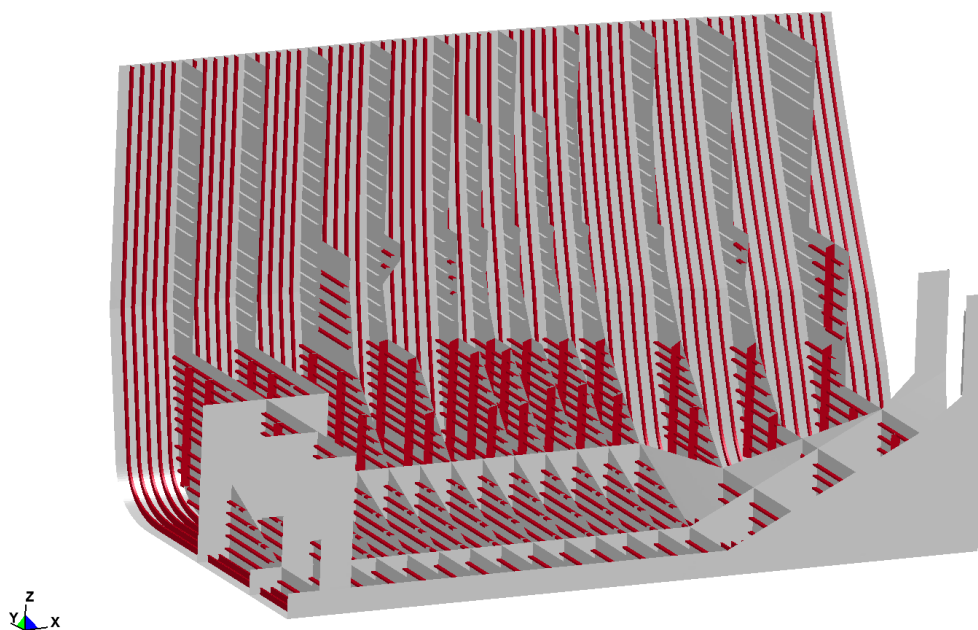


Figure 6.1: Frames and stiffeners supporting outer shell

As seen from figure 6.1, the ship is also stiffened by three longitudinal frames. These frames are for simplicity not modelled with traditional stiffeners, but "smeared stiffeners" which will cause larger modelled thickness than the on the real frames.

In the front tank area, 5 decks are modelled, including the inner bottom and top deck. All of these decks are largely supported with transverse L-stiffeners. In addition, the top deck is supported with large longitudinal flat bar stiffeners along the ship side. Parts of the deck are for simplicity supported with longitudinal stiffeners. The flat bar stiffeners on the top deck are modelled in dimension 550 x 48 mm. The deck carrying the load of the LNG tank is supported by L-stiffeners with dimensions L450 x 150/12 x 20 mm while the deck stiffeners for all other decks are modelled in dimension L300 x 120/11 x 15 mm.

The dimensions of the stiffeners in the ship are large. In general, the strength in the ship side and bottom must be large in ships with large cut-outs for cargo. In addition, the ship modelled in this thesis is ice strengthened, which also contributes to larger dimensions of plating and stiffeners.

The modelled stiffeners in the front tank area are shown without plating in figure 6.2.

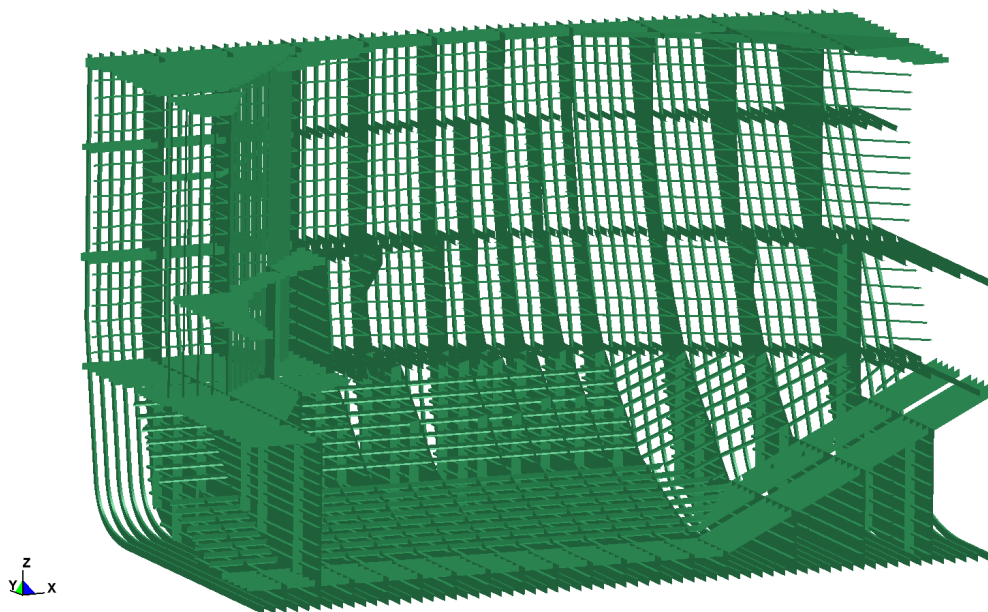


Figure 6.2: Stiffeners in front tank area

Figure 6.3 show some of the modelled details. All the details are modelled to get a simulation which represents the physics in the best possible extent. Figure 6.3a shows seven brackets supporting the main deck and the tank cover. These are modelled to distribute the weight and forces from the tank cover into the transverse frames of the ship. If these brackets had been left out from the model, large stress concentrations would have been found in the boundary along the tank cover.

Figure 6.3b shows the side ballast water tank. Unstiffened tanks are modelled for the whole structure, but in the front tank vertical stiffeners are also included to prevent non-realistic deformations.

Figure 6.3c and 6.3d shows details in the skirt. The skirt support which connects the skirt to the deck, figure 6.3c, are modelled with extra support at spots where it is connected to the frames. These "brackets" are created to avoid large stress concentrations at these spots. Figure 6.3d indicates the different materials in the skirt. The green part of the skirt is the steel part, while the red part is the aluminium part. The skirt is created in this way to prevent the steel material from being in contact with the cold temperature in the tank. If the steel material is exposed for this temperature, it may become brittle, which will contribute to fracture.

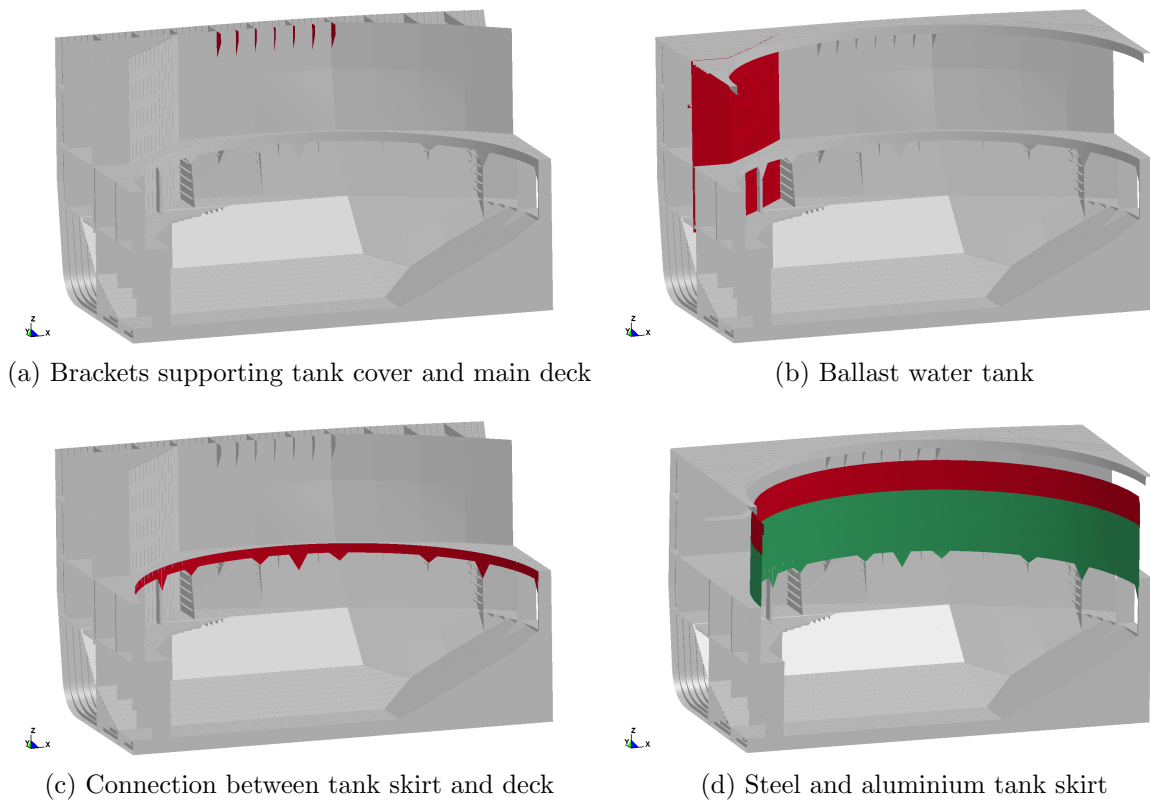


Figure 6.3: Modelled details in front tank section

### 6.1.2 Meshing

To obtain accurate results for large indentations, the model is meshed with fine mesh in all of the port front tank side. The results obtained from a collision analysis will strongly depend on the mesh used, as this forms the basis for the description of the geometry and mechanisms involved. 4-node Belytschko-Tsay shell elements with five integration points over the thickness are used as the main element type for the entire model. In regions with advanced geometry, and in some regions where coupling of elements led to small structural parts with difficult geometry, 3-node shell elements are used to avoid very small critical time step. According to [12], the use of 3-node elements should be limited due to less accuracy compared to 4-node elements. 3-node elements are therefore only used where it is required by the geometry and where the aspect ratio of the 4-node elements turns out to be too large.

The mesh size is important to consider. A convergence study of a grounding scenario has been carried out in [13], and this study can be adopted into a collision scenario. This study concludes that, in order to give a good physical approach, the element length should preferably be 5 to 10 times larger than the plate thickness. Due to the ice strengthened hull, the shell thickness varies between 15 mm and 40 mm, while the stiffeners have thickness varying between 11 mm and 48 mm. The front tank area is modelled with 150 mm 4-node shell elements, which gives 3 elements over the web height of the stiffeners. From this it follows that, for the geometry with largest thickness, the mesh is not included

in the size domain.

The element size results in a very large amount of elements, approximately 650 000 for the front tank model, which leads to large computation time. The purpose of this thesis is to obtain accurate results to verify error sources in simplified analysis methods, and the computation time is therefore of lower priority. The majority of the elements are located along the collision side of the model, and a reduction of elements in parts of less relevance for the results will not reduce the total amount of elements significantly.

To simplify the meshing, many of the stiffeners are cut to avoid coupling of elements in spots where this is not necessary. In some situations, it is very difficult to couple all surfaces and at the same time get a preferable mesh in these spots. The cutting will therefore reduce the time spent on meshing, and it will contribute to a more accurate result. An example of the cutting is shown in figure 6.4. The figure shows a transverse frame (grey) with a cut L-stiffener (green). The white L-stiffener coupled to both the bottom deck and the frames.

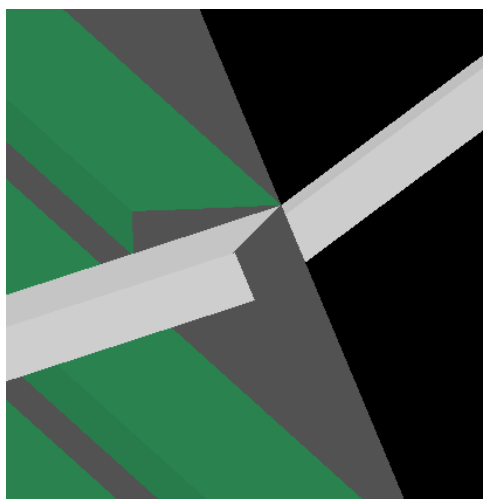


Figure 6.4: Cutting of frame stiffener

Surface coupling is required to transfer stresses and forces. MSc. Patran includes a node modification option, where nodes can be moved and connected to other nodes. This modification tool has been used a lot to connect free edges.

The stiffener webs are coupled with all connected plates, while the flanges are not coupled. In real ship structures the flanges often are placed in cut-outs in opposing plates, and uncoupled flanges makes therefore a good representation of the physics.

Ideally, 4-node elements should be perfectly shaped quad-elements with aspect ratio equal to one. In regular shaped areas this is achieved, but in areas with advanced geometry the elements will be distorted. To obtain an accurate result, it is important to minimize the use of distorted elements. The plates from the original geometry modelling have been divided into several smaller pieces to simplify the meshing and in a comprehensive extent get undistorted elements.



### 6.1.3 Time step considerations

The model of the front tank area has a critical time step of 3.41E-06 s. To avoid contact instabilities in LS-DYNA, time step sizes larger than 5E-05 s. is not recommended. At the same time, too small time steps will cause high computational time, and is therefore not desirable. Small time steps occur in e.g. elements with large aspect ratio. Large aspect ratios are a problem in corners and other spots where undistorted elements are necessary for a good representation of the geometry. It is important to address these spots and improve the meshing here to get results of adequate accuracy after a reasonable use of computation time.

### 6.1.4 Materials

Two different materials are used for the front tank section.

#### Steel material in ship structure

For the steel parts of the ship a user defined material model is used. The material model is developed by Alsos, [13], and includes an element size dependent fracture criterion. The basis of the model is a modified power law hardening material, and the fracture criterion is applied to the maximum allowed plastic strain in an element. Small elements are needed to get accurate representations of fracture. On the other hand, small elements are critical with respect to the time step, and are therefore unfavourable in an explicit analysis.

According to Alsos and Storheim, [9], the mesh size is a concern in structural analyses. Fine mesh is required to capture strain concentrations and fracture, and is therefore necessary for getting a satisfying result of the analysis. On the other hand, a fine mesh requires large computer resources and long computation time. A coarse mesh will not capture the strain concentrations typically seen in ship structures. Shell elements are in addition sensitive to mesh scale effects, and a coarser mesh is therefore generally not compatible with a complex damage model required to predict fracture.

Failure mechanisms such as local necking typically take place in narrow bands where the width is in order of the sheet thickness itself. A mesh size which is 5-10 times larger than the shell thickness will not capture these instabilities, and a proposed way to deal with the mesh sensitivity is to apply an element size scaling law. The material model includes such element scaling law, which implicitly accounts for local instability effects within large elements by calculating the volume averaged fracture strain from an assumed strain distribution. It is not guaranteed that the strains are located prior to fracture, and the scaling law should be applied with caution. In ship structures the criterion is in general acceptable to use. By assuming the localized mechanisms to appear parallel to the element side, the average equivalent strain at fracture for various element sizes can be given as eq. 6.1.

The width of the virtual neck is assumed to be as wide as the element thickness which gives a neck volume of  $V_n = t^2 l_e$  where  $l_e$  is the element length and  $t$  the element thickness. This gives the volume of the remainder of the element as  $V_r = V_{el} - V_n = t l_e^2 - t^2 l_e$ . Inserting this into eq. 6.1 gives the equation used as basis for the plastic strain rupture criterion, eq. 6.2.

$$\epsilon_{cr} = \frac{\epsilon_r V_r + \epsilon_n V_n}{V_{el}} \quad (6.1)$$

$$\epsilon_{cr} = n + (\epsilon_n - n) \frac{t}{l_e} \quad (6.2)$$

Here,  $V_{el}$  is the total element volume,  $V_n$  is the volume of a virtual neck,  $V_r$  is the volume outside the instability,  $\epsilon_n$  is the strain of the virtual neck and  $\epsilon_r$  the strain outside the instability. The scaling law is illustrated in figure 6.5.

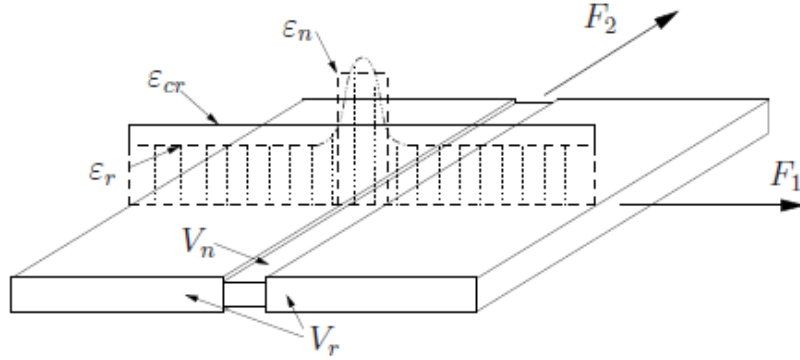


Figure 6.5: Critical strain for an element exposed to necking

The nominal stress-strain relationship is represented by a modified power law formulation which includes the plateau strain, given in eq. 6.3;

$$\sigma_{eq} = \begin{cases} \sigma_y & \text{if } \epsilon_{eq} \leq \epsilon_{plat} \\ K(\epsilon_{eq} + \epsilon_0)^n & \text{otherwise} \end{cases} \quad (6.3)$$

where  $\epsilon_{plat}$  is the equivalent plastic strain at the plateau exit and  $\sigma_y$  is the initial yield stress. The strain  $\epsilon_0$  describes an expression which allows the plateau and power law expression to intersect at  $(\epsilon_{plat}, \sigma_y)$ , and is given as eq. 6.4.

$$\epsilon_0 = \left( \frac{\sigma_y}{K} \right)^{\frac{1}{n}} - \epsilon_{plat} \quad (6.4)$$

The input parameters used in the material model are given in table 6.2.

Parameter	Value
Density, $\rho$	7850 $kg/m^3$
$\sigma_y$	285 MPa
Young's modulus, $E$	210 GPa
$G$	80.77 GPa
$B$	175 GPa
$K$	740 MPa
$n$	0.24
Poisson's ratio, $\nu$	0.3
$\epsilon_{plat}$	0
$\epsilon_n$	0.7

Table 6.2: Steel material properties

### Aluminium in cargo tanks and tank skirts

The aluminium material used in the cargo tanks and the skirts supporting the tanks are based on 5083-0 aluminium. The chosen elastic modulus and Poisson ratio is based on analyses of temperature dependent material behaviour provided by Moss Maritime, [14]. The collision scenario is assumed to occur in loaded condition, and the aluminium material will therefore have the same temperature as the LNG cargo, i.e. approximately  $-162\text{ }^\circ\text{C}$ .

The power law parameters are calculated based on equation 6.5.

$$\sigma = K\epsilon^n \tag{6.5}$$

Based on  $\sigma_{ULT} = 275\text{ MPa}$  and  $\sigma_y = 125\text{ MPa}$ , the parameters,  $K$  and  $n$ , have been calculated by solving eq. 6.5. The two stresses are found according to Mazzolani, [15], and Eurocode 9, [16]. The different parameters for the aluminum material are given in table 6.3

Parameter	Value
$\sigma_y$	125 MPa
$\sigma_{ULT}$	275 MPa
$K$	424.56 MPa
$n$	0.1968
Young's modulus, $E$	79.25 GPa
Poisson's ratio, $\nu$	0.35
Density, $\rho$	2650 $kg/m^3$

Table 6.3: Aluminium material properties

### 6.1.5 Properties

The ship model is divided into a lot of different groups, based on properties. The different properties are based on structural drawings of similar ships. Figure 6.6 shows the different

thicknesses in the outer hull. As seen from the figure, the upper part of the outer hull is modelled with very large thickness. This is, as mentioned in section 6.1.1, done to compensate for the reduced strength in the structure due to the cut-outs for cargo.

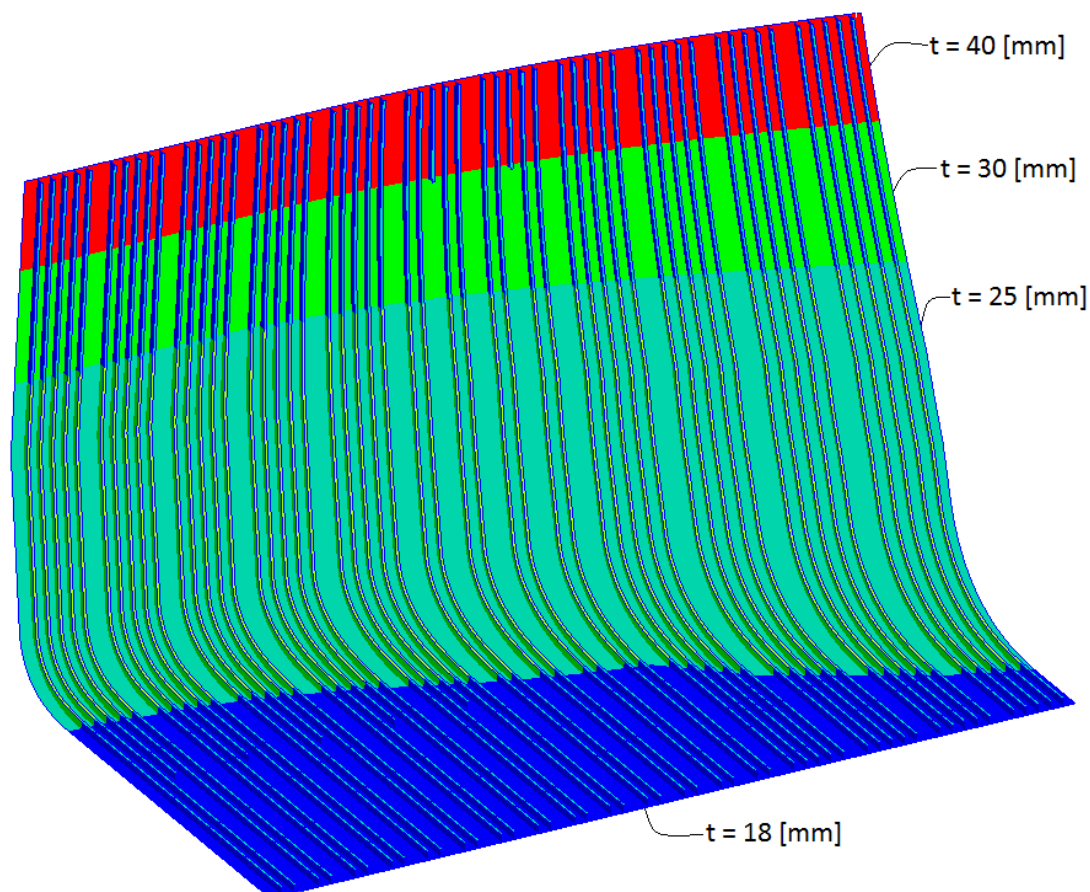


Figure 6.6: Thickness on outer shell

Members of the structure which carry large weight or are exposed to large loads are in general modelled with larger thickness. E.g. the main deck is modelled with larger thickness in both deck plating and stiffeners near the ship sides.

In parts which are not exposed for large loads, the dimensions of plating and stiffeners are smaller. This will give a realistic approach to the strength in the real ship.

A good definition of groups from the modelling part of the thesis simplifies the post processing, since LS-DYNA sorts the model part based on the properties.

## 6.2 Global model

The global model is included in purpose of getting correct boundary conditions into the simulations. It is important to get the total mass and the centre of gravity approximately correct to give a reasonable physical approach to the simulation. The detailed front tank

section is integrated in the global model to obtain accurate results from the collision, which still is assumed to collide in the front tank area.

### 6.2.1 Geometry modelling

As mentioned, only coarse geometry is modelled in the global model. The coarse geometry includes transverse frames, longitudinal frames, decks, ballast water tanks, all cargo tank details, wheelhouse and outer shell geometry. The modelled frames and decks contribute to satisfying stiffness of the hull. Figure 6.7 shows a vertical cut at the centre line of the ship. In this figure the tanks are left out, and the frames and stiffeners can be seen as dark grey parts.

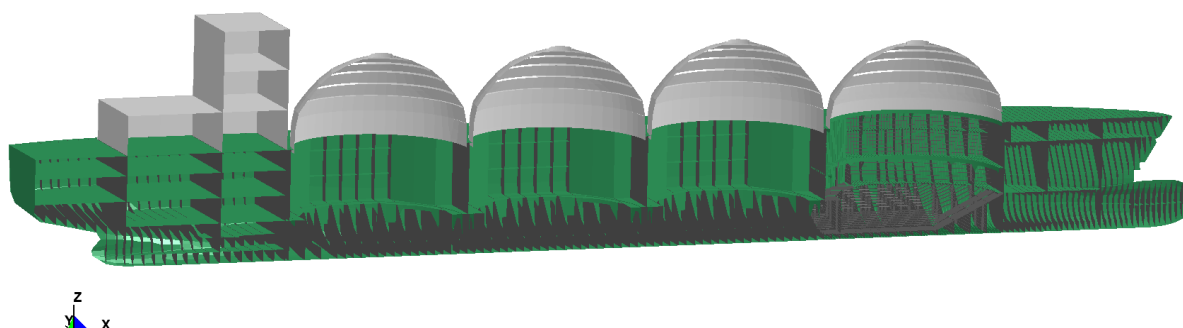


Figure 6.7: Vertical cut of global model at centre line, tanks are not showed

The detailed stiffener layout is not modelled, which is based on the assumption that this will not contribute to the results of the collision analyses. The deformations are expected to be limited to the front tank area, and the global model is included to get correct boundary conditions and external mechanics.

### 6.2.2 Meshing

The global model is meshed with element side lengths of 2 - 2.5 m. This is sufficient, since this part is not in contact with the iceberg, and is not capturing any deformation. The front tank section is included in the global model, and all shared surfaces between the global model and the front tank have been re-meshed. It is important to couple all large surfaces to ensure a physical relevance regarding force and stress transferring, and the transitions must be checked to avoid free edges.

The total model includes approximately 750 000 elements, which is a very large amount of elements. The largest amount of these elements is located in the front tank area, and the model will therefore yield accurate results. The drawback with this is the large computation time such amount of elements will provide.

### 6.2.3 Time step considerations

The global model has a critical time step of 2.41E-06 s, which indicates that some of the elements in the transitions are more distorted than in the front tank model. This value does not cause trouble for the analyses, and the simulation can be performed.

### 6.2.4 Materials

In the global model, six different materials are used in the analyses. The materials are based on the steel material and aluminium material described in section 6.1.4, but the density is modified to include the LNG cargo, the added mass of the ship and to get correct total mass of the vessel.

The different materials and modifications are described in the following.

#### Steel for general use in ship

This material is the same as used for the front tank area, described in section 6.1.4, with no applied modifications.

#### Steel for use on outer shell below water line

To include the added mass, the steel material used in the outer shell below the water line has increased density. The steel material is the same as used for the front tank, but the density is modified based on volume calculations of the steel volume below the water line. The added mass are calculated to be approximately 125 000 tons, and this must be included in the density of the relevant steel material. The new density, including the added mass, is calculated to 345900  $kg/m^3$ .

#### Steel for use on main deck

Due to the details which are not modelled; engine weight, equipment weight, detailed stiffener layout, etc., the mass of the model is lower than the real value. To compensate for this, the density of the main deck is increased. This is done by the same method as for the outer shell below the water line, and the result is a new density of 100799  $kg/m^3$ .

#### Steel for use in wheelhouse

The wheelhouse geometry is made of large plates without stiffeners. To avoid deformation of the elements in this part, which do not contribute to the result of the collision analyses, a rigid steel material model is applied. Only basic material parameters is therefore necessary for modelling this part, and these parameters are the same as for the material model used in the general global model.

#### Aluminium for general use

The aluminium used in the tank skirts and tank towers has the same properties as described for the front tank area.

#### Aluminium for use in tank shell

The four tank shells are modelled in the previous described aluminium material model, but the weight of the LNG cargo is included in the density. The calculation of the new

density is based on the total mass of the cargo and the material volume of the cargo tanks. This new density is then set to  $74084 \text{ kg/m}^3$ .

Figure 6.8 shows a vertical cut at the center line, where the materials which differs from the original material models are numbered. The modified materials are also described in table 6.4.

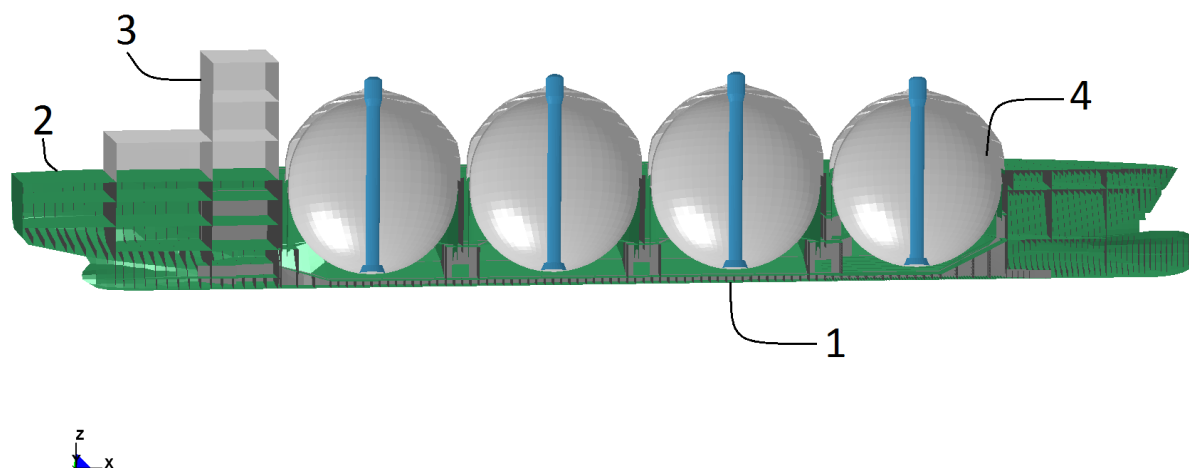


Figure 6.8: Vertical cut of global model at centre line

Number	Material	Density [ $\text{kg/m}^3$ ]
1	Steel below water line	345 900
2	Main deck	100 799
3	Wheelhouse	7850
4	Aluminium tank shell	74084

Table 6.4: Modified material properties

### 6.2.5 Properties

In the same way as for the simplified model, the parts in the global model are divided into a lot of different groups based on the properties. The outer hull is modelled in the same way as for the simplified model, and all the different property groups are included in the global model.

## 6.3 Iceberg

The modelling of the iceberg was complicated due to the ice material model used in this thesis. This model requires a very dense mesh, which will give a very large amount of elements when a reasonable large iceberg is modelled. The ice strengthened ship structure is built to sail in arctic areas, and a large iceberg is necessary to cause serious damage on the hull. A large iceberg with very fine mesh will cause long computation time, and

is not practical for analyses. It is therefore important to mesh the iceberg with various mesh size, sufficiently fine in the collision area and coarse in the other areas.

Three different icebergs are modelled. One iceberg is used for the initial velocity analyses, another for the prescribed displacement analyses, and the last one is a large iceberg modelled to cause serious damage on the hull. A collision with such an iceberg is possible, but the analyses require long computation time and have therefore not been the main focus in this thesis. The different analyses are further described in section 6.4.3 and 6.4.4.

### 6.3.1 Geometry modelling

The geometry of the iceberg is difficult to model in a way which gives a good physical representation. Spherical icebergs have been used in previous master thesis', e.g. [2] and [17], but such shape is not realistic. The thesis description describes that a very simple iceberg shape are to be modelled, but to get realistic results of the analyses, a more irregular shape must be used as colliding body.

After discussing different options with Ph.D. Candidate Martin Storheim, a box iceberg with irregular cut corners and edges were chosen, see figure 6.9. The iceberg used in most of the analyses has side lengths of 15 m, while the large iceberg has side lengths of 30 m.

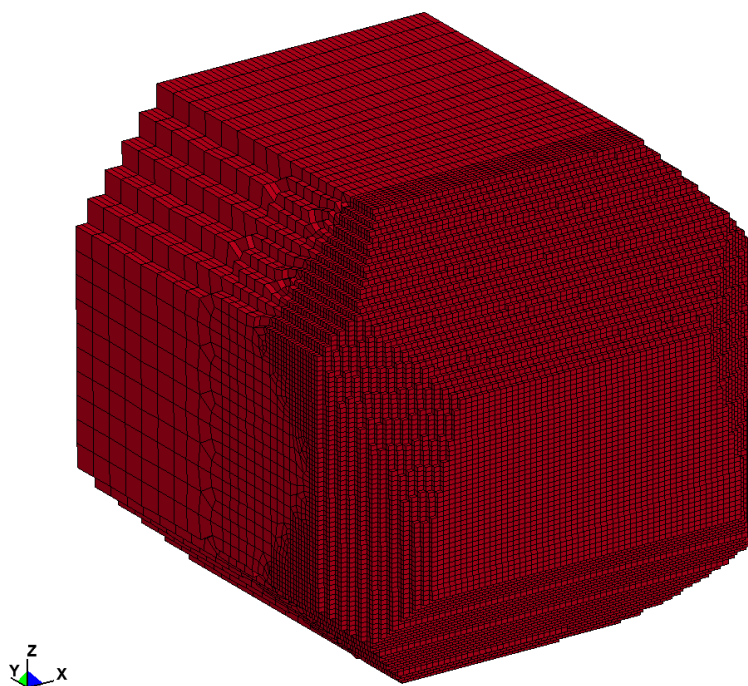


Figure 6.9: Modelled iceberg

### 6.3.2 Meshing

The meshing of the iceberg was challenging. The ice material model requires very fine mesh, and elements with side lengths of 150 mm are used in the collision zone. Even this



element size is large according to the material model, but it is chosen to keep the amount of elements on a reasonable level. 150 mm hexahedral elements for the whole iceberg will give a very large amount of elements, and the model must be coarser meshed in the areas not affected by the collision. This is done by a tool in MSc. Patran where a surface with the wanted iceberg dimensions are created and meshed. This mesh is then extruded into a cube. In this way the mesh can easily be made coarser in areas where fine mesh is not required. Still, the total number of elements in the 15 m iceberg are approximately 200 000. The side of the iceberg showing the mesh variation is shown in figure 6.10.

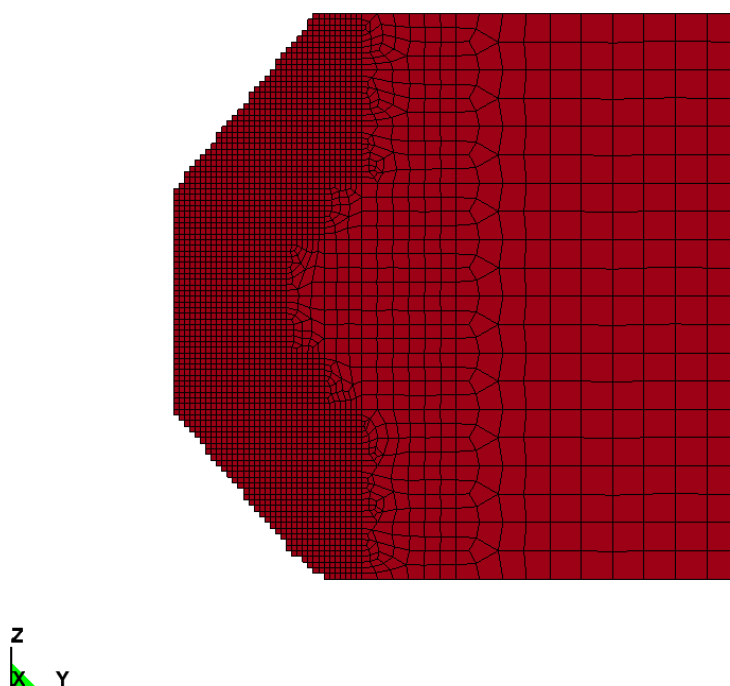


Figure 6.10: Side view of iceberg

The two other modelled icebergs are meshed in the same way. For the large iceberg with side lengths of 30 m, the large amount of elements, a total number of approximately 1 000 000, causes very high requirements for the computer performance. Due to this, only two different analyses with this iceberg have been carried out.

For the analyses including the prescribed displacement option, the iceberg is cut to save computation time. In these analyses, the mass of the colliding bodies is of no relevance since the front tank structure is pinned and the iceberg is given a prescribed displacement, and some elements can therefore be deleted. The mesh in the collision zone is not changed, and only the rear side of the iceberg is cut, see figure 6.11.

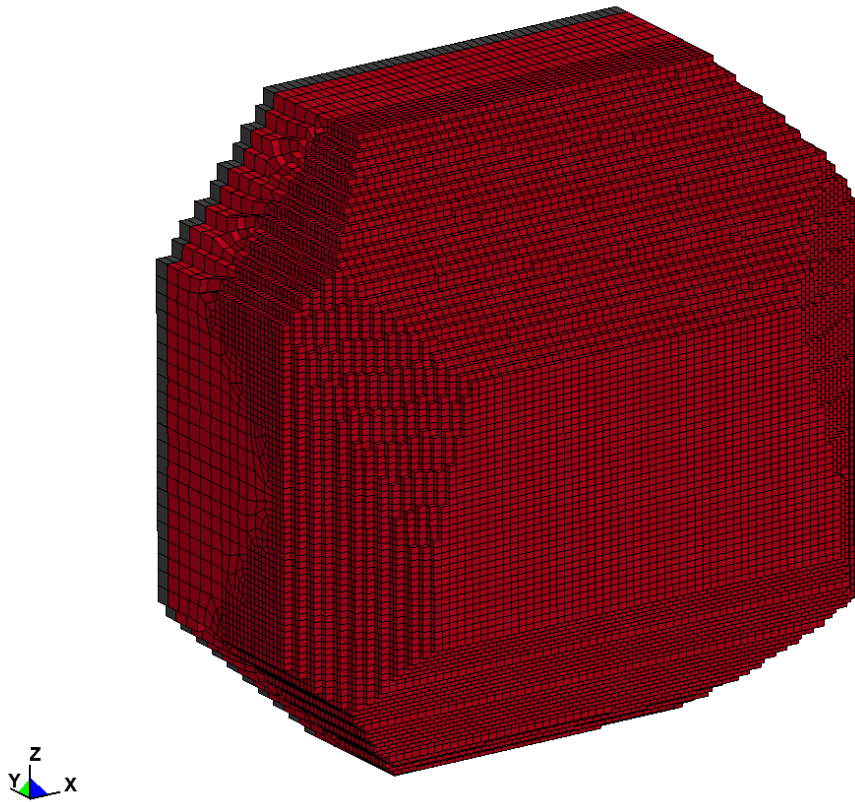


Figure 6.11: Cut iceberg for prescribed displacement analyses

### 6.3.3 Materials

#### General ice material

The ice material model used in this thesis is developed by Zhenhui Liu, [1]. An elliptical yield surface is adopted to describe the iceberg behaviour, and the yield surface is described as the *Tsai-Wu* yield surface, see eq. 6.6. The temperature profile of the iceberg has been studied by Liu. It is found that for the submerged part of the iceberg ablation during the late winter, spring and summer seasons gives rise to a steep gradient that reaches the core temperature approximately 3 m into the ice. Corresponding to this gradient a change in the strength can be included in the Tsai-Wu yield surface.

$$f(p, J_2) = J_2 - (a_0(T) + a_1(T)p + a_2(T)p^2) = 0 \quad (6.6)$$

where T is the temperature.

Liu has also proposed an empirical failure criterion based on effective plastic strain and hydrostatic pressure. The equivalent plastic strain is given in eq. 6.7.

$$\epsilon_{eq}^p = \sqrt{\frac{2}{3} \epsilon_{ij}^p : \epsilon_{ij}^p} \quad (6.7)$$

and the failure strain is given by eq. 6.8:

$$\epsilon_f = \epsilon_0 + \left( \frac{p}{p_2} - 0.5 \right)^2 \quad (6.8)$$

where  $\epsilon_{ij}^p$  is the plastic strain tensor and  $\epsilon_0$  is the initial failure strain which should be adjusted according to experimental data.  $p_2$  is the larger root of the yield function. If  $\epsilon_{ij}^p > \epsilon_f$  or the pressure is not larger than the cut-off pressure,  $p_{cut}$ , erosion is activated.

The properties of the ice material are given in table 6.5.

Parameter	Value
$a_0$	22.93 MPa <sup>2</sup>
$a_1$	2.06 MPa
$a_2$	-0.023
Initial failure strain, $\epsilon_0$	1 %
Young's modulus, $E$	9.5 MPa
Poissons's ratio, $\nu$	0.3
Density, $\rho$	900 kg/m <sup>3</sup>

Table 6.5: Ice material properties

### Rigid ice material

For the analyses where the iceberg is given a prescribed displacement, a rigid ice material is defined at the rear side of the iceberg. This part is given the displacement, and will not contribute to the results, and will have no crushing. Only basic ice material parameters are included in this material model.

## 6.4 Settings for analyses

A lot of studies on ship collisions have been carried out, and a lot of simplifications are used to decrease the computation time of the calculations. The most common way to analyse collision scenarios is to give one of the colliding bodies a prescribed displacement and calculate the damage at a given dissipated energy level. This does not represent a real collision scenario, and it is interesting to compare the results obtained from such analysis with results from a more realistic situation. A more realistic situation demands more computer resources and longer computation time, but such analyses are important for getting better knowledge of the error sources of the simplified approach. If the error in the simplified method is small, it can be justified to carry on with such simplifications, but if the comparison study shows that there are large errors, use of the simplified method should be limited to analyses where an overview of the energy dissipation is the aim.

When a more realistic collision scenario between a ship and an iceberg is simulated, one, or both, of the colliding bodies are given an initial velocity towards the other body. Throughout the analysis, the energy will dissipate between the colliding bodies, and they will behave in the same way as in a real collision.

The impact angle is important, and collisions with two different impact angles are investigated. The first impact angle is calculated based on the impact scenario described in [7]. Here, the radial velocity of a turning ship is given as 10 % of the forward speed. In addition to this scenario, it is interesting to investigate how an increased impact angle will impact the results. Increased impact angle can occur if the iceberg is drifting towards a turning ship, which is a realistic situation for iceberg sizes which not appear on the radar.

Two different sets of analyses are carried out. A simplified approach only including the front tank area and the iceberg are first analysed for both initial velocity and prescribed displacement. In these analyses, simplifications regarding the boundary conditions are used. To verify these boundary conditions, a full analysis of the global model for both impact angles is carried out. Throughout these analyses, an overview of the deviations between the methods is established.

Specific settings for each analysis are described in detail in section 7.

#### 6.4.1 Boundary conditions

##### Front tank in a simplified analysis

It is difficult to apply correct boundary conditions for the front tank structure when the global ship model is not included. As previously described, the iceberg is given the motion and is considered as the colliding body. This is due to the boundary conditions of the problem, i.e. pinned boundary conditions for the front tank section. In a real situation, the ship will collide into the iceberg, and the iceberg will slide away. For a small iceberg, as investigated in this analysis, the ship will be the dominating structure, and global effects will probably not be significant.

Several options for boundary conditions exist, e.g. inertia controlled boundary conditions and pinned boundary conditions. In the inertia controlled conditions, the mass of the whole ship is included as a distributed mass along the boundaries and the inertia forces will resist the impact. For the pinned conditions, no pushing of the side is allowed. According to Martin Storheim, [9], the two different options are practically identical when maximum indentation is compared. For, at least, small expected deformations, pinned boundary conditions yields satisfying results, and are therefore chosen in this thesis.

Another concern when deciding boundary conditions for the front tank area in these analyses is the LNG cargo tank. If no boundary conditions are applied to this member, it will collapse of its own weight. A pinned boundary condition will avoid this collapse.

##### Global model

A full analysis of the global model is significantly more time consuming than a simplified analysis, both with respect to modelling time and computational time, but the issues regarding modelling correct inertia effects and boundary conditions are avoided. The forces in the front tank area will now be transferred and dissipated into the global model, and the connection between the front tank area and the rest of the model does not need to be considered.

In a global analysis the external mechanics are represented in a satisfying way. The collision energy will be captured in the colliding bodies, and they behave as in a real collision.

### Iceberg

For the simplified analyses where only the front tank is included, the velocity and displacement is given to the iceberg. No other boundary conditions are applied to this body.

In the collision simulations between global ship and iceberg, no boundary conditions are applied to the iceberg. The iceberg is therefore free in both translational and rotational degrees of freedom throughout the simulation.

#### 6.4.2 Contact

Three different types of contact have been defined; one specifying the internal contact between the different members of the ship, one specifying the internal contact in the iceberg, and one specifying the contact between the iceberg and the ship.

**\*CONTACT\_AUTOMATIC\_SINGLE\_SURFACE** The contact within the ship is an automatically updating single surface penalty algorithm. Both static and dynamic friction coefficients are defined as 0.3, as given in [18].

**\*CONTACT\_ERODING\_SINGLE\_SURFACE** The internal contact in the iceberg is described by a master-slave contact where only the slave side is included, [19]. In this contact the friction coefficient is set to 0.15.

**\*CONTACT\_ERODING\_SURFACE\_TO\_SURFACE** The last contact defined is the contact between the iceberg and the ship. The friction is set to 0.15, and the contact allows the ice elements to be deleted when crushing is simulated. In this contact, the command which creates the nodal contact force output must be included. This is done by setting the MPR option to 1, which will write an output file including the nodal contact force data for the steel (master) part of the contact.

#### 6.4.3 Initial velocity

For the analyses of the collision between the front tank and the iceberg, the initial velocity is given to the iceberg at two different impact angles. This simplifies the problem, but is not simulating the real situation. The simplification is applied due to the pinned boundary conditions of the tank section. To further simplify the collision setup, the ship is rotated by the impact angle, and the iceberg is given an x-directed velocity. In LS-PrePost, this setup is easier than giving the iceberg a velocity with both x- and y-components.

When the global ship model is analysed, the initial velocity is given to the ship, and *not* the iceberg. This situation gives the best representation of the physics, and is therefore preferred. The initial velocities and impact angles are the same as for the analysis of the front tank area.

For all the analyses, it is assumed that the turning is initialized, but the loss in velocity due to the turning has not started. This is an assumption which possibly will cause a small error in the result, but this error will in any case be conservative.

#### 6.4.4 Prescribed displacement

The most common analysis method for collision scenarios is to give the striking body a prescribed displacement or motion. This method requires less computer performance for the calculations, and is therefore an efficient simplification for reducing computational time.

The iceberg is in this scenario given a prescribed displacement into the ship side. The displacement is based on a curve which defines the displacement distance at a given time. This curve is adjusted to be equivalent to the initial velocity setup described in section 6.4.3.

The deformation calculation in such analysis is based on an energy consideration. In this thesis, the energy levels obtained from the prescribed displacement analysis are compared to the energy levels obtained from the initial velocity analysis, and the deformations at equal energy levels for the two analyses can be compared. This is a possible method of investigating the conservatism obtained from a prescribed displacement analysis.

#### 6.4.5 Mass and centre of gravity

The mass of the different bodies is calculated by use of the FEM modelling software MSC. Patran. A built-in tool calculates the mass of the elements based on the input properties of each element. For the front tank analysis, the mass of the ship is not relevant due to the pinned boundary conditions.

The global model is modelled with coarse geometry, and the detailed stiffener layout is not modelled. This means that the mass of the model will be lower than the real mass before modifications of the model are applied.

The centre of gravity is calculated based on the applied properties. A spreadsheet including volume, weight and centre of gravity for each part has been established, see appendix D, and the total centre of gravity has been calculated. Based on information from stability calculations of the modelled ship, the real centre of gravity is given in table 6.6. Details in the global model are not modelled, and the centre of gravity is therefore not correct before any modifications are applied. The total ship weight, including cargo, is given as 125 000 tons, and the modelled ship weight are approximately 107 600 tons before modifications.

The added mass are added to the outer hull below the water line, which is described in detail in section 6.4.6, and the centre of gravity will therefore be moved against the keel. 17 400 tons needs to be added to the total mass of the ship. Since the added mass will bring the centre of gravity towards the keel, extra mass can be added to the main deck to contribute to a higher centre of gravity. The density of the main deck has therefore been increased to a level which give 17 400 tons extra mass to the model.

Stability parameters					
	$CG_x$ [m]	$CG_y$ [m]	$CG_z$ [m]	Mass [ton]	M + A [ton]
Real value	132.20	0	21.80	125 000	250 000
Original model	141.44	0.12	22.58	103 967	207 934
Modified model	136.52	0.07	13.47	125 000	250 000

Table 6.6: Stability parameters for modelled ship

The mass of the iceberg in the analyses where initial velocity is applied is calculated in the same way as for the ship. For the analyses where the iceberg is given prescribed displacement, the mass of the iceberg is not relevant.

#### 6.4.6 Added mass

Added mass will contribute to higher energy levels in the analyses, and must be included to give a realistic representation of the physics. The added mass coefficients are included only to get a realistic energy level of the moving structures, and are therefore included as an additional density of the structure. The external mechanics will be correct by using this assumption. The assumption will cause an error in the internal mechanics, but this is of lower priority.

For the front tank section the added mass will not contribute to the results due to the pinned boundaries.

The added mass of the ship is an addition which contributes below the water line, and it is therefore added to the outer shell below waterline in the simulation. The coefficient is based on discussions with Ph.D. Candidate Martin Storheim and is set equal to 1 for sway translation, based on an assumption that the added mass for the ship structure is approximately equal to the total mass of the ship. This leads to a centre of gravity which is lower than for the ship structure, but after a discussion with Professor Jørgen Amdahl it was concluded that this was reasonable.

For the iceberg, the added mass is added to the whole body, although it only will contribute to the part below the water line. This is done for simplicity, and will possibly cause a conservative error in the results. Due to its irregular geometry, a reasonable value for the iceberg was more complicated to find. After discussing with Professor Jørgen Amdahl and by use of a figure describing coefficients for hexagons and rectangles by Korotkin, [20], the coefficient was set to 0.8 for translational degrees of freedom.

#### 6.4.7 Radius of gyration

The radius of gyration indicates how the cross sectional area is distributed around the centroidal axis of the ship. This means that it indicates inertia in a collision. For a ship, the radius of gyration in x- and y-direction normally is between 1/4 and 1/3 of the total ship length. The gyration radius for the model is presented in table 6.7 together with values calculated by generic formulas given by Liu, [1].

Values for gyration radius			
	$RG_x$ [m]	$RG_y$ [m]	$RG_z$ [m]
Model	73.4	72.9	20.7
Generic formulas	69.11	75	16.02

Table 6.7: Gyration radius for model

As seen from the table, small deviations between the values are found. 1/4 of the length over all is 75 m, and it is seen that the values x- and y- gyration radius are close to this value. No accurate calculations for the gyration radius of the ship are given.

One of the error sources in the calculation of the gyration radius in MSc. Patran is the considerations of the added mass and the cargo weight used in this thesis. In a real situation, the gas cargo will flow inside the tanks, and the weight does not have to be moved in the same manner as the ship structure. The same considerations are done for the added mass. In the model, this "extra mass" needs to be moved in the same manner as the ship structure, which is not a realistic physical approach.

Based on these observations it can be concluded that the gyration radius probably seems to be close to the real value. The error can nevertheless be neglected by adjusting the collision point either ahead or astern.



## 7 Analysis setup

When comparing the two different methods described in section 6.4, the setup for the different analyses must be as equal as possible. The different parameters for each analysis are given in table 7.1, and will be further discussed in the following sections.

Part 1 - Front tank vs. iceberg						
Method	$\alpha$	$V_x$ [m/s]	$C_{A,ice}$	$C_{A,ship}$	$M_{ice}$ [ton]	$M_{ship}$ [ton]
Initial velocity	5.71	10.24	0.8	1.0	2457	125000
Prescribed displacement	5.71	10.24	0.8	1.0	1129	125000
Initial velocity	30	8.91	0.8	1.0	2457	125000
Prescribed displacement	30	8.91	0.8	1.0	1129	125000
Part 2 - Global ship vs. iceberg						
Initial velocity	5.71	10.24	0.8	1.0	2457	125000
Initial velocity	30	8.91	0.8	1.0	2457	125000
Part 3 - Large iceberg impact						
Front tank, initial velocity	30	10.24	0.8	1.0	19100	125000
Global model, initial velocity	30	10.24	0.8	1.0	19100	125000

Table 7.1: Setup parameters for the different analyses

### 7.1 Part 1 - front tank vs. iceberg

For the first set of analyses the scenario is described as a collision between a ship in turning and an iceberg. Only the front tank is included in the ship structure, and the simulation is simplified by defining the iceberg as the colliding body and the ship as the struck body.

The two different methods are described in detail in section 6.4.3 and 6.4.4. The prescribed displacement is based on a curve which gives the iceberg a displacement equivalent to the calculated initial velocity. This is done by giving the iceberg a motion into, and through, the ship side, and the analysis are stopped at the point where the dissipated energy has reached the same level as for the analysis with initial velocity. At this energy level, the deformation of the ship side for the two analyses is compared, and this forms the basis for the comparison study.

#### 7.1.1 Iceberg

It is assumed that 10 % of the iceberg will be visible above the water line. This is based on the material model used for the iceberg, where the density is specified as  $900 \text{ kg/m}^3$ . The water line for the ship is located at  $z = 11 \text{ m}$ , and for the iceberg with height  $15 \text{ m}$ , this means that the top point of the iceberg is located at  $z = 12.5 \text{ m}$ , as shown in figure 7.1

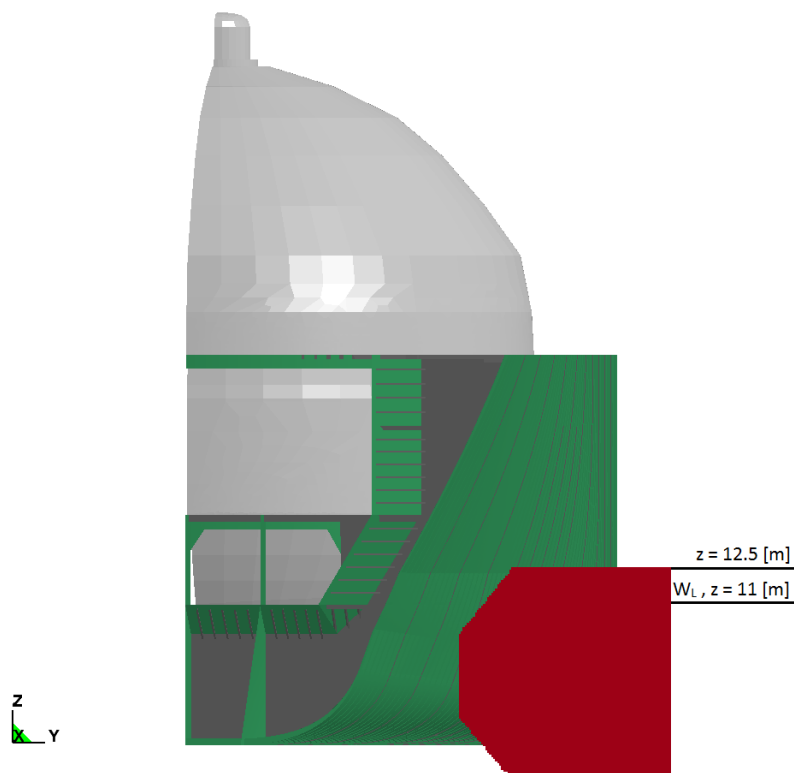


Figure 7.1: Iceberg position, front tank analyses

### 7.1.2 Initial velocity

#### Small impact angle

The forward ship speed is 20 knots, and based on the assumption in [7], the radial velocity is then given as 2 knots. An impact angle representing the two velocity components is given in eq. 7.1.

$$\alpha = \arctan \frac{V_r}{V} = \arctan \frac{2}{20} = 5.71^\circ \quad (7.1)$$

The ship is rotated by this angle to simplify the initial velocity vector, which originally includes both a x- and a y-component. When the ship is rotated, the velocity vector can be directed in x-direction only.

The collision setup is shown in figure 7.2.

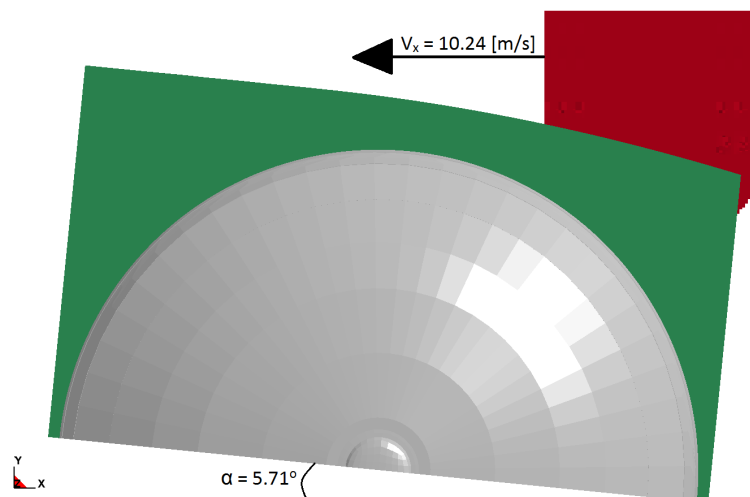


Figure 7.2: Setup of front tank and iceberg for the small impact angle

From the figure it seems like the iceberg will hit the side where the boundary conditions are applied. The figure shows a top view at the bow shoulder where the ship has its largest breadth at the main deck. The collision point yields therefore no problems related to the boundary conditions.

### Large impact angle

After discussing relevant impact scenarios with Professor Jørgen Amdahl, the second impact angle was assumed to be  $30^\circ$ . The impact angle affects the initial velocity of the iceberg, and the new velocity is calculated by eq. 7.2.

$$V_x = \cos 30 * V = \cos 30 * 20 \text{ knots} = 17.32 \text{ knots} = 8.91 \text{ m/s} \quad (7.2)$$

The collision setup for the large impact angle scenario is illustrated in figure 7.3.

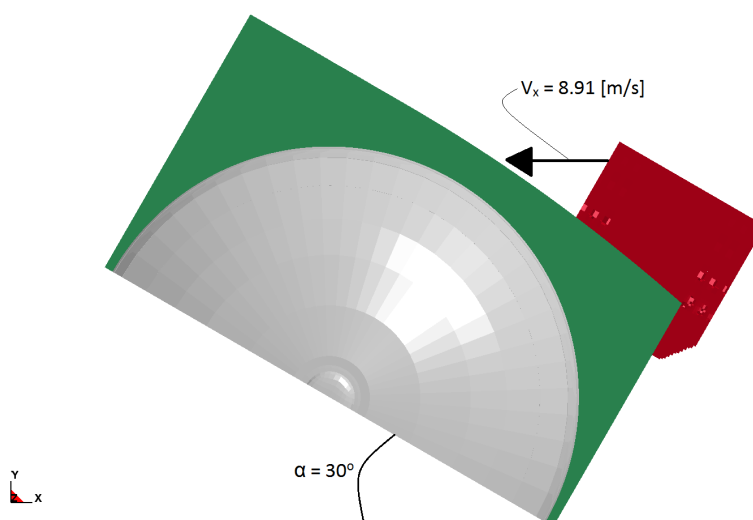


Figure 7.3: Setup of front tank and iceberg for the large impact angle

### 7.1.3 Prescribed displacement

As described in section 6.4.4, the most common method for collision analyses is to give the striking body a prescribed displacement or motion. Pinned boundary conditions are applied to the front tank section, and the iceberg is therefore given the prescribed displacement.

To get as comparable results as possible, the prescribed displacement equals both the initial velocity and the impact angles described in section 7.1.2. To avoid a large gradient in the energy curve between the two first time steps, an initial velocity has also been applied to the iceberg. This velocity will not affect the collision, since the prescribed displacement is set to equal the velocity.

### 7.1.4 Boundary conditions

Based on the information described in section 6.4.1, pinned boundary conditions are chosen for the front tank area. Pinned boundary conditions are applied on both bow side, aft side and at the center line of the model. This is the most simple boundary condition regarding both application and computation time, and the error of this method will be investigated further in the analysis of the global model. The boundary conditions are presented in table 7.2.

Side	Translation			Rotation		
	$T_x$	$T_y$	$T_z$	$R_x$	$R_y$	$R_z$
Bow side	1	1	1	0	0	0
Aft side	1	1	1	0	0	0
CL side	1	1	1	0	0	0

1 = fixed, 0 = free

Table 7.2: Boundary conditions for the analysis

## 7.2 Part 2 - global model vs. iceberg

By repeating the analyses performed in part 1 with the complete global ship model, possible errors are verified. For these analyses, the setup with prescribed displacement is not considered. Prescribed displacement requires that one of the colliding bodies is constrained against translation, which is avoided in these analyses.

The global ship model collision is analysed for both impact angle scenarios described in section 7.1.2

An overview of the collision scenario is shown in figure 7.4.

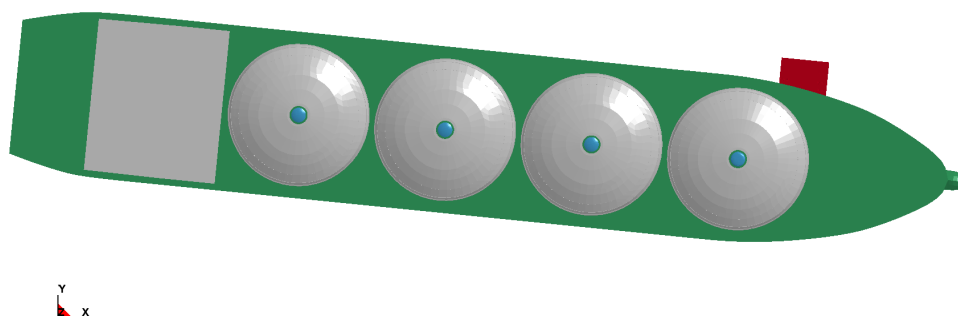


Figure 7.4: Setup of global model at small impact angle

### 7.2.1 Iceberg

The iceberg position is given in the same way as described in section 7.1.1.

### 7.2.2 Initial velocity

As described in section 6.4.3, the initial velocity is now given to the ship. The ship is rotated in the same way as for the analyses of the front tank, and the velocities are the same. This means that two different simulations are performed with the following parameters.

Analysis	$V_x$ [m/s]	$\alpha$ [°]
Small angle	10.24	5.71
Large angle	8.91	30

Table 7.3: Velocity and angle for global model analyses

### 7.2.3 Boundary conditions

No boundary conditions are applied to the global analysis. Both the ship and the iceberg are free to move in all directions.

## 7.3 Part 3 - Large iceberg impact

To obtain the deformations and energy dissipation for a collision scenario with an large iceberg, an iceberg with mass of approximately 19100 tons has been modelled. This analysis requires large computation time, and only two different analyses are performed,

i.e. a simplified analysis of the pinned front tank area where the iceberg is given initial velocity and a full analysis of the global model.

To ensure that the largest deformations of the hull are obtained, the impact angle of the iceberg is chosen to  $30^\circ$ . This means that the setup is equal to the  $30^\circ$  analysis described in section 7.2, except from the iceberg size.

The collision setup for the large iceberg is shown in figure 7.5.

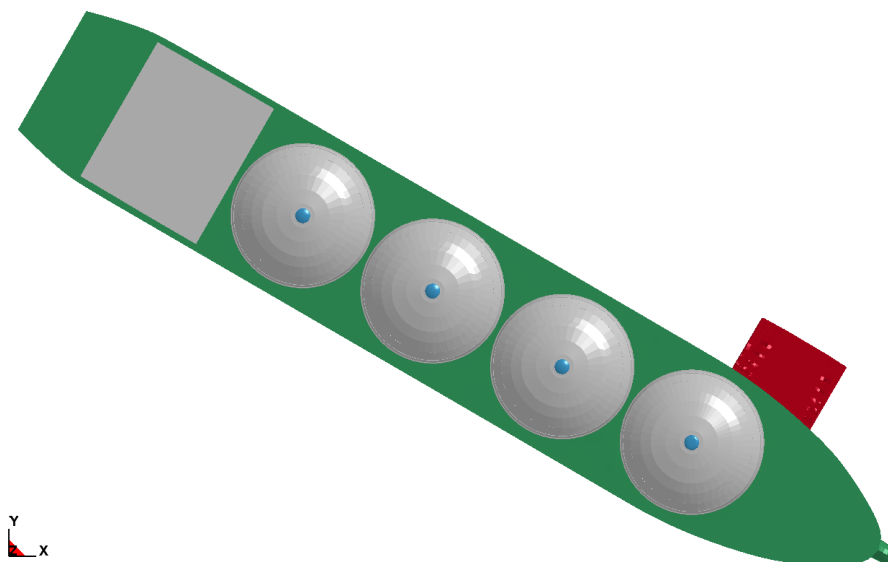


Figure 7.5: Setup of global model vs. large iceberg scenario

## 8 Results

A large amount of results are obtained from the analyses in LS-DYNA. These can be post-processed in several ways, and different aspects can be considered. In this thesis the focus has been to compare different approaches to the collision scenario, and, in addition, to compare results from analyses of simplified geometry with results from analyses of the global ship model.

A selection of data for each analysis are post-processed and presented in this section. The most important results in this thesis are the energy dissipation and deformation of the ship structure. Other important results are the contact forces, contact area and pressure between the two colliding bodies and the accelerations within the bodies. Some figures presenting a picture of the hull deformations are given in appendix A.

MATLAB has been used to post-process the results from the LS-DYNA analyses. Large output files from the analyses have been read and included in matrices in MATLAB. These matrices are further compacted into vectors where different parameters are calculated for each time step. Using MATLAB as post-processor ensures large possibilities in comparing different results. Results from several analyses can be post-processed at the same time, and figures comparing e.g. contact forces and energies for different approaches can easily be presented.

To ensure that the MATLAB codes are post-processing the results correctly, comparisons with results directly from LS-DYNA and simple hand calculations have been performed.

When the results are presented, the following notation is used for the different analyses:

### **Local model:**

The simplified model which only includes the front tank area.

### **Initial velocity analysis:**

Initial velocity is given to the iceberg, which is defined as the colliding body.

### **Prescribed displacement analysis:**

A prescribed displacement which is defined to equal the initial velocity is given to the iceberg, which is the colliding body. This option is only used for the local model analyses.

### **Global model:**

The full global model of the LNG carrier.

When the local model and the global model are compared, the initial velocity setup is used for both models.

### 8.1 Pressure-area relationships

Based on the contact forces and the reference area, given from the LS-DYNA analysis, pressure-area relationships for the two icebergs colliding with the ship are established. In addition, a pressure-area relationship for the ice model colliding with a rigid plate is established. The relationships are compared to a curve given in ISO 19906, 2007, [21]. This curve is based on local pressures for thick, massive ice features having thickness larger than 1.5 m. The curve is given by eq. 8.1.

$$p_L = \begin{cases} 7.40A^{-0.70} & \text{for } A \leq 10 \text{ m}^2 \\ 1.48 & \text{otherwise} \end{cases} \quad (8.1)$$

where  $p_L$  is the local pressure given in [MPa] and A the loaded area.

The pressure-area relationship established from the simulations are calculated as total force at the actual contact area. The pressures from the ice impact at the rigid plate is higher than the pressures obtained from the ship-iceberg collision. This is due to the lower strength in the steel material model used compared to a rigid plate which will totally resist the impact. The obtained pressure-area relationships for all three collision approaches in addition to the rigid plate collision and the ISO 19906 curve are shown in figure 8.1.

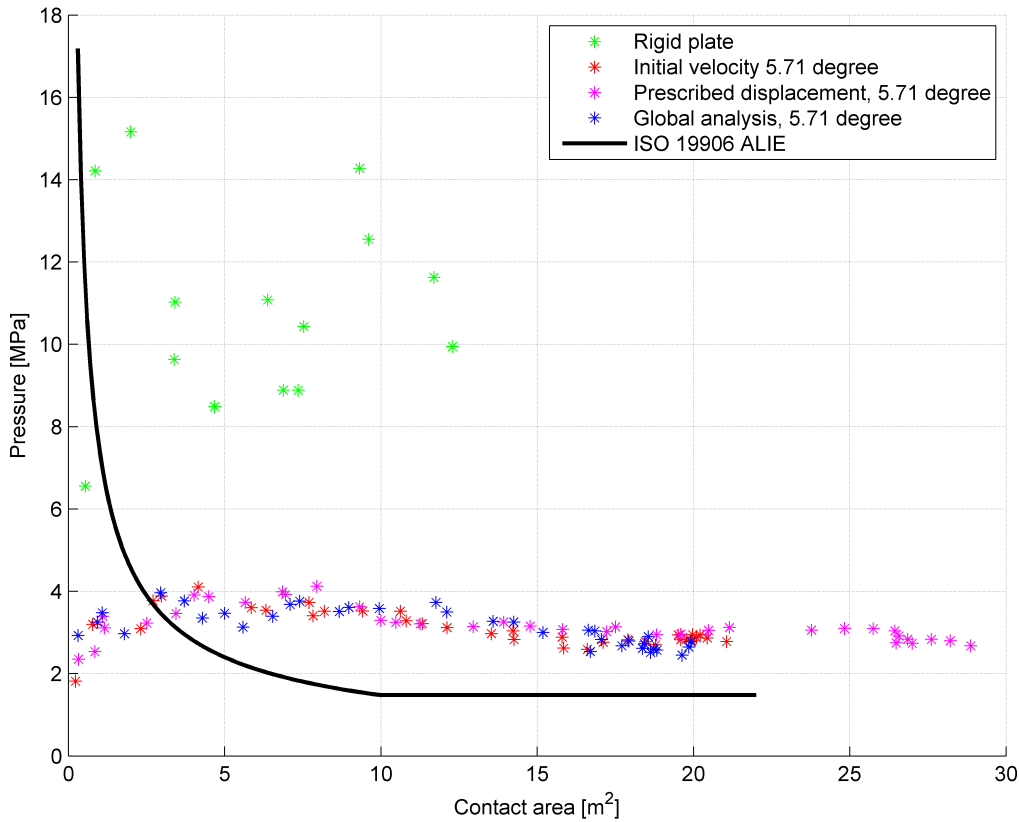


Figure 8.1: Pressure-area relationships



As seen from the figure, all the observed pressures are low, and does not match the ISO curve for low areas. This do not match since global pressures and not local pressures are observed. If local pressures had been investigated, a better fit to the ISO curve for low areas would have been obtained.

Another way to present the pressures obtained in the simulations are by plotting a contour plot of the impacted area. An example of such presentation is shown in figure 8.2. This figure shows the pressure at each node in the impact area at the time step where max contact force is obtained.

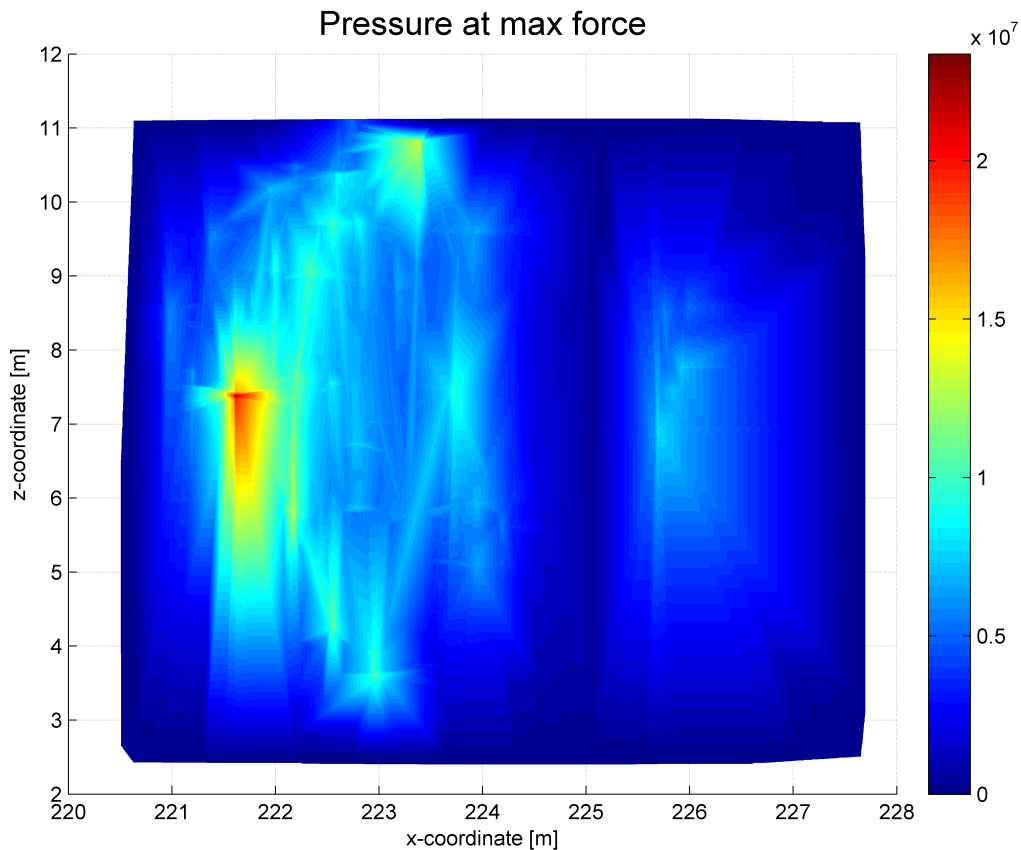


Figure 8.2: Contour plot of contact pressure at max force for initial velocity,  $5.71^\circ$

## 8.2 Contact forces and deformations

During the collision, large deformations of the outer shell is expected. The node displacement has been tracked for a large selection of the nodes in the outer shell, and the largest indentation is found and presented. The node displacement can be tracked in two different ways:

- The displacement is tracked for every single node, and the displacement of the node with the largest total displacement is presented as maximum indentation.
- The largest indentation for each time step is found and added in a vector which gives the largest indentation for all nodes at each time step.

To capture the deformation at early time steps, the method where the largest displacement for each time step is tracked has been chosen. This method will give the same results as the other method for late time steps, while it will deviate at early time steps. By using this method, a good representation of the indentations will be given.

The contact forces are calculated as the resultant force at each time step. A common way of presenting the forces and the displacements is to create force-displacement curves. For some of the analyses it has been decided not to present these curves due to poor readability. In these sections, other ways of presenting the forces and deformations are chosen. It is important to notice that the force-displacement curves presented in this thesis do not represent the total deformation, but the largest indentation. This means that the area under the curves do not represent the absorbed energy in the structure.

### 8.2.1 Simplified approach - pinned local model

For the simplified approach, both initial velocity and prescribed displacement has been applied to the iceberg, as described in section 7. Comparing the contact forces and deformations of these two methods will give large deviations, since the deformations in the prescribed displacement analysis will increase independent of the resistance in the hull. Nevertheless, the deformations and forces for the first time steps of the simulation are interesting to investigate, and a comparison for both impact angles are presented in the following.

#### 5.71° impact angle

Figure 8.3 shows the force-displacement relationships for the two local simulation methods at 5.71° impact angle.

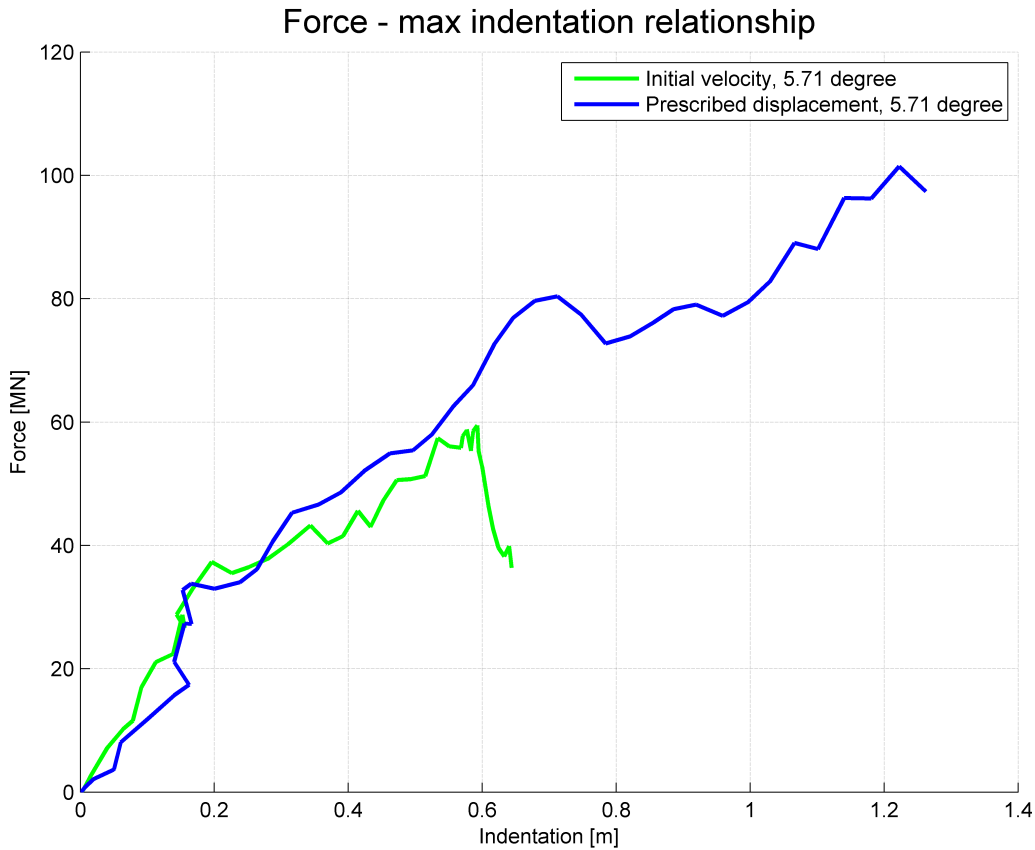


Figure 8.3: Force - indentation relationship, initial velocity and prescribed displacement for local model,  $5.71^\circ$

As expected, the analysis with prescribed displacement yields larger forces and deformations than the initial velocity analysis. On the other hand, it is interesting to see that the contact force and the indentation are similar until approximately indentation of 0.6 m is obtained. At this indentation the resistance in the hull is large enough to resist more deformation given by the iceberg impact. For the prescribed displacement scenario, the iceberg is forced to give further deformation, and it is seen that both contact force and indentation is increasing further on.

In addition to this observation, figure 8.4 and 8.5 also shows the difference in deformation after  $t=0.6$  s. The deformations seen in the prescribed displacement analysis, figure 8.4d, are significantly larger than for the initial velocity simulation, figure 8.5d, and already at 0.6 s of simulation yields the prescribed displacement analysis over-conservative results.

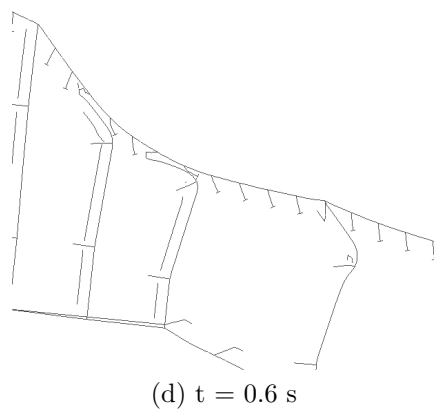
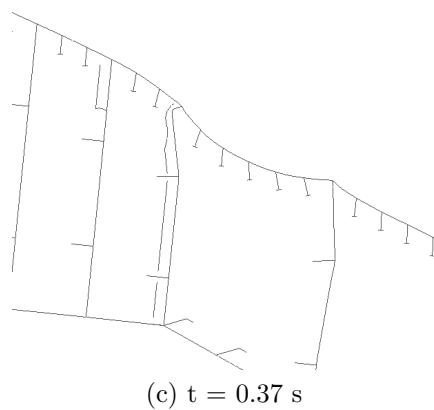
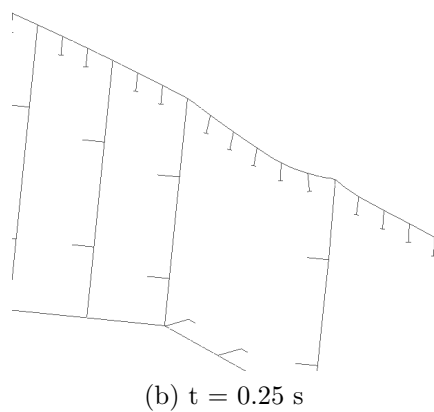
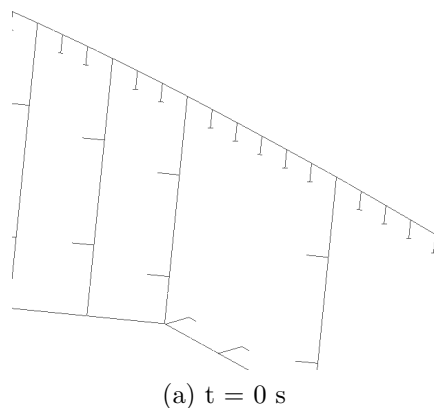
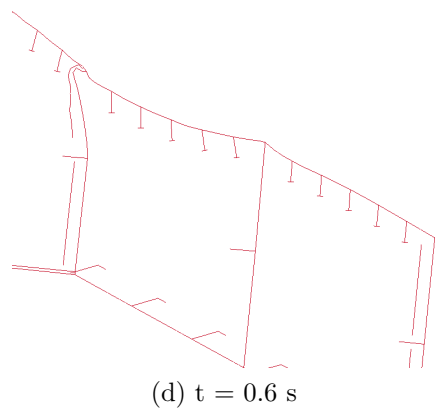
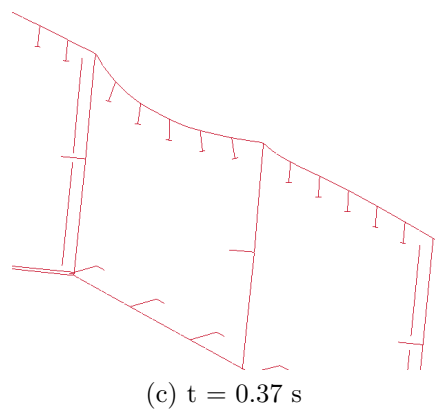
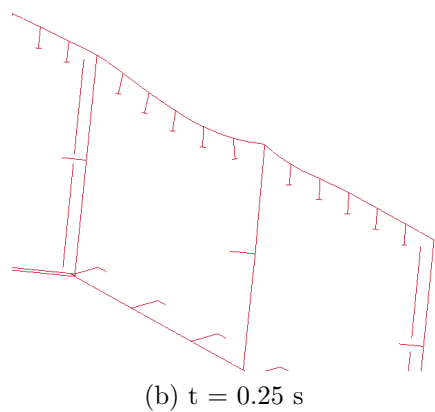
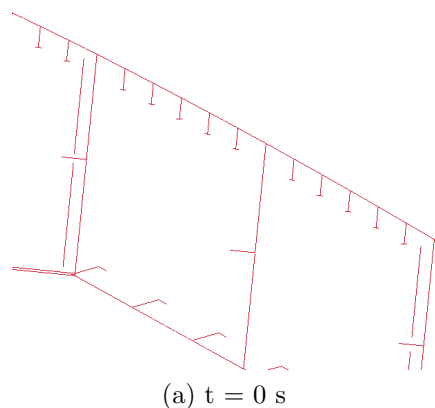


Figure 8.4: Horizontal cut for local initial velocity analysis,  $5.71^\circ$

Figure 8.5: Horizontal cut for local prescribed displacement analysis,  $5.71^\circ$

Figure 8.6 shows the contact force for each time step. As previously discussed, it seems like the deformation and contact force is similar for the two methods until approximately 0.25 s. The same observation is done in this figure. The contact force seems to be approximately the same for both methods until 0.25 s, where the prescribed displacement analysis is beginning to get larger contact forces and deformations.

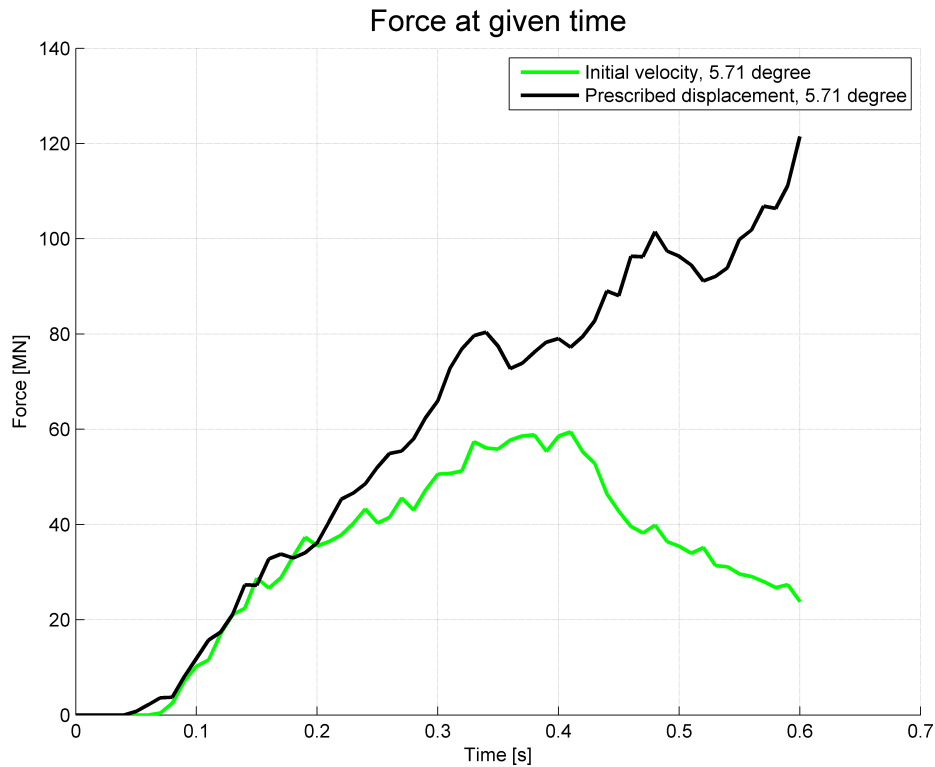
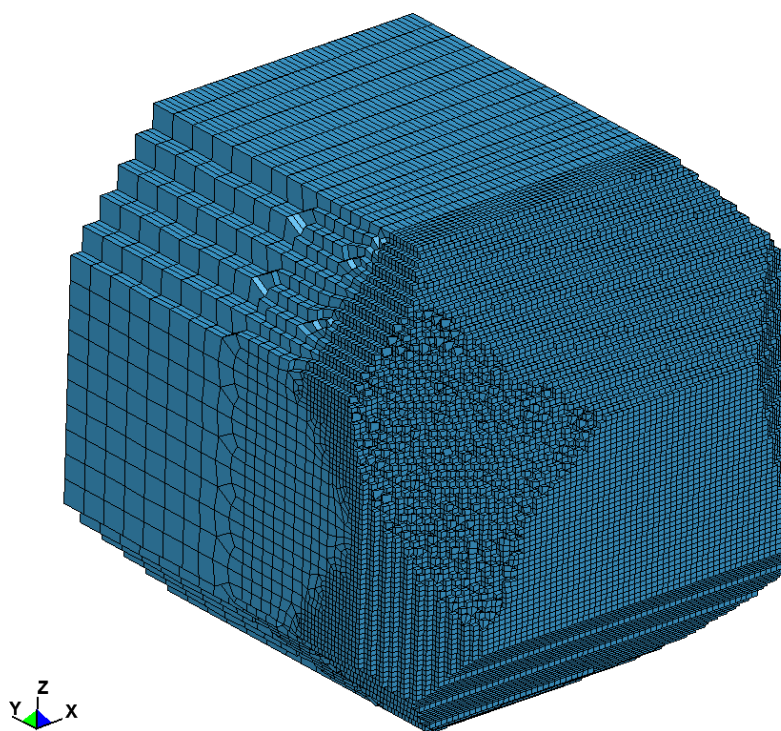


Figure 8.6: Force - time, initial velocity and prescribed displacement,  $5.71^\circ$

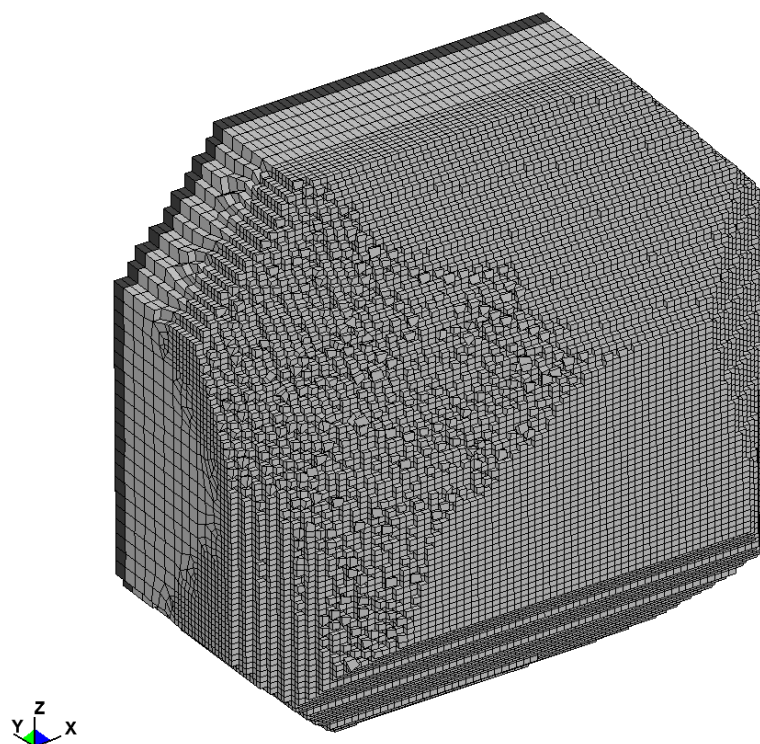
The iceberg crushing for the two methods is shown in figure 8.7. The original shapes can be seen in section 6.3.1 and 6.3.2. It is difficult to get accurate tracking of the iceberg deformations due to the crushing of elements, and it is therefore chosen to give a visual consideration of the iceberg crushing only. It is possible to track the displacement, but the irregularity in the iceberg shape will cause a large possibility of errors in the measurements, and the tracking will be misleading.

The figures show that the crushing of the prescribed displacement iceberg is significantly larger than for the initial velocity iceberg. The icebergs are shown at 0.6 s, which is the last time step of the prescribed displacement analysis, and the large deformation in the iceberg is therefore as expected. Based on the simulation, it seems like the ice material model yields realistic crushing of the material, and it is clearly seen from the figures that the contact corner of the iceberg is smoothed due to crushing.

The size of the mesh used in the icebergs is a bit large according to Liu's material model. This can possibly lead to small instabilities in the crushing, which again can cause small deviations in the results.



(a) Crushed iceberg for local initial velocity analysis



(b) Crushed iceberg for local prescribed displacement analysis

Figure 8.7: Ice crushing for local initial velocity and prescribed displacement analyses,  $5.71^\circ$

### 30° impact angle

For the 30° impact angle analyses of the local model larger forces is obtained. The relationship between force and max indentation is given in figure 8.8. From the figure it is seen that the maximum force for the local initial velocity analysis at 30° impact angle is approximately 18 MN larger than the maximum force for local initial velocity at 5.71° impact angle, shown in figure 8.6. The corresponding indentation obtained from the largest impact angle is approximately 0.6 m larger than for the small angle, which is near 100 % increase.

For this impact angle it is seen that the two simulation methods yield similar results until an indentation of approximately 0.8 m. Beyond this indentation, the prescribed displacement analysis yields larger forces and indentations than the initial velocity analysis, which is expected. On the other hand, it is seen that the prescribed displacement analysis yield significantly larger contact forces between 0.3 m indentation and 0.5 m indentation. This is probably caused by the deformation of the transverse frame, shown in figure 8.10c and 8.10d, which is a lot more resistant to deformations than the plating between the frames.

The observation of similar indentations for longer simulation time indicates that the difference in the simulation approaches is less for larger impact angles. At small impact angles, the iceberg will more easily be deflected from the ship side. This deflection will not be simulated in analyses where a prescribed displacement is defined, and the difference between the initial velocity approach and the prescribed displacement approach will be introduced at an early time step. For larger impact angles the deflection will be limited, and the initial velocity approach will therefore give similar results as the prescribed displacement approach for a larger range in indentation.

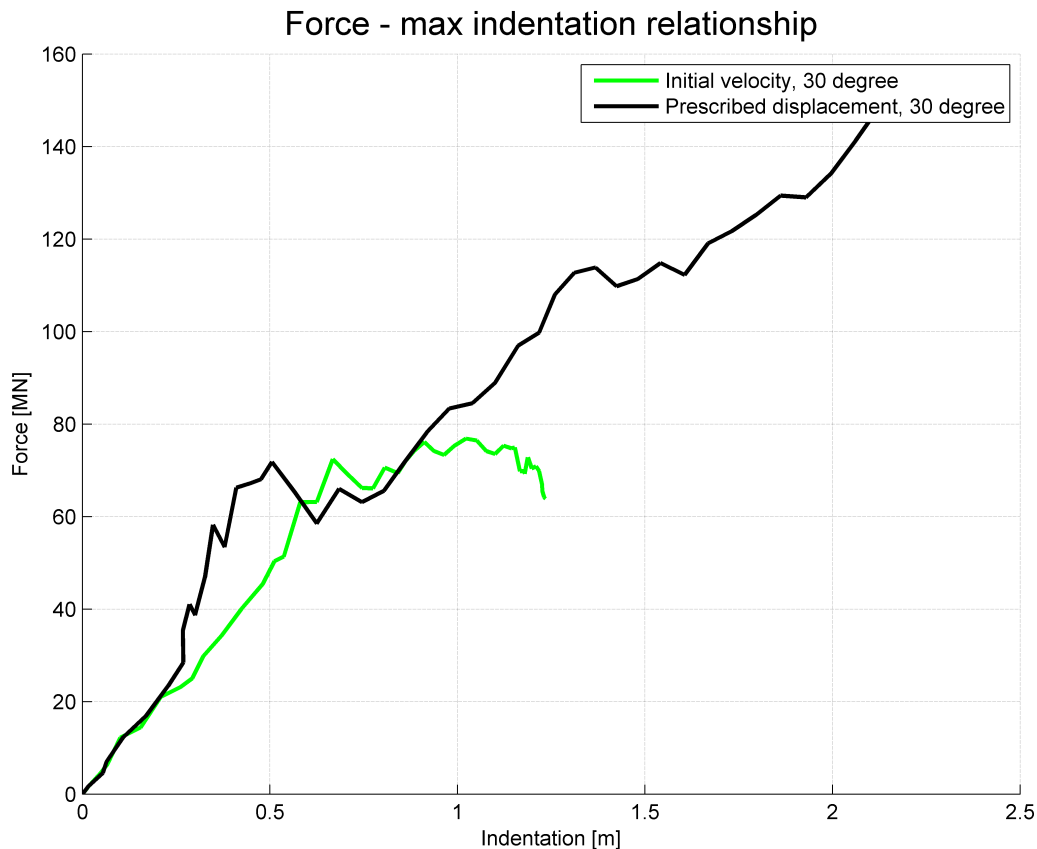


Figure 8.8: Force - indentation relationship, initial velocity and prescribed displacement analysis for local model,  $30^\circ$

Figure 8.9 and 8.10 shows the deformation obtained by the two different simulation methods. It is interesting to see that already after 0.25 s a deformation in the transverse frame is seen. This shows that the impact at  $30^\circ$  impact angle yields larger contact forces than for the impact angle of  $5.71^\circ$ , and the energy absorption in the bodies needs to be larger. This is further discussed in section 8.3.1.

It is also seen from the figure that the deformation of the prescribed displacement analysis is significantly larger than for the initial velocity analysis at the last time step shown. This indicates that the prescribed displacement analysis also at this impact angle is over-conservative.



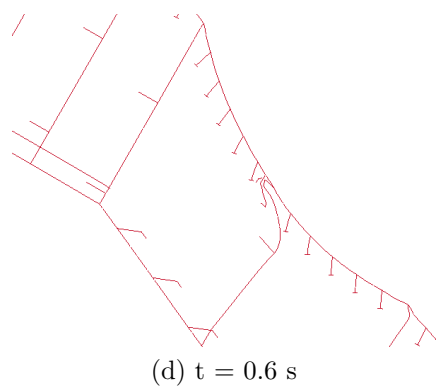
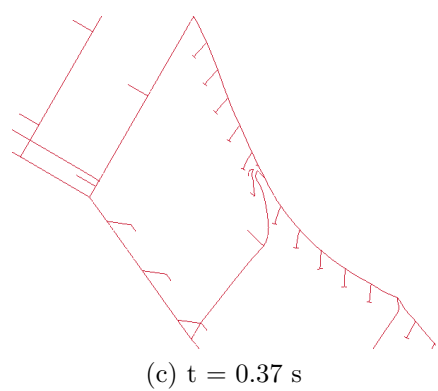
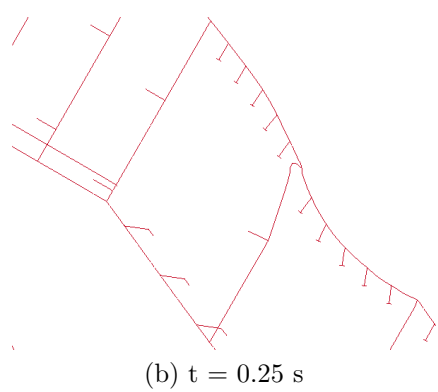
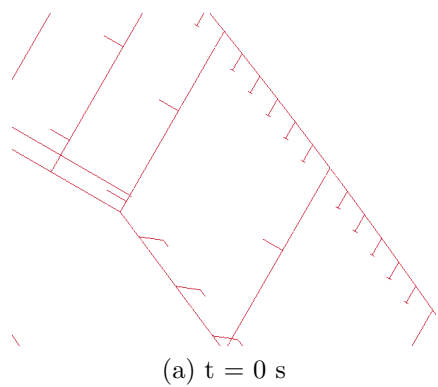


Figure 8.9: Horizontal cut for local initial velocity analysis,  $30^\circ$

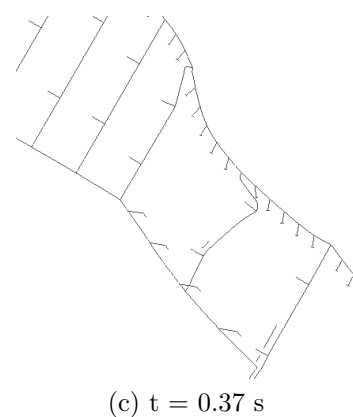
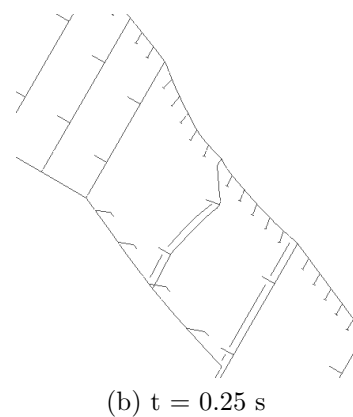
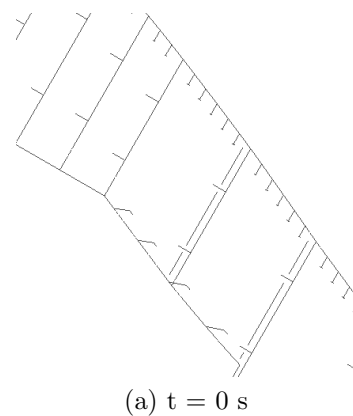


Figure 8.10: Horizontal cut for local prescribed displacement analysis,  $30^\circ$

### 8.2.2 Local model compared to global model

To verify the effect the boundary conditions have on the result, it is interesting to do a comparison of the results from the local and the global model simulation.

#### 5.71° impact angle

In figure 8.11 the force progress for each time step is shown for an impact angle of 5.71°.

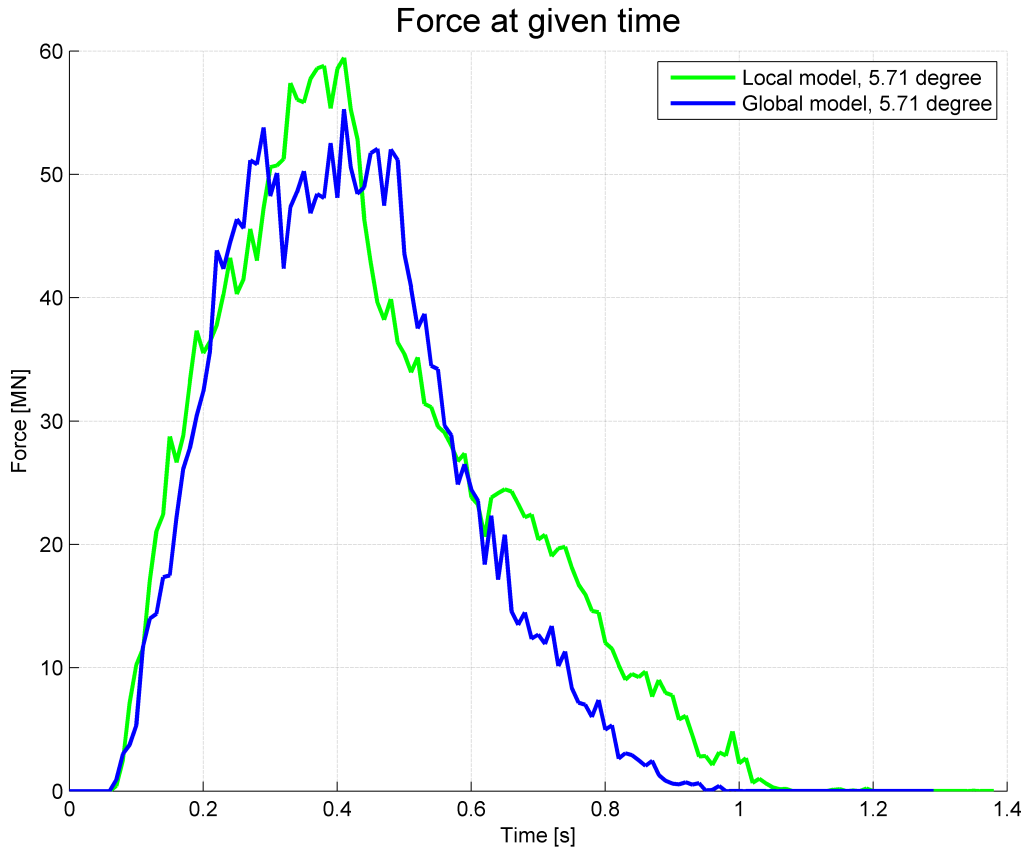


Figure 8.11: Force - time for local and global model, 5.71°

The contact force is similar until approximately 0.3 seconds, where some deviations occur. When studying the deformations in figure 8.12 and 8.13 this seems reasonable. The deformations at  $t=0.25$  s seems similar, while the deformations of the local model at  $t=0.37$  s, see figure 8.12c, shows larger deformations than for the global model analysis, figure 8.13c.

At time  $t=0.7$  s it is seen that the analysis of the local model yields some more deformations of the ship than the global analysis. One of the vertical frames has been deformed, which is not happening for the global model. This indicates that the pinned boundary conditions leads to a conservative result which is an expected outcome of the comparison. Based on this, the boundary conditions seem to introduce conservatism to the results. When relating the boundary conditions to the physics, this is reasonable, since no damping in the system is introduced when pinned boundary conditions are applied.

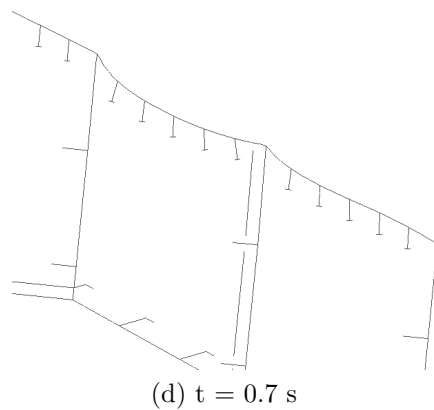
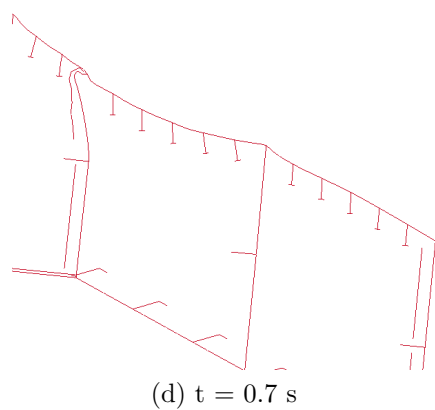
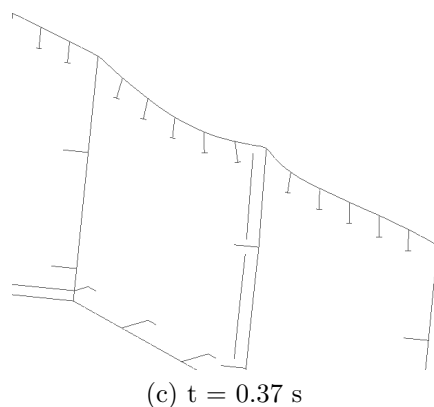
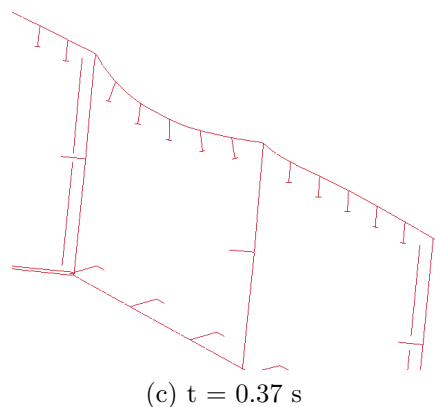
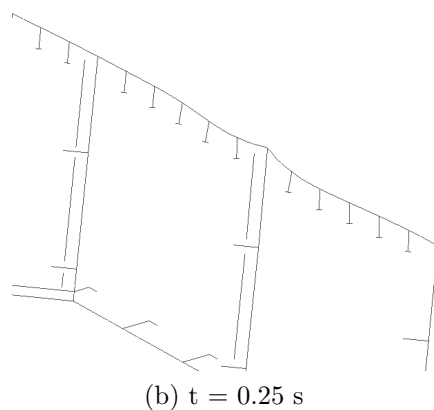
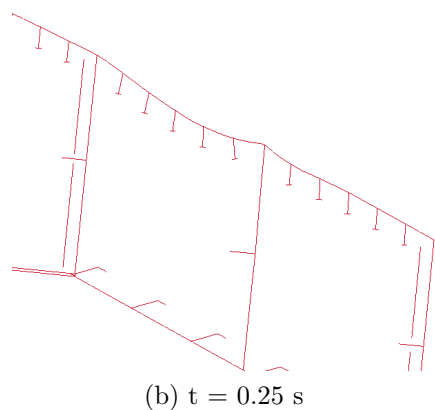
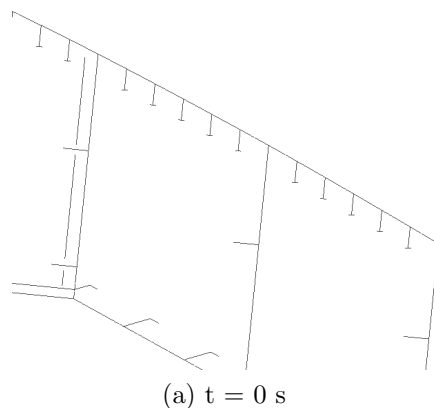
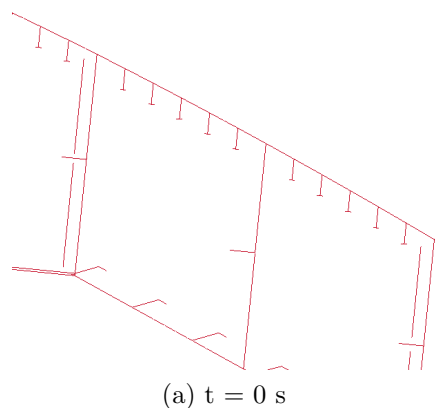


Figure 8.12: Horizontal cut for local model initial velocity analysis,  $5.71^\circ$

Figure 8.13: Horizontal cut for global model analysis,  $5.71^\circ$

When plotting the indentation for each time step, an unexpected large difference is found, see figure 8.14. Larger deformations was expected, but based on figure 8.12d and 8.13d an increase in indentation of approximately 200 % for the local analysis seems too large. The displacement shown is the resultant displacement. This means that both x- and z-displacement, which is difficult to observe in figure 8.13, contributes to the displacement, and this can be some of the explanation of the large difference.

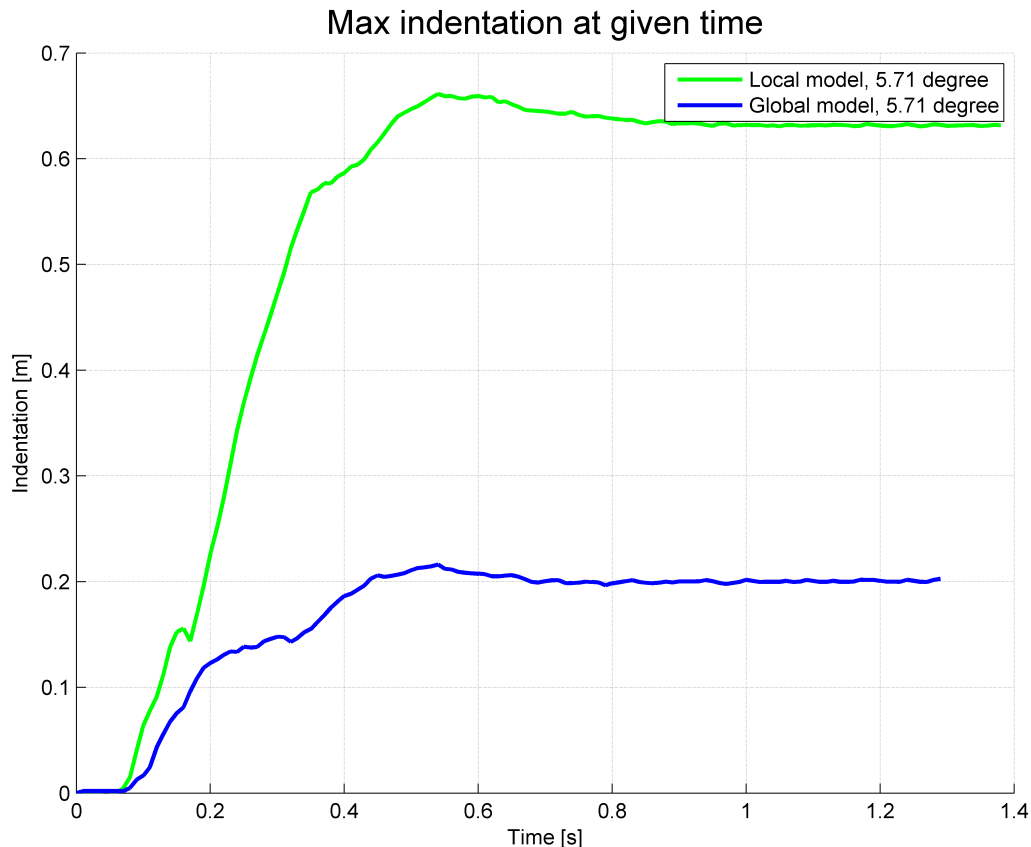
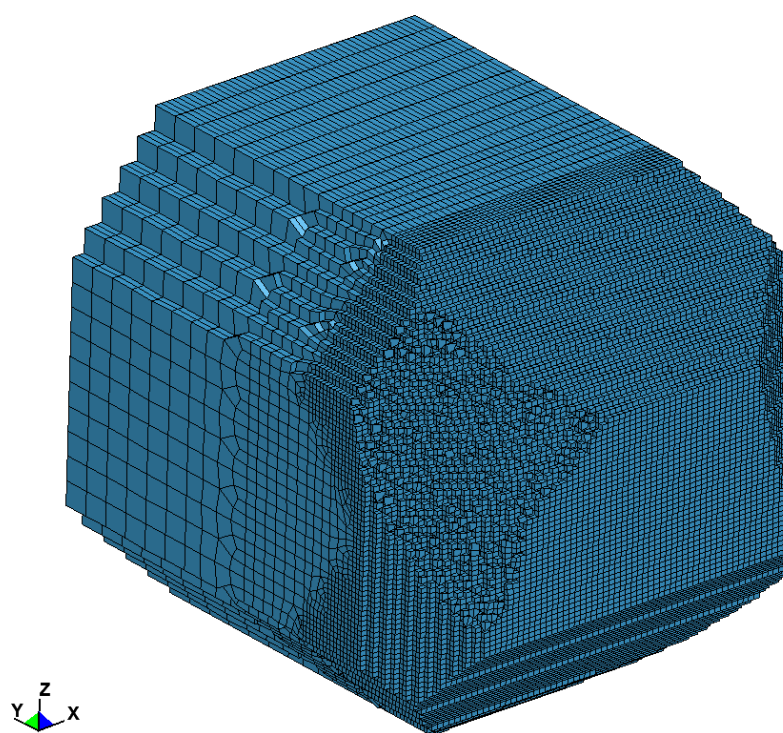
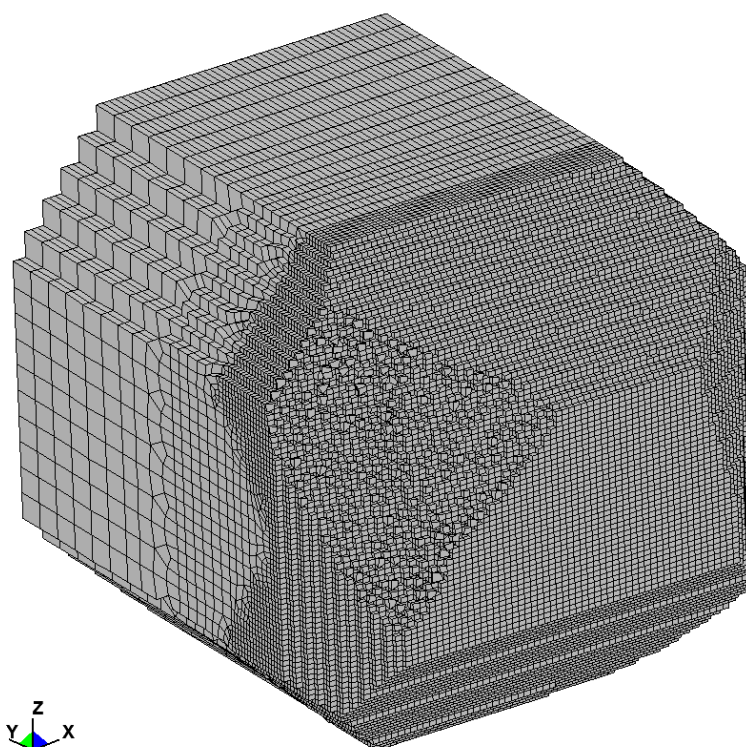


Figure 8.14: Max indentation plotted against time for local and global analysis,  $5.71^\circ$

The iceberg crushing is given in figure 8.15. The difference here is small. This means that, according to figure 8.14, that most of the energy in the local analysis for later time steps than  $t=0.25$  s is absorbed by the ship. The energy considerations for these analyses are investigated in section 8.3.2.



(a) Crushed iceberg for local model analysis



(b) Crushed iceberg for global model analysis

Figure 8.15: Ice crushing for local and global analysis,  $5.71^\circ$

### 30° impact angle

The force-indentation relationship for the local and global analyses for impact angle 30° is shown in figure 8.16. The same trend as for the collision at 5.71° impact angle is seen. The local analysis yields larger deformations for equal contact force. As expected, the deformations obtained from these analyses are significantly larger than for the small impact angle.

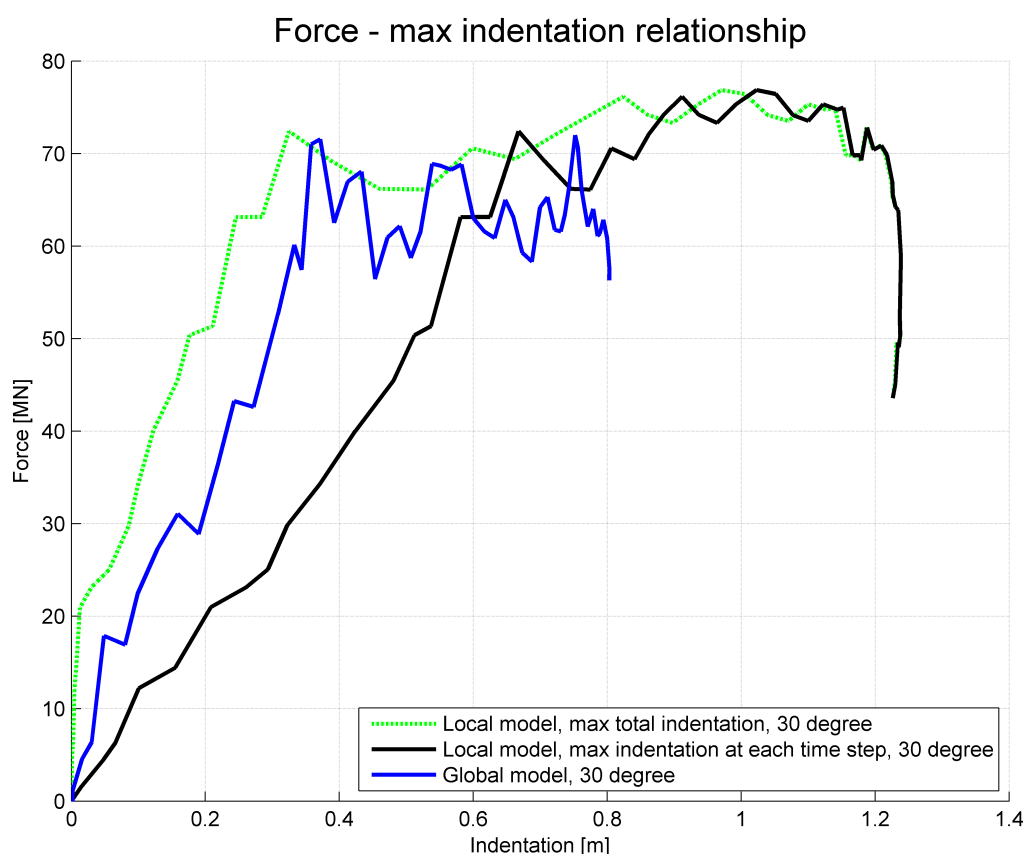


Figure 8.16: Relationship between force and max indentation for local and global analysis, 30°

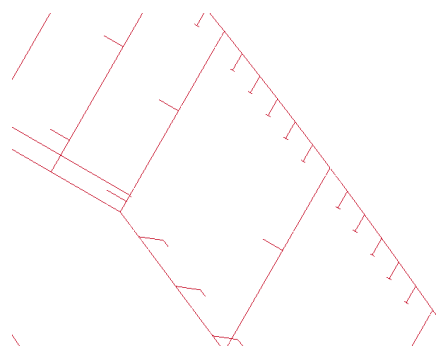
In figure 8.16 the deviations in the two different methods of tracking indentation can be clearly seen. The green curve shows the indentation for all time steps of the node which gets the largest total displacement while the black dotted line shows the largest displacement at each time step for all nodes. The black dotted line yields results which better describes the physics in the problem, and it is seen that for late time steps the results are similar for the two tracking methods. It is reasonable that the local model will get larger deformations at lower contact force due to its pinned boundary conditions. This effect is captured by the chosen method to track node indentation.

The deformations of the ship side for the two analyses are shown by horizontal cuts in figure 8.17 and 8.18. The deformation is, as expected, quite similar for the first 0.25 s. The indentation seems not to change from  $t=0.4$  to  $t=0.8$  s. One of the transverse frames

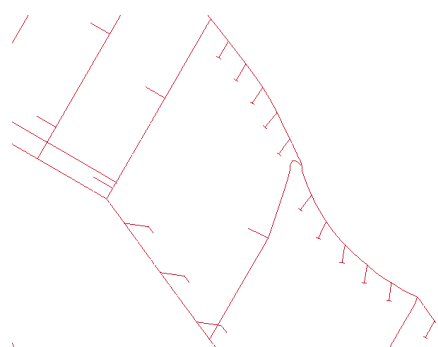
is deformed and this will therefore not give a large contribution to the strength in the ship side at this time, but the strength in the two neighbouring frames is apparently large enough to resist the iceberg impact.

Figure 8.18d shows that the iceberg has deformed the transverse frame on the left side of the figure. This frame is not deformed at the same time step for the local analysis, which is an observation that does not support the observed result of larger deformations in this simplified analysis. In the global analysis, the ship is given an initial velocity which apparently leads to a deformation pattern which is spread over a larger part of the ship side. This means that the collision forces will be captured over a larger area, which again will contribute to a smaller maximum deformation, as shown in figure 8.16. It is also for this impact angle seen that deformations obtained from the simplified local analysis seems to be conservative with respect to deformations.

Compared to the collision scenario at  $5.71^\circ$  impact angle, the iceberg seems to absorb more energy in crushing in the simulation of  $30^\circ$  impact angle. According to figure 8.19, the crushing of the iceberg seems to happen over a larger area than for the small impact angle scenario, which seems reasonable when it is known that the collision yields larger deformations in the ship.



(a)  $t = 0$  s



(b)  $t = 0.25$  s

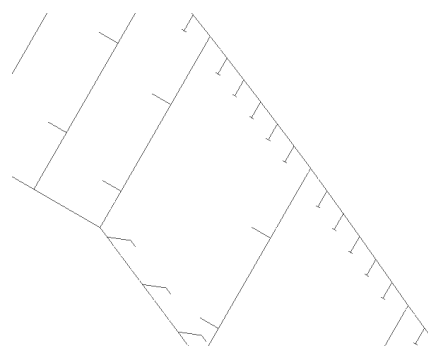


(c)  $t = 0.4$  s

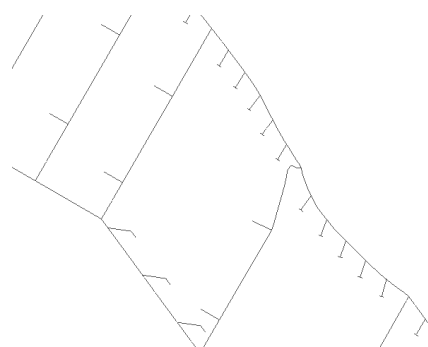


(d)  $t = 0.8$  s

Figure 8.17: Horizontal cut for local initial velocity analysis,  $30^\circ$



(a)  $t = 0$  s



(b)  $t = 0.25$  s



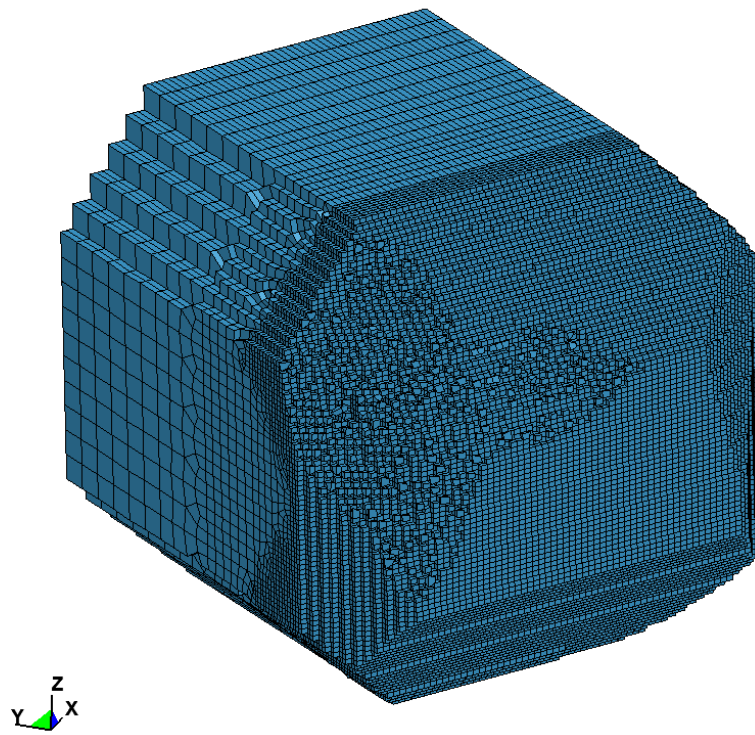
(c)  $t = 0.4$  s



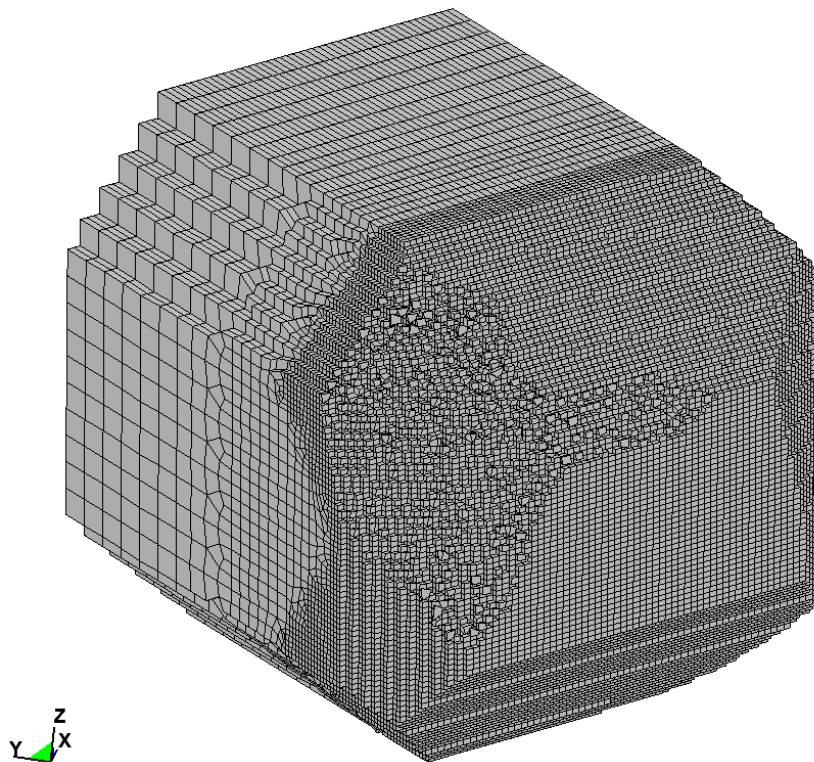
(d)  $t = 0.8$  s

Figure 8.18: Horizontal cut for global analysis,  $30^\circ$





(a) Crushed iceberg for local analysis



(b) Crushed iceberg for global analysis

Figure 8.19: Ice crushing for local and global analysis,  $30^\circ$

### 8.2.3 Comparison of both impact angles for the global model

It is interesting to investigate the differences in the collision scenario for the two different impact angles. The relationship between force and max indentation for the global model simulation at  $5.71^\circ$  and  $30^\circ$  impact angle is shown in figure 8.20.

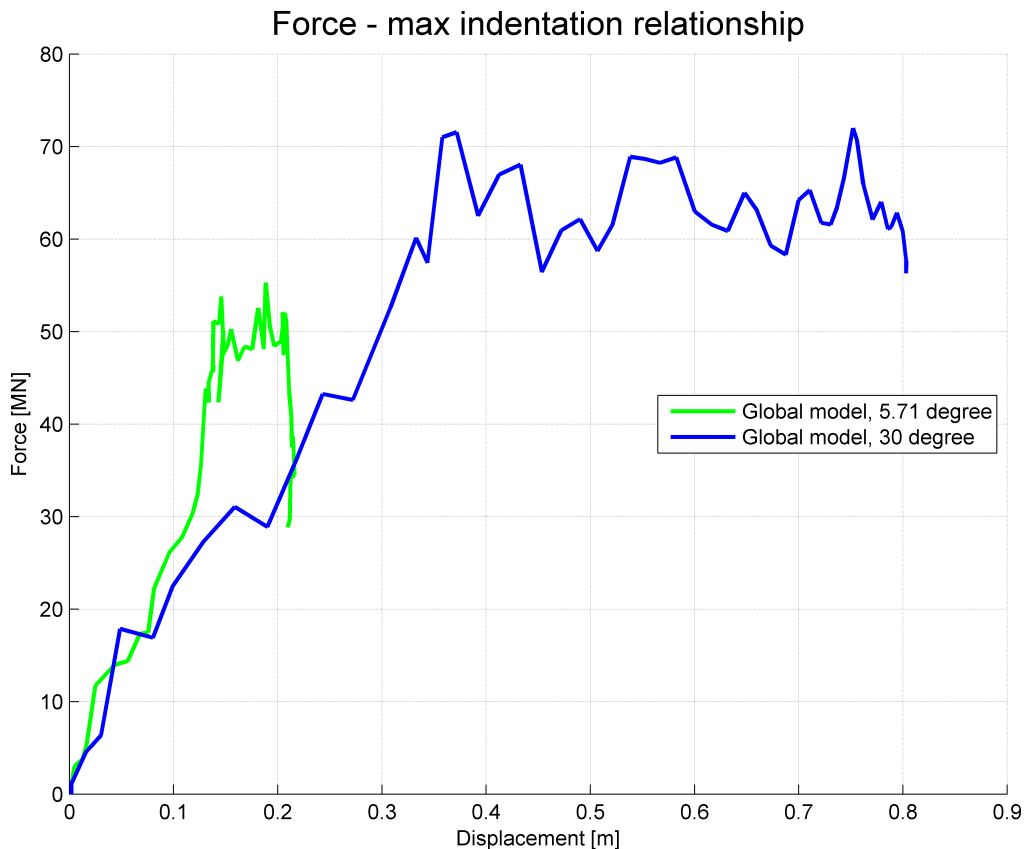


Figure 8.20: Relationship between force and max indentation for both impact angles, global analysis

As discussed in section 8.2.2, the deformations obtained from the global analysis for  $5.71^\circ$  impact angle seems remarkable small compared to the deformations in the other analyses. The same observation is done in this comparison. Here, the displacement tracking is common for both analyses, and this possible error source is therefore eliminated. On the other hand, if the two initial velocity analyses of the local model are compared, it is seen that the difference between the deformations for  $5.71^\circ$  and  $30^\circ$  is approximately 0.55 m. The difference in deformation for the global analyses is, according to figure 8.20, approximately 0.6 m. This means that the difference in deformations for the two impact angles is approximately the same for the local analyses as for the global analyses. When figure 8.21 is included in the consideration, it is seen that the largest deformation at  $30^\circ$  impact angle is significantly larger than for  $5.71^\circ$  impact angle. Based on this figure, the force-indentation relationship shown in figure 8.20 seems reasonable.

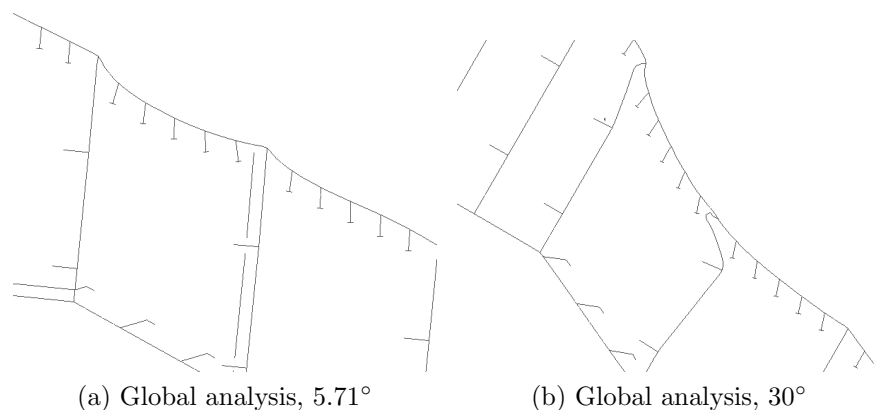


Figure 8.21: Largest deformation of ship for the two different impact angles, global analysis

#### 8.2.4 Large iceberg

Two different collision simulations are performed with the large iceberg; a local initial velocity analysis and a global analysis. These analyses demands very large computer resources and the computation time is very long. The local analysis had to be stopped after approximately 81 hours to release computer resources for other simulations, and only 0.52 s of the collision scenario is therefore simulated. This means that the results from this analysis only will indicate how the deformation will be, and larger deformations and energy absorptions than obtained from the analysis must be assumed to occur. The global model was stopped after approximately 400 hours and 0.88 s of the collision scenario is simulated. From the simulations it seems like the large iceberg will not deflect in the same way as the small iceberg, and the area of deformation is therefore larger. The results are, as mentioned, presented for the analysed time steps, but the trend is clear: Larger forces, deformations and internal energy levels must be expected to occur throughout the simulation.

The relationship between force and max indentation for these simulations are shown in figure 8.22. In this figure the max indentation at each time step is shown.

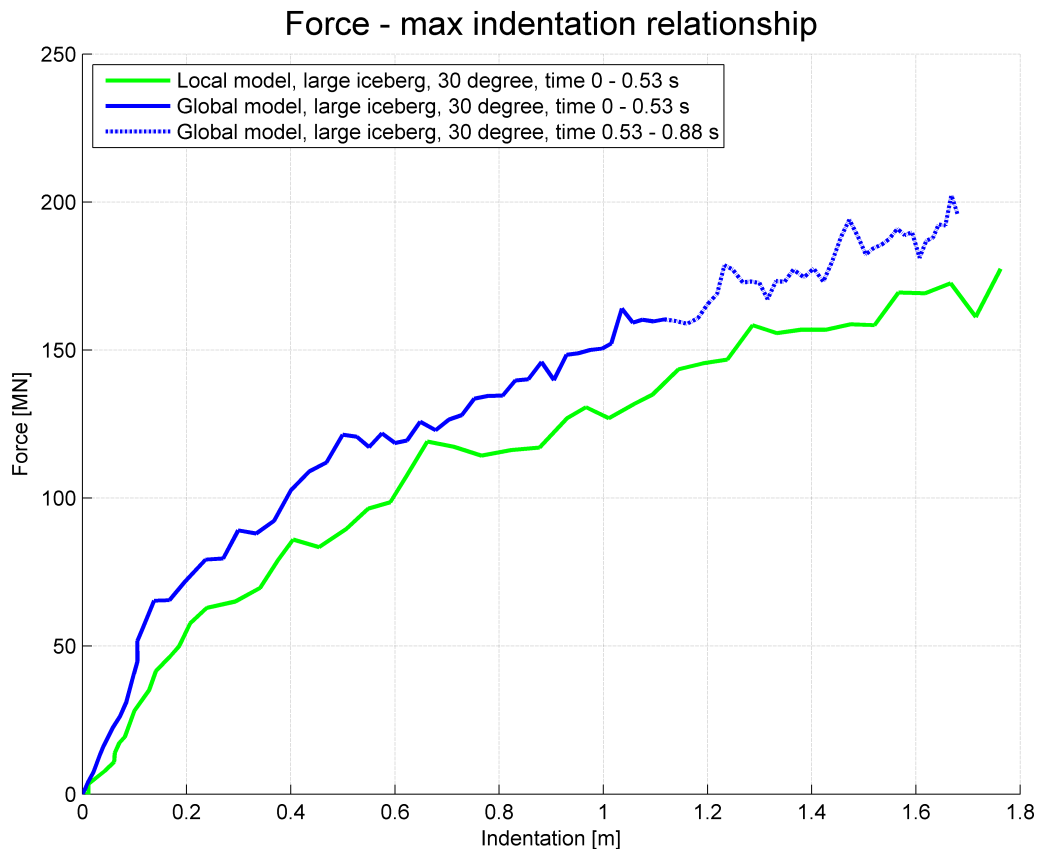
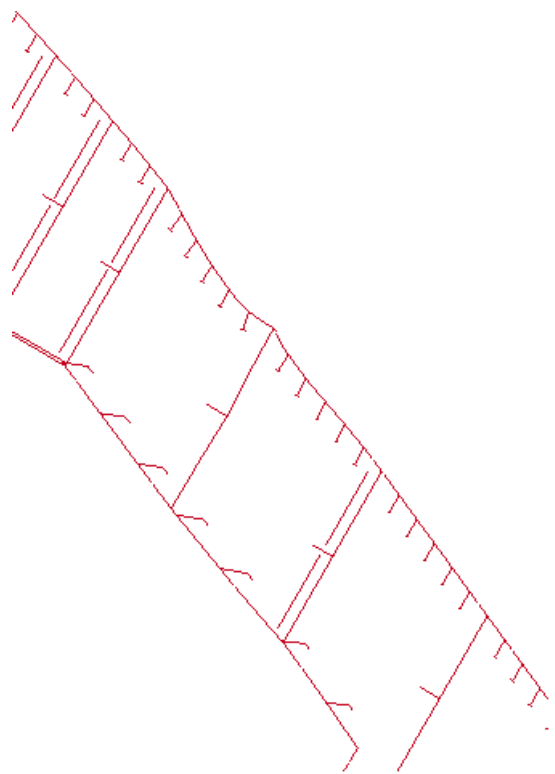


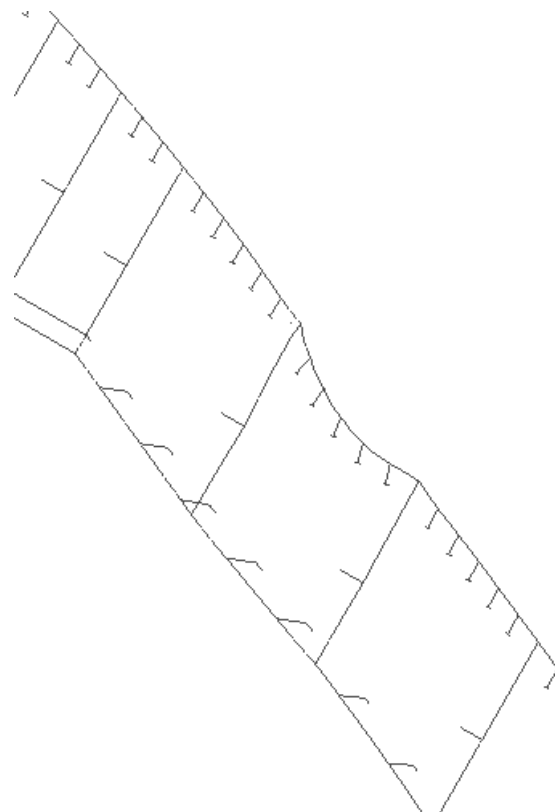
Figure 8.22: Relationship between force and max indentation for local and global analysis, large iceberg at 30° impact angle

As seen from the figure a very similar force-deformation relationship is obtained from these analyses. This is reasonable since the ship structure in this collision will have a significant reduction in structural resistance due to large deformations. It is also seen that the indentation of the hull is significantly larger for the large iceberg than for the small iceberg. A requirement for the accidental stability of the structure is that leakage of two ballast tanks is acceptable. This means that if the indentation leads to any leakage it is not critical for the ship as long as fracture is limited to a small area. From the simulations it seems like the deflection of the large iceberg is smaller than it was for the small iceberg. This means that the indented area will be more comprehensive than for the small iceberg, and the impact can therefore possibly be larger than two ballast tanks during the collision. No fracture is observed during the simulated scenario, but as seen from the figures, even larger deformations can be expected. A max indentation of approximately 1.7 m is observed, and at this point the inner hull has started to deform, see figure 8.23 and 8.24.

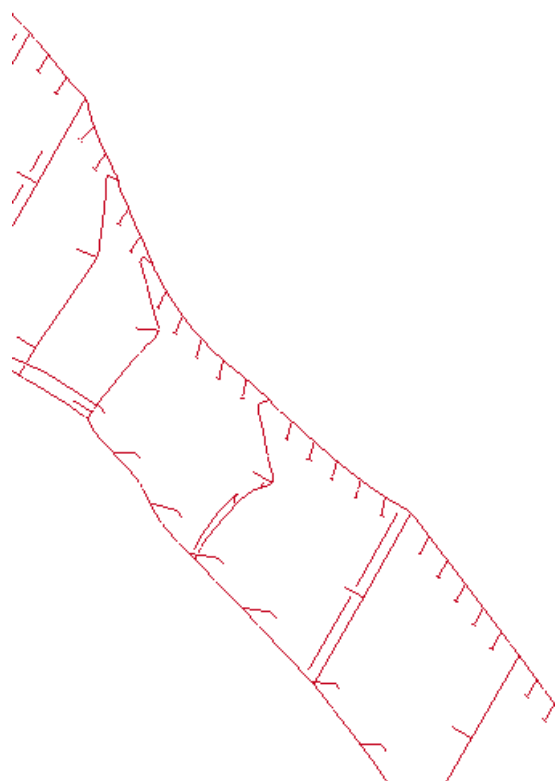
The horizontal cuts shows that the deformation for the two approaches is approximately equal at  $t=0.52$  s. This observation matches figure 8.22 well. It is also seen that the inner hull has started to deform for both approaches.



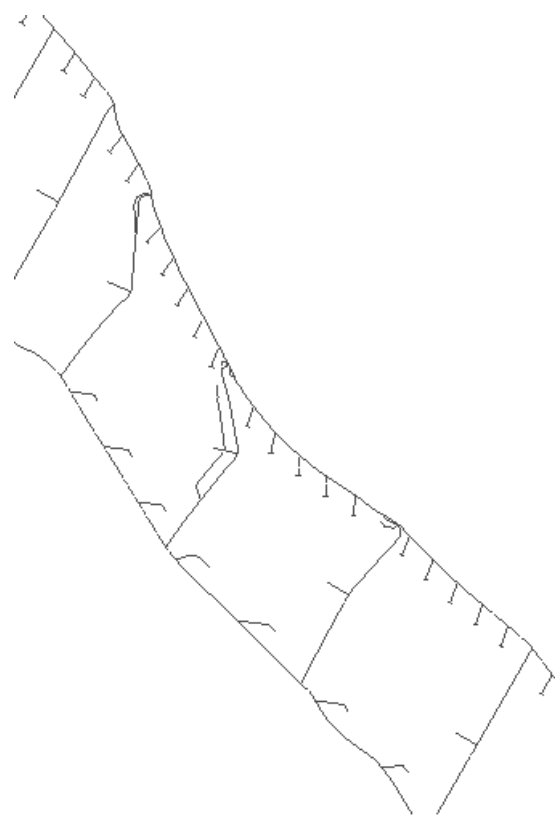
(a)  $t = 0.25$  s



(a)  $t = 0.25$  s



(b)  $t = 0.52$  s



(b)  $t = 0.52$  s

Figure 8.23: Horizontal cut for local initial velocity analysis, large iceberg,  $30^\circ$

Figure 8.24: Horizontal cut for global analysis, large iceberg,  $30^\circ$

The global simulation is as previously described analysed for a longer time than the local analysis. The deformations of the ship structure at  $t=0.88$  s are shown in figure 8.25.

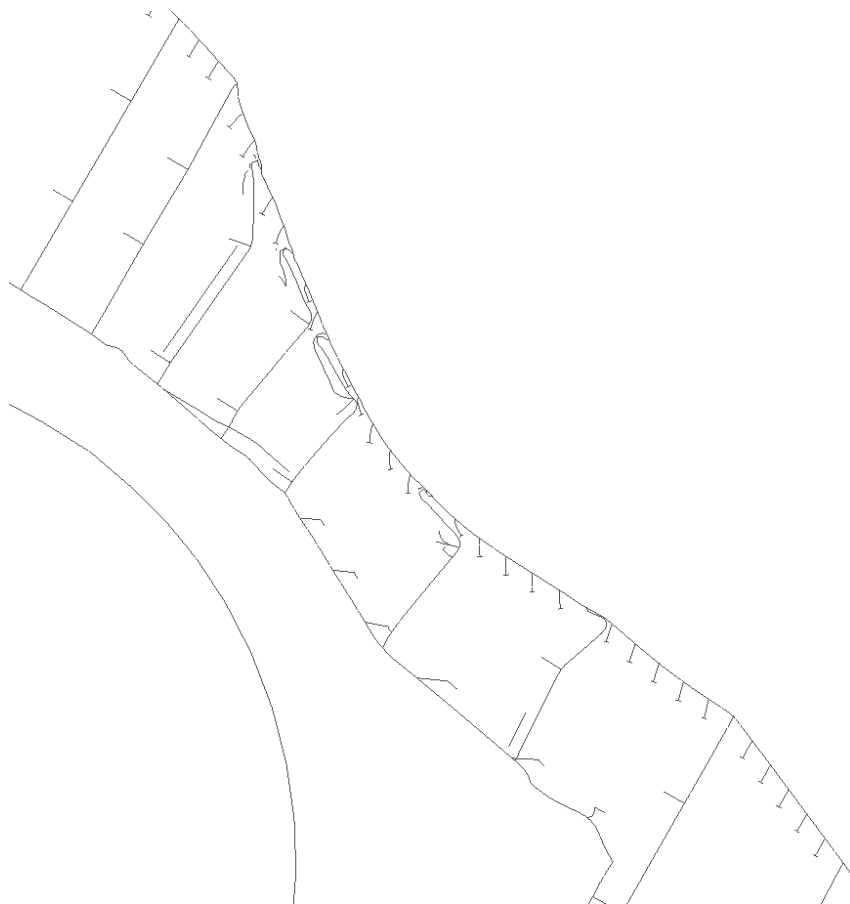


Figure 8.25: Horizontal cut for global analysis, large iceberg at  $30^\circ$  impact angle and  $t=0.88$  s

The deformations at this time step is very large. From figure 8.25 it is seen that the deformation of the inner hull is significant. On the other hand, it is seen that there still is a large distance to the cargo tank, which is shown in the left corner. From the simulations it is observed that the connection between the tank skirt and the ship structure not is deformed, but deformation of the deck at the connection has started. The impact is therefore yet not critical to the cargo, but further indentation can be critical.

### 8.3 Energy considerations

During the collision scenario, kinetic energy from the striking body will be transformed into internal and kinetic energy in the two colliding bodies. The energy will mainly be absorbed as deformation in the ship and crushing of the iceberg, but some energy will be absorbed as kinetic energy in the two bodies.

The energy absorption indicates how the two bodies will deform and move after the collision. A comparison of the energy dissipation in the different collision scenarios will therefore indicate if the simulation approach is reasonable.

As a control of the calculations performed in MATLAB, the initial kinetic energy of the iceberg in the local initial velocity analyses has been calculated by a simple hand calculation. The initial kinetic energy is given by eq. 8.2.

$$E_{kin,iceberg} = \frac{1}{2}(1 + C_{A,ice})m_{iceberg} * v_{ice}^2 \quad (8.2)$$

This equation gives an initial kinetic energy of approximately 232 MJ. This is the same value as given by the MATLAB calculation, which indicates that the result calculations are correct.

#### 8.3.1 Simplified approach - pinned local model

By comparing the internal energy of the colliding bodies for the two collision approaches, initial velocity and prescribed displacement, an indication of the difference in the deformations are found. Initially, the total energy in the system only consists of kinetic energy in the iceberg. Throughout the analysis, parts of this energy are dissipated into the ship and the iceberg, mainly as deformation and crushing respectively. For the local analyses, the ship structure in its entirety will not have any kinetic energy at the end of the simulation due to the pinned boundary conditions. Nevertheless, the deformed parts of the ship will get small amounts of kinetic energy due to the deformation motion.

#### 5.71° impact angle

The internal energy for ship and iceberg is shown for both collision approaches in figure 8.26. The horizontal and vertical lines indicate the energy levels at the same time steps as for the deformations shown in figure 8.4 and 8.5. The dissipated energy in the two bodies are approximately equal until  $t=0.25$  s. This is the same observation as done for the contact forces, and the deformations at this time step is also similar.

Throughout the simulation it is seen that the two bodies in the prescribed displacement analysis dissipates a larger amount of energy than the bodies in the initial velocity analysis. The total dissipated energy in this analysis is larger due to the kinetic energy which is not decreasing during the analysis.

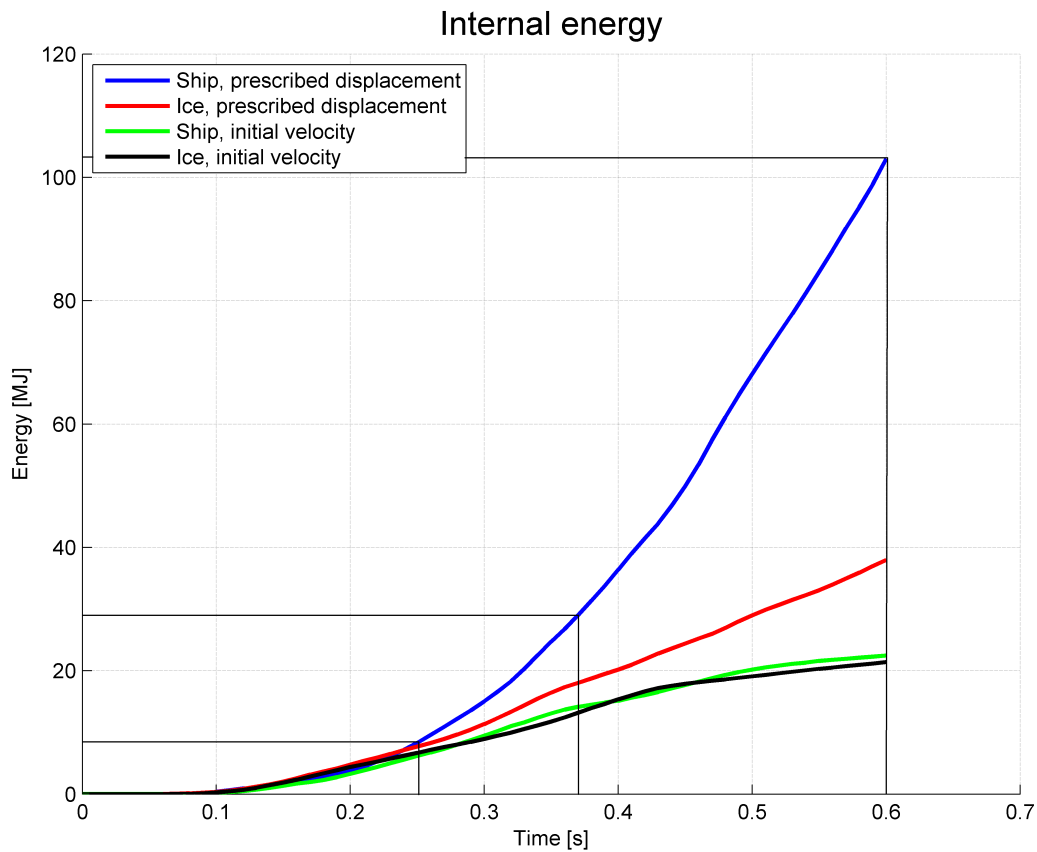


Figure 8.26: Internal energy for local initial velocity and prescribed displacement analysis,  $5.71^\circ$

The figure indicates that for the local initial velocity analysis, the ship and iceberg absorb an approximately equal amount of energy. For the prescribed displacement analysis, it seems like the ice crushing part of the total absorbed energy declines while the energy absorbed by the ship increases during the simulation. This is further discussed in section 8.4.

Figure 8.27 shows the distribution of internal energy in the iceberg for the two different simplified approaches. It is clearly seen that the largest contribution to energy absorption in the iceberg is the iceberg crushing.



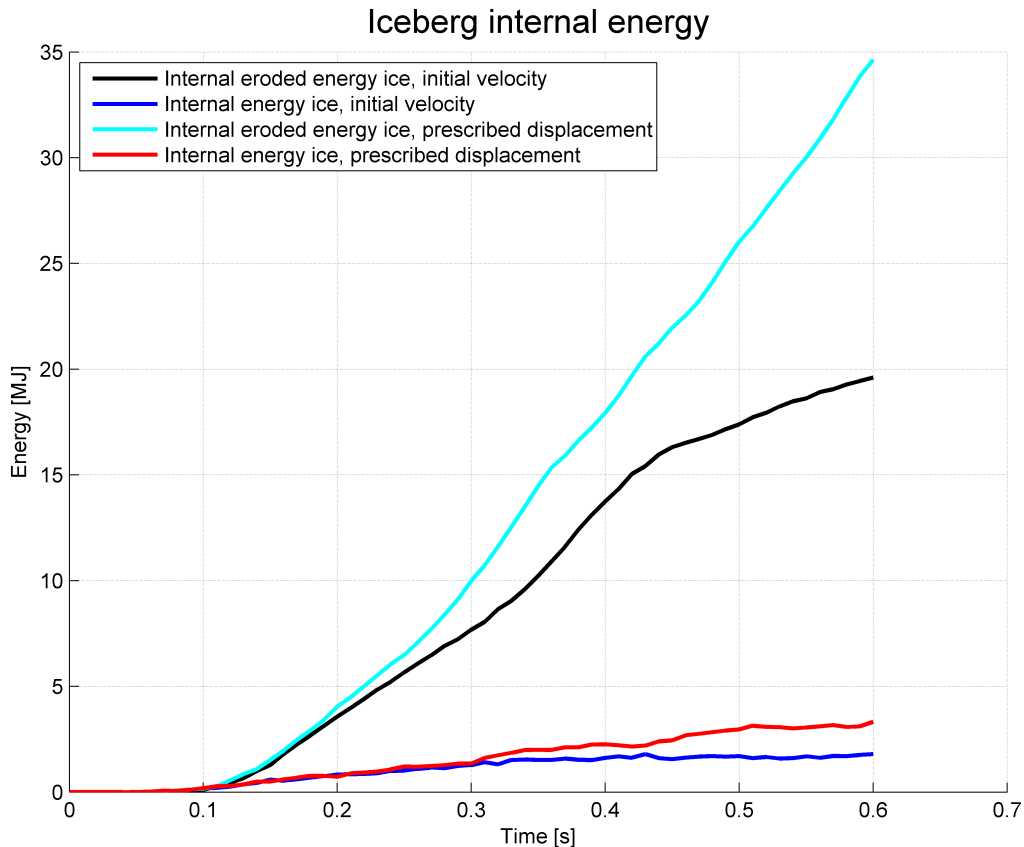


Figure 8.27: Internal iceberg energy for local initial velocity and prescribed displacement analysis,  $5.71^\circ$

As expected, the iceberg absorbs a larger amount of energy in the prescribed displacement analysis than in the initial velocity analysis. 75 % more energy is absorbed as crushing, and this supports the observation of the iceberg crushing done in figure 8.7.

### 30° impact angle

At the impact angle of  $30^\circ$  an internal energy curve which is very similar to the curve shown in figure 8.26 is obtained, see figure 8.28. The energy levels are larger, but the dissipation of the energy is similar. The prescribed displacement analysis yields very large energy levels in the ship, which indicates that the energy absorbed as ice crushing is decreasing during the simulation. This is further discussed in section 8.4. In the same way as for  $5.71^\circ$  impact angle, the total amount of energy absorbed by the two bodies in the prescribed displacement analysis is significantly larger than for the initial velocity analysis. This is also in at this impact angle caused by the kinetic energy in the iceberg which does not decrease during the analysis.

The difference in absorbed energy for the ship and the iceberg for the initial velocity analysis is larger at  $30^\circ$  impact angle than at  $5.71^\circ$  impact angle. At  $30^\circ$  impact angle the ship is absorbing significantly more energy than for the small impact angle, while the iceberg absorbs approximately the same amount of energy. This indicates that the energy absorption of the iceberg is less sensitive to the impact angle than the ship structure.

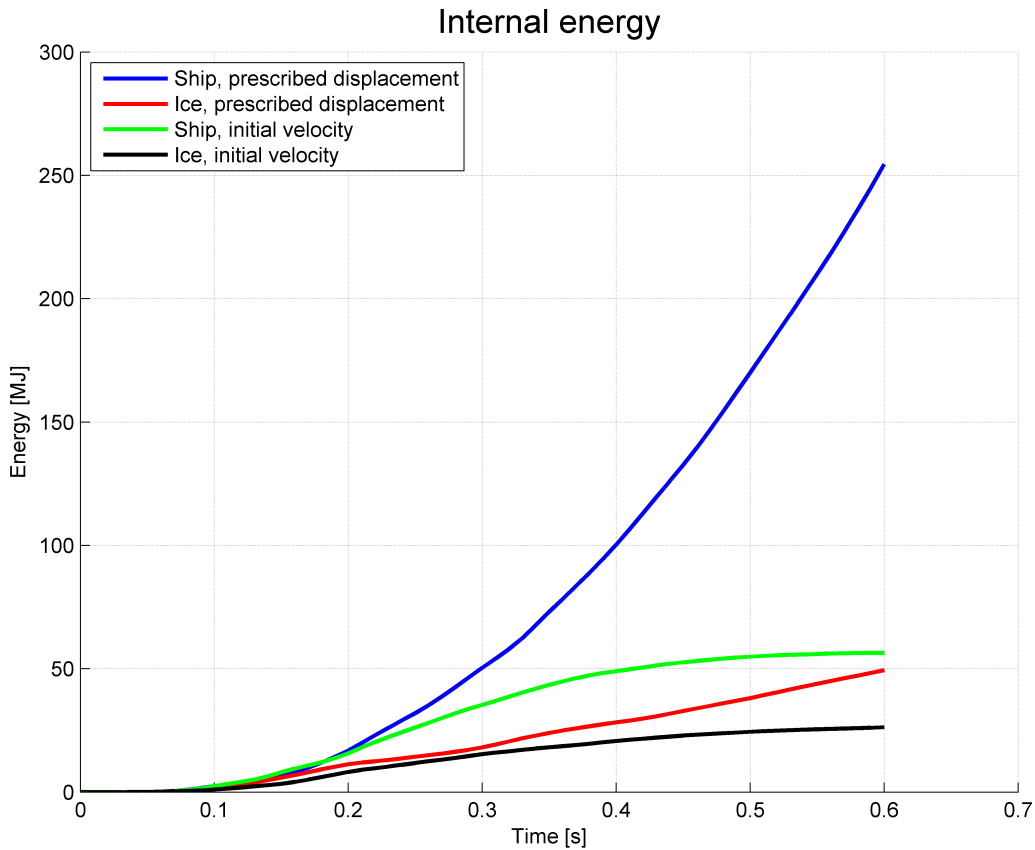


Figure 8.28: Internal energy for local initial velocity and prescribed displacement analysis, 30°

As discussed in section 8.2.1, the deformation curves indicates that a larger amount of energy is absorbed in the ship for the prescribed displacement analysis than for the initial velocity analysis for later time steps than  $t=0.25$  s. This is verified by studying the internal energies in figure 8.28. At  $t=0.25$  s it is seen that the slope of the internal energy curve in the ship for the local prescribed displacement analysis is increasing while the corresponding curve for the initial velocity analysis has a decreasing slope. It is also seen that the ship in the prescribed displacement analysis has absorbed a larger amount of energy than for the initial velocity analysis, which explains why the deformation at this stage is larger.

### 8.3.2 Local model compared to global model

#### 5.71° impact angle

The internal energy in the two colliding bodies is shown for both the global and the local initial velocity analysis in figure 8.29. The horizontal and vertical lines show the time steps for the horizontal cuts in figure 8.12 and 8.13. Also in this comparison, the internal energy in the ship for the global analysis rises in line with the energy in the local analysis until approximately 0.25 s. The deformation until this point is according to the

deformation figures similar. After this point in time, larger deformations are observed for the constrained local model. This matches the curves for internal energy well.

A remarkable observation in the internal energy curves is the energy absorbed by the ice for both analyses, which is larger than the energy absorbed by the ship. It is also seen that the total amount of absorbed energy in the two different approaches is almost the same. It is interesting to observe that for the local analysis, the energy absorption in the ship is approximately 8 MJ larger than in the global model, which will lead to a conservative result of the analysis.

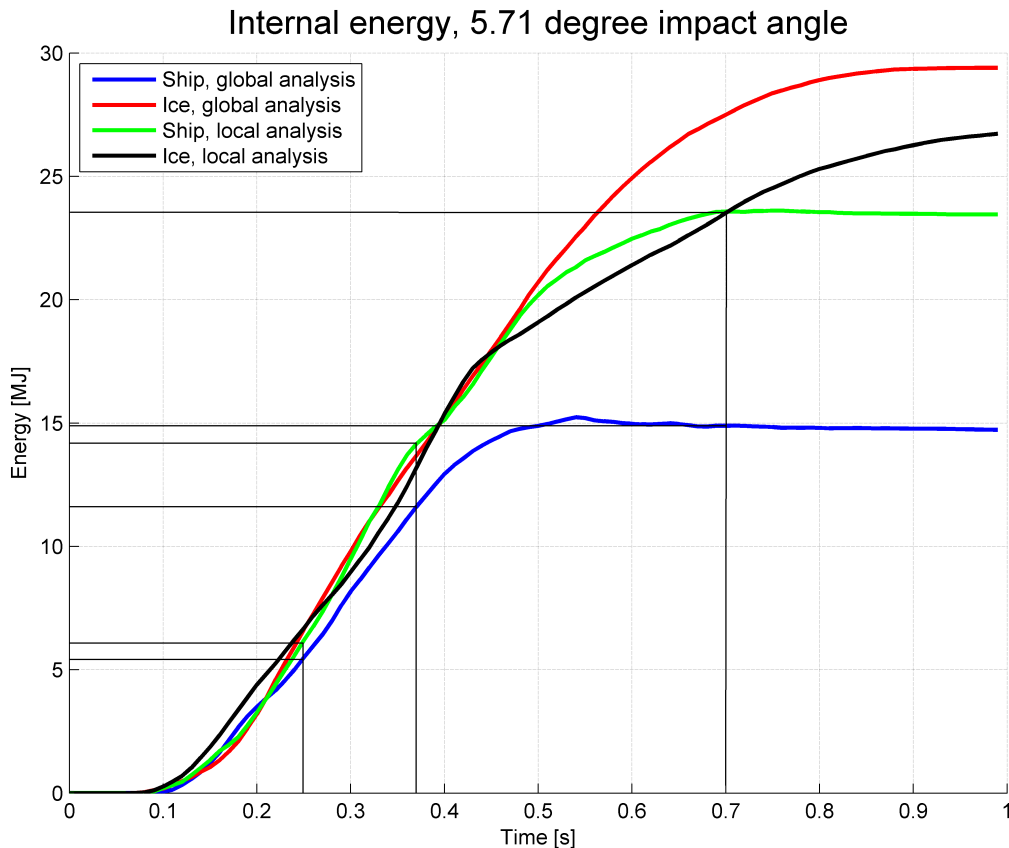


Figure 8.29: Internal energy comparison for local and global model, 5.71°

As previously stated, the internal eroded energy creates the major contribution of the energy absorption in the iceberg and is therefore the only part discussed. Figure 8.30 shows the internal eroded energy for the two different approaches. The energy absorbed by the iceberg for the global analysis is larger than for the local initial velocity analysis. In section 8.2.2 it is shown that the local analysis yields significantly larger deformation in the ship than the global analysis. The eroded ice energy indicates then that a large amount of the energy in the global analysis is absorbed by the iceberg.

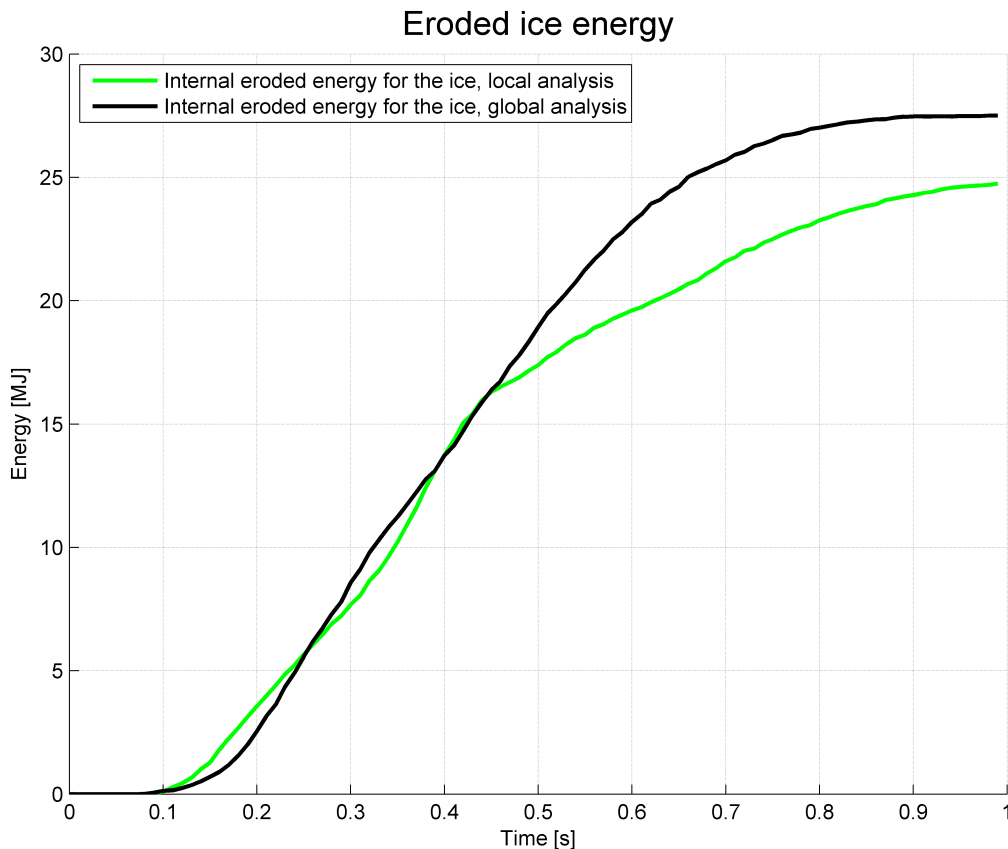


Figure 8.30: Ice energy comparison for local and global model, 5.71°

### 30° impact angle

When comparing the local analysis with the global analysis for an impact angle of 30°, it is interesting to observe that the internal energy in the ship for the global analysis is of the same magnitude as the internal energy for the ship in the simplified approach. The internal energy for the local analysis is slightly larger, but the difference is small. Based on figure 8.31, the deformations in the ship are expected to be of equal magnitude. In section 8.2.2 a significant difference in the deformations of the two approaches was found. These two observations do not match each other, and this is probably due to the presentation method of the force-indentation relationship.

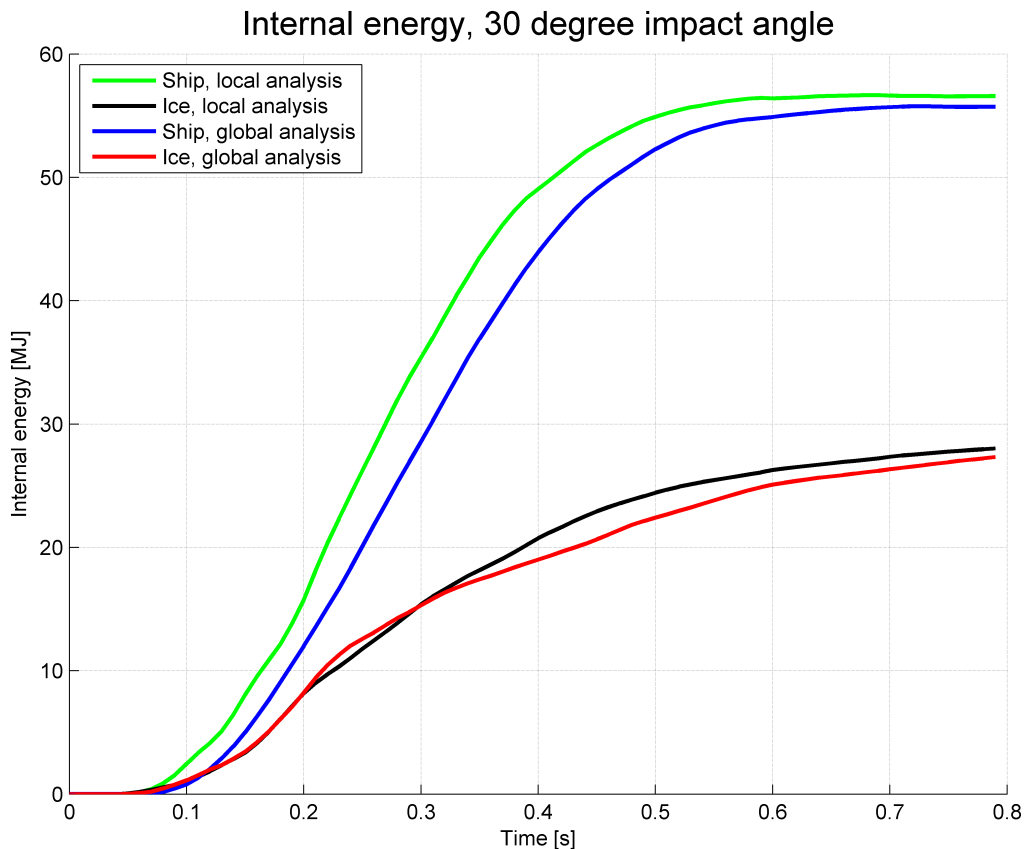


Figure 8.31: Internal energy comparison for local and global analysis, 30°

The force-indentation relationship given in figure 8.16 is based on the maximum node displacement, but no information on the deformation pattern is given by this figure. This means that the total absorbed energy is not represented by the given force-displacement relationship. The internal energy curve can therefore, despite the non-logical connection between the force-displacement curve and the internal energy curve, give a good representation of the physics in the real collision scenario.

It is interesting to see the difference between 5.71° impact and 30° impact. The absorbed energy is significantly larger for the 30° impact, and it seems like the local analysis for 30° impact angle gives a more realistic approach of the real scenario than for the small impact angle. The local analysis is more conservative regarding energy absorption for the small impact angle than for the large impact angle. The explanation to this is probably complex, but, based on the simulations, one of the reasons seems to be that the deflection of the iceberg is larger for the global analysis than for the local analysis at 5.71° impact angle. This deflection is not seen to the same extent at 30° impact angle.

Figure 8.32 shows the internal eroded energy in the iceberg for the two discussed collision approaches. Based on the curves the deformation of the icebergs seems to be similar, which is an observation that matches the visual comparison done in figure 8.19.

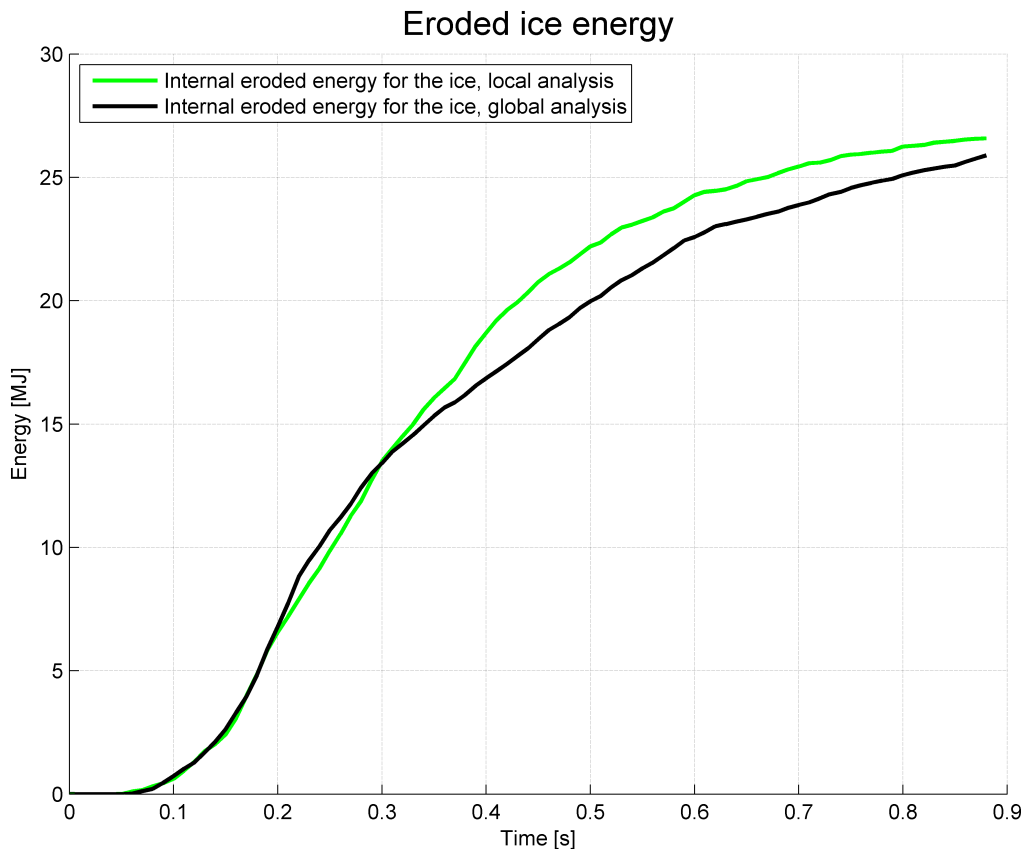


Figure 8.32: Ice energy comparison for local and global analysis,  $30^\circ$  impact angle

### 8.3.3 Comparison of both impact angles for global model

A figure showing the internal energy for the two global analyses with impact angles  $5.71^\circ$  and  $30^\circ$  is presented in figure 8.33. As the deformation plots in section 8.2.3 indicated, the absorbed energy in both ship and iceberg is significantly larger for the impact angle of  $30^\circ$ . The total amount of absorbed energy at  $30^\circ$  impact angle is approximately twice as large as for  $5.71^\circ$  impact angle, and it is clear that a collision at this impact angle is more critical for the ship. On the other hand, it is seen from the deformation figures that no visible deformations are found in the inner hull. The plastic strains are investigated in section 8.5, and based on these strains it is possible to verify if fracture is reached in the outer shell.

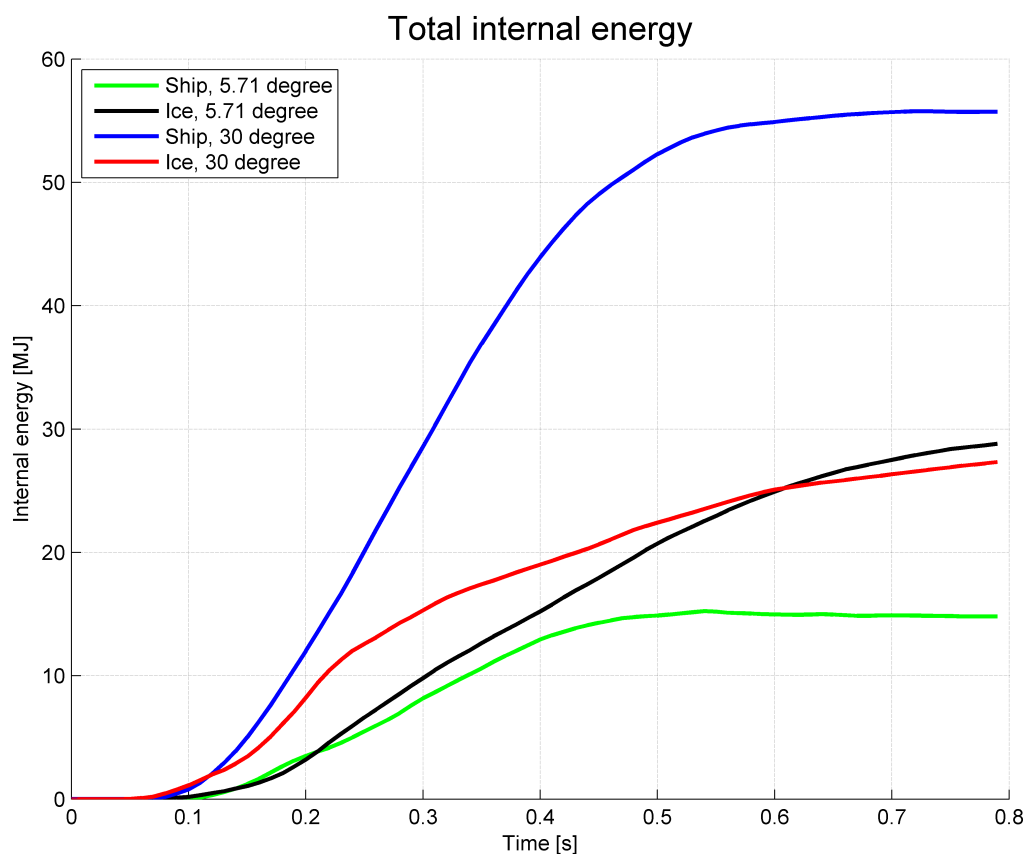


Figure 8.33: Comparison of internal energy for both impact angles, global model

### 8.3.4 Large iceberg

When the forces and deformations caused by the large iceberg were considered, the results from the local initial velocity analysis and the global analysis were very similar. Based on this, similar energy absorption of the two methods is expected. The energy absorption for both ship and iceberg is shown for both approaches in figure 8.34.

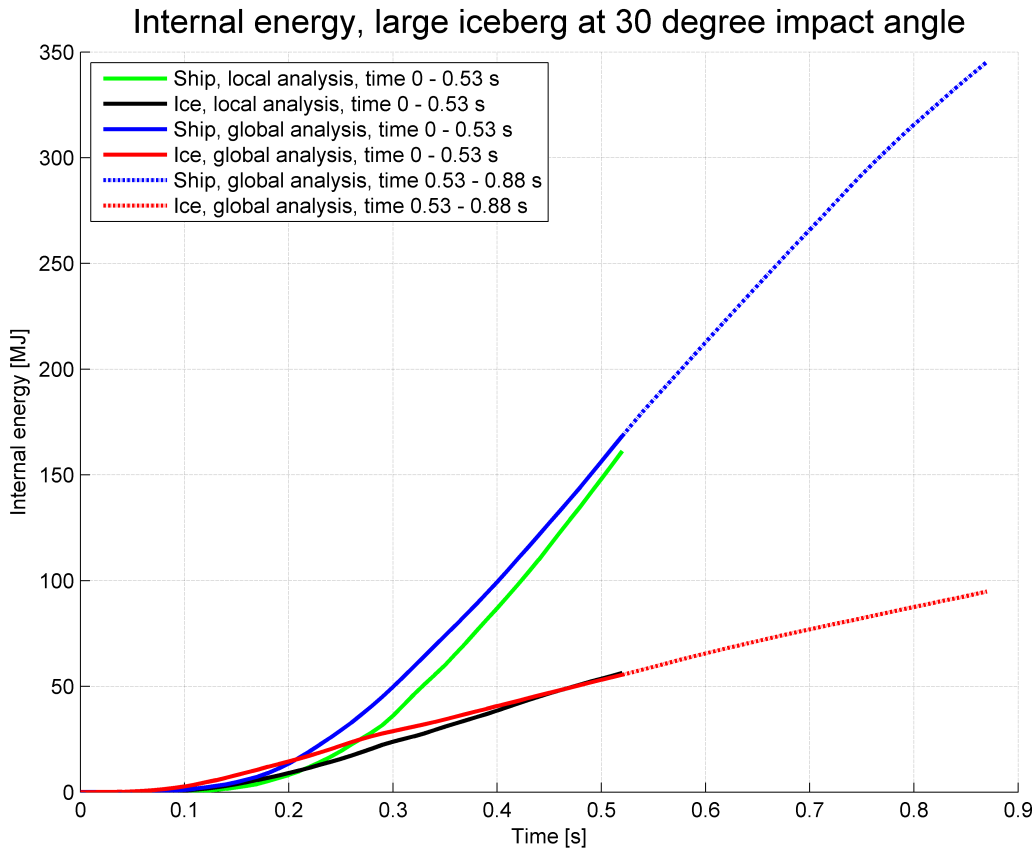


Figure 8.34: Internal energy, large iceberg at 30° impact angle

It is seen that the absorption of energy is very similar both for the ship and the iceberg. This was expected based on the deformation considerations. On the other hand, the result deviates from what was expected based on the physics. For the large iceberg it was expected that the pinned boundary conditions of the local model should influence the result to a larger extent than for the small iceberg. It was assumed that significantly larger deformations should be obtained from the local analysis than for the global analysis due to large deflection of the ship in the global analysis. Based on the energy absorption, this effect seems to be over-estimated.

The energy absorption for the last time steps which is analysed for the global model only is given in the figure as dotted lines. It is clearly seen that both ship and iceberg is absorbing more energy, and especially the ship will absorb a large amount of energy as absorption.

## 8.4 Ice crushing energy

### 5.71° impact angle

To investigate the distribution of the absorbed energy between the ship and the iceberg, the total internal energy in the iceberg are divided by the total dissipated energy to get



an energy ratio for the iceberg absorption. This energy ratio is then plotted against the total internal energy in the system. The ration for the different approaches is shown in figure 8.35.

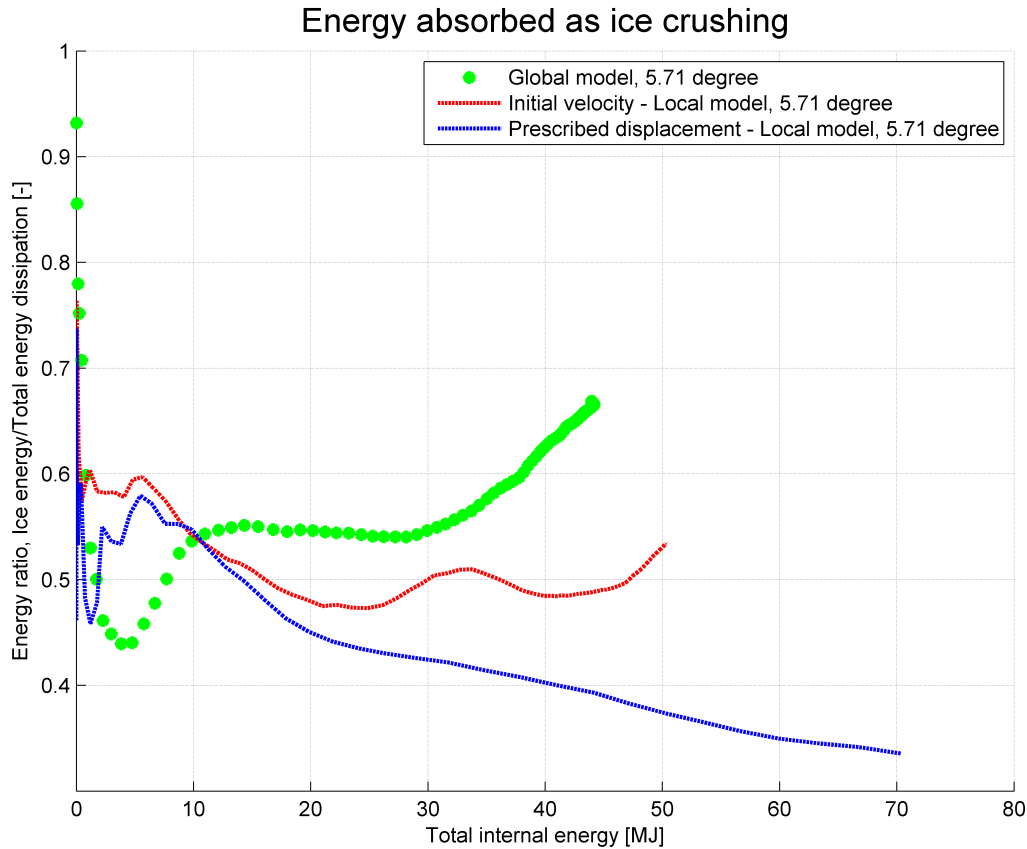


Figure 8.35: Energy ratio for ice crushing, 5.71° impact angle

From the figure it is seen that for the local prescribed displacement analysis, the energy absorption in the iceberg is decreasing throughout the simulation. This means that the ratio of energy absorption in the ship must increase during the analysis. For the local initial analysis and the global analysis no clear trend is seen.

### 30° impact angle

For 30° impact angle the same trend as for 5.71° impact angle is seen for the local prescribed displacement analysis. At this impact angle it seems like the local initial velocity analysis and the global analysis also has a decreasing trend during the simulation. This trend seems realistic since the resistance of the ship structure will decrease when it is deformed.

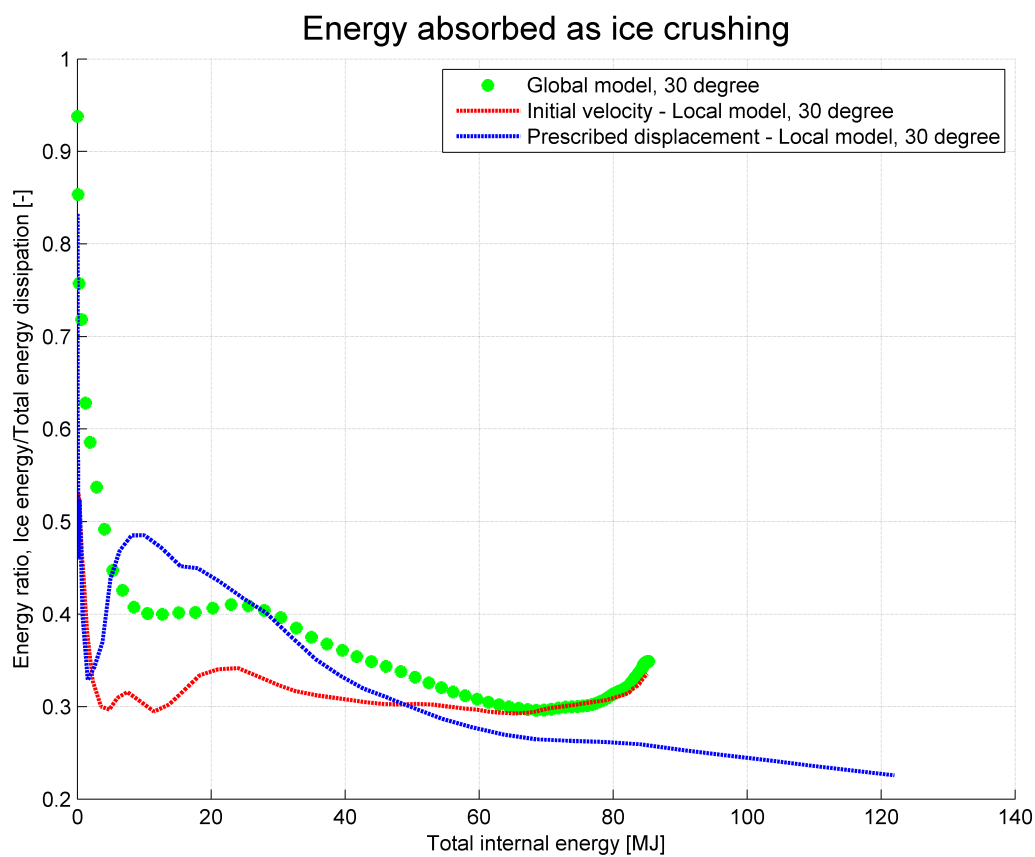


Figure 8.36: Energy ratio for ice crushing, 30° impact angle

## 8.5 Plastic strain

Collapse of the elements is based on the plastic strain in each element. The damage is calculated from the RTCL criterion in the material model, described in section 6.1.4, and the element is removed when the damage exceeds the criterion. The damage is also scaled by mesh size and it is therefore difficult to know exactly for which strain the element is collapsing.

In the following sections the plastic strain is presented with example screenshots from the outer shell and transverse frames. To show the difference between the different analysis methods, screenshots are shown for the local initial velocity and prescribed displacement analysis and the global analysis for 5.71° impact angle. The critical strains for all analyses are given in table 8.1 in section 8.5.4. More screenshots of the plastic strains are shown in appendix B.

### 8.5.1 Local initial velocity analysis

#### 5.71° impact angle

The first impact angle which is investigated is 5.71°. At this impact angle, as seen from figure 8.37, large deformations of the outer shell and the transverse frames are obtained. The yield stress of the steel material model is given as  $\sigma_y = 285 \text{ MPa}$ . Based on the figure, we can see that plastic strain of approximately 18 % is obtained in the outer shell.

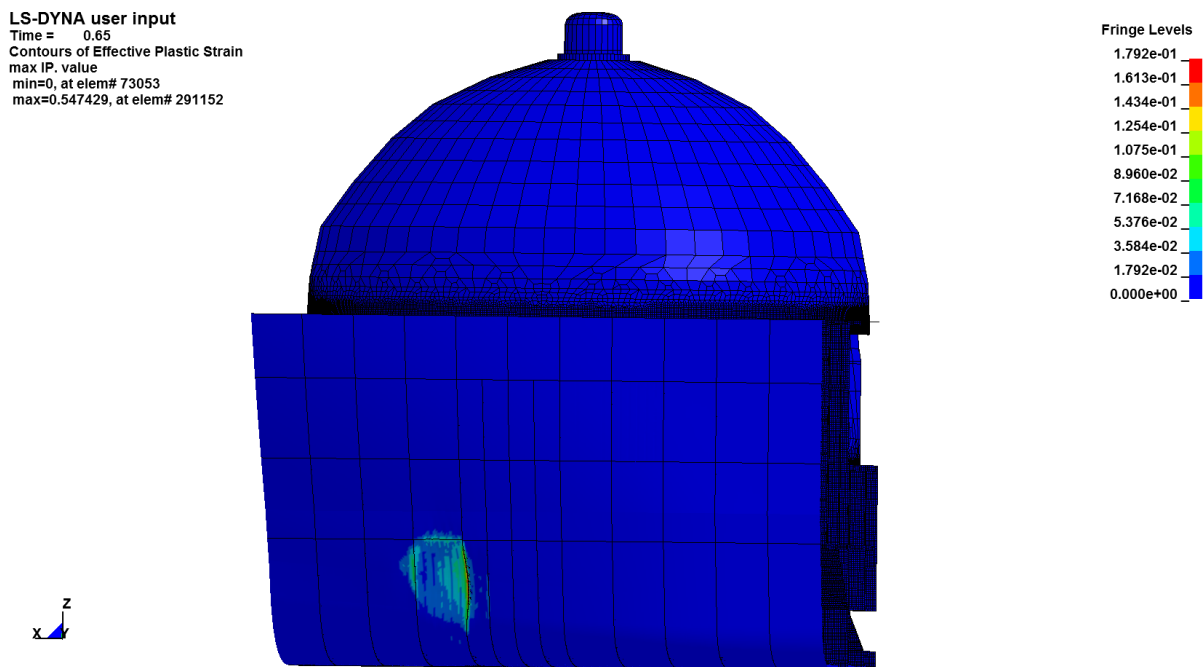


Figure 8.37: Plastic strain at local 5.71° initial velocity impact

Larger plastic strain is obtained in the transverse frames, see figure 8.38b. Here, plastic strain of more than 30 % is observed. At this stage, some of the elements in the transverse frame stiffeners has reached the maximum allowed plastic strain and is collapsing.

This level of plastic strain is higher than maximum allowed strain in regulations for ship structures, but it is interesting to observe the strains in the ship structure beyond these regulations.

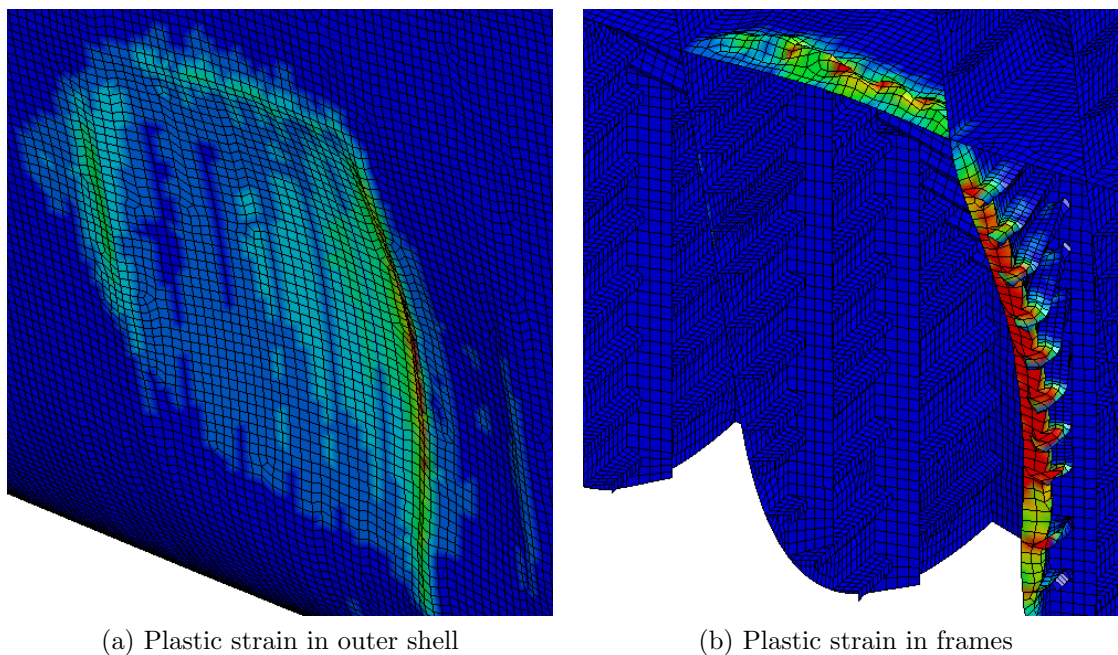


Figure 8.38: Plastic strain in outer shell and vertical frames, initial velocity for local analysis,  $5.71^\circ$ .

It is difficult to clearly see how the frame will deform by studying the screenshot of the plastic strain. The deformation of the frames can be seen in the horizontal cuts in section 8.2. The deformation of the frames in figure 8.38b can be seen in figure 8.4d.

## 8.5.2 Prescribed displacement for local model

### 5.71° impact angle

Compared to the initial velocity analysis, the difference in plastic strain is large when studying the prescribed displacement analysis. Figure 8.39 shows the plastic strain in the outer hull and the transverse frames with the same color scaling as for the initial velocity.

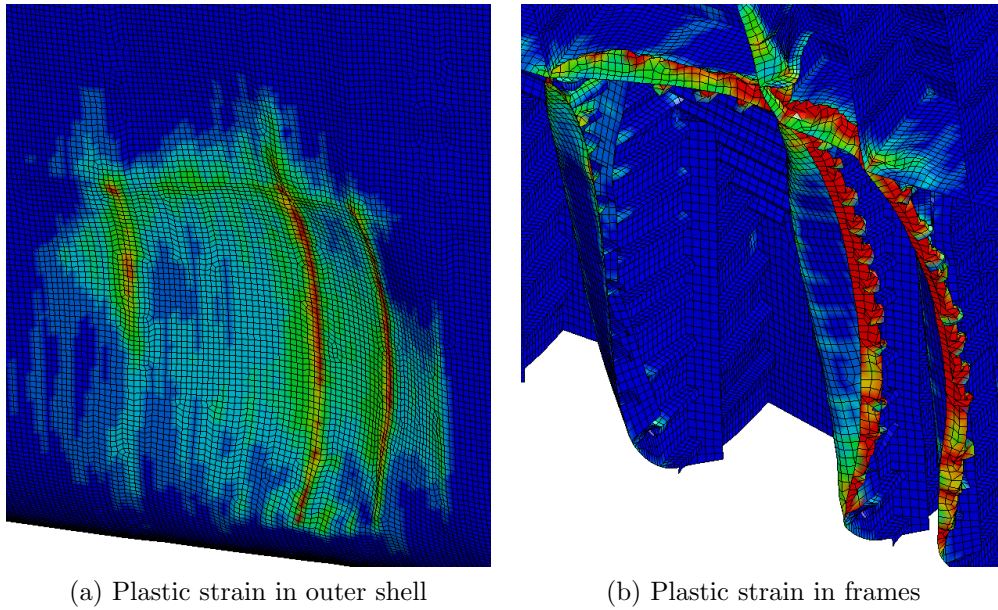


Figure 8.39: Plastic strain in outer shell and vertical frames, prescribed displacement analysis for the local model, 5.71°.

It is seen that especially the transverse frames have larger plastic strain than the maximum level of the color scale, which is approximately 18 %. Figure 8.40 shows the same frames as figure 8.39b, here with scale up to 30 %. It is seen that strains of more than 30 % are found in large areas of two of the transverse frames, and elements in these frames have started to collapse.

As for the initial velocity analysis, it is difficult to study the deformations from these screenshots. Figure 8.5d can be used to better observe the maximum deformation of the transverse frames.

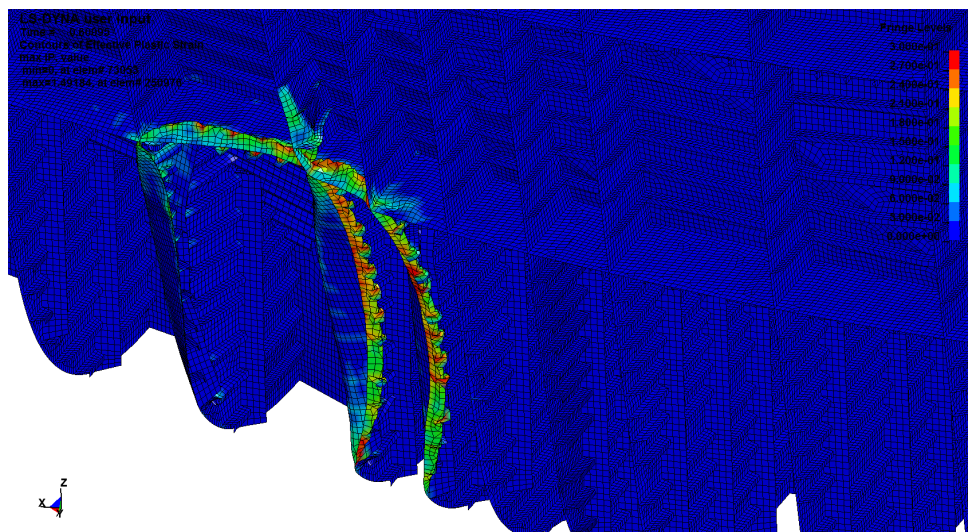


Figure 8.40: Plastic strain at 5.71° prescribed displacement impact on local model

### 8.5.3 Global model

#### 5.71° impact angle

After studying the contact forces, deformations and internal energies from the global analysis for 5.71° impact angle, it is expected that the plastic strains obtained from this analysis is smaller than for the simplified analysis. Figure 8.41 shows the plastic strain in the same scale as for the other analyses. It is clearly seen that the strains obtained is smaller than for the simplified analyses, and the critical strain is given as approximately 14 %. This strain is not critical to the material, and indicates that the ship will resist an impact of an iceberg of this size.

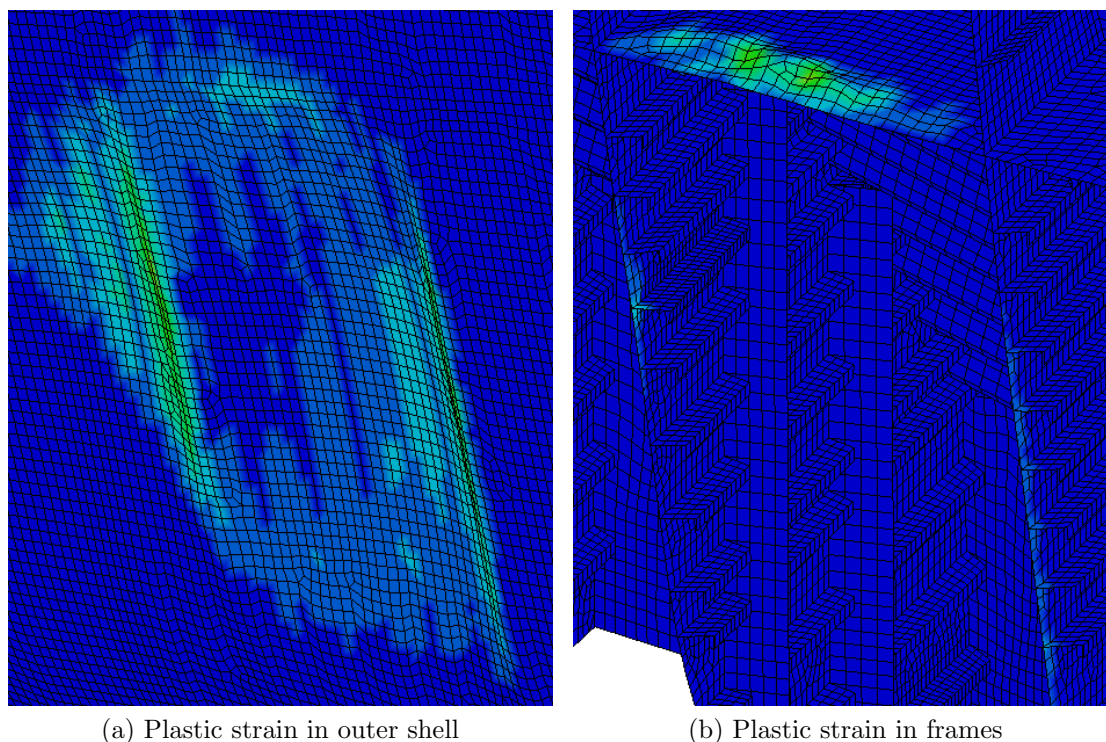


Figure 8.41: Plastic strain in outer shell and vertical frames, global model, 5.71°.

#### 8.5.4 Observed plastic strains for all analyses

The largest observed plastic strains for the different analyses are shown in table 8.1. All the largest strains are observed in the transverse frames.

<b>Local initial velocity</b>	
Impact angle	Strain
5.71°	28-30 %
30°	30-35 %
<b>Local prescribed displacement</b>	
Impact angle	Strain
5.71°	30-35 %
30°	30-35 %
<b>Global initial velocity</b>	
Impact angle	Strain
5.71°	12-14 %
30°	30-35 %
<b>Large iceberg</b>	
Analysis	Strain
Local	30-35 %
Global	30-35 %

Table 8.1: Largest observed plastic strains for the different analyses

As seen from the table, it is difficult to conclude on the conservatism of the simplified local approaches based on the plastic strains. No collapse of elements is observed during the simulated analyses, but this is probably due to too short simulated time.

On the other hand, it is clearly seen the difference between the two impact angles for the global simulation. As seen from all the other considered results, the simulations of 5.71° impact angle yields significantly smaller strains than the other analyses. An impact of a 2500 tons iceberg at 5.71 degree impact angle seems therefore not to be critical to the ship structure.

## 8.6 Accelerations, velocities and deformations

In previously investigated collision scenarios, e.g. in numerical simulations carried out by InnoQual Co., Ltd, [7], unreasonable large accelerations are found in spots in large distance from the collision point. In these simulations, a cubic iceberg with collision point at the flat side is used. This can cause large vibrations in the ship structure, which again can lead to large accelerations.

Accelerations of large magnitude are also found in the simulations performed by Stine Aas Myhre, [2], and Andreas Berling, [17]. To investigate if this is a problem in the collisions simulated in this thesis, the accelerations, velocities and displacements at three spots in the fastening point of the tank are observed. The three different spots are shown in figure 8.42.

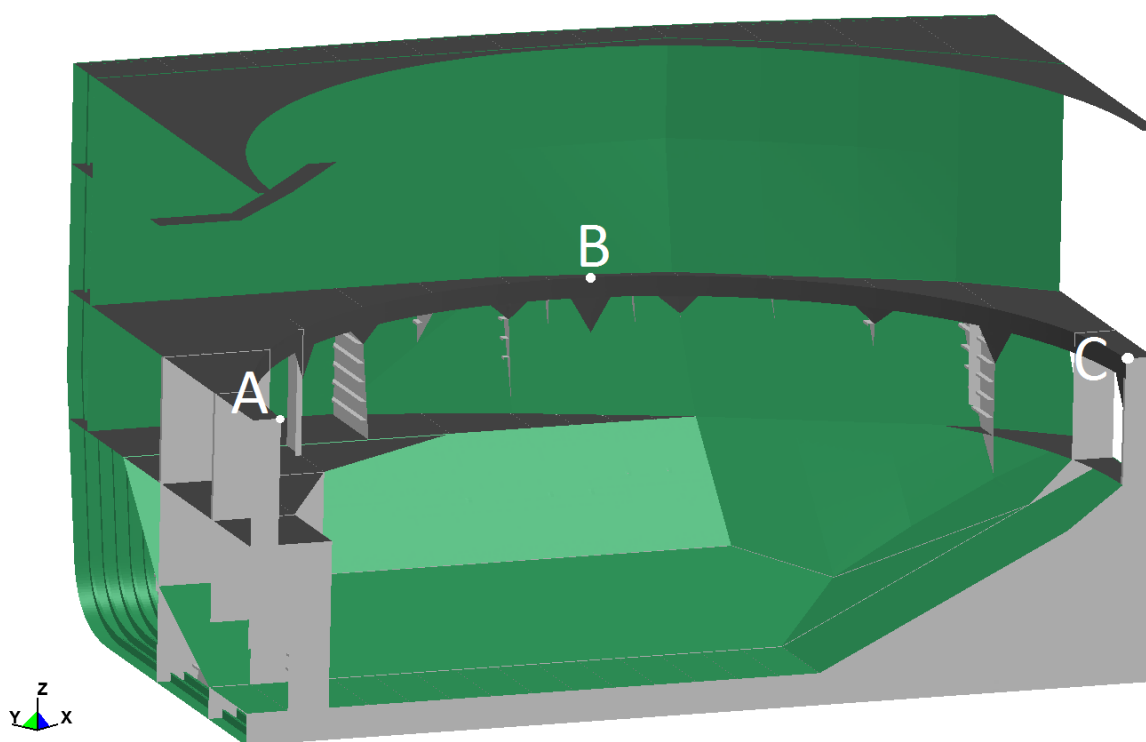


Figure 8.42: Spots for measuring accelerations

In addition to these spots, two points in the top of the tank cover and tank tower are observed. These points are shown in figure 8.43. The relative motion between these two parts is critical for small displacements due to the tank tower. This tower includes motion sensitive parts, and an impact between the tank tower and the tank cover is therefore critical. The tank tower has for a real ship a cover surrounding it, but this detail is not modelled.



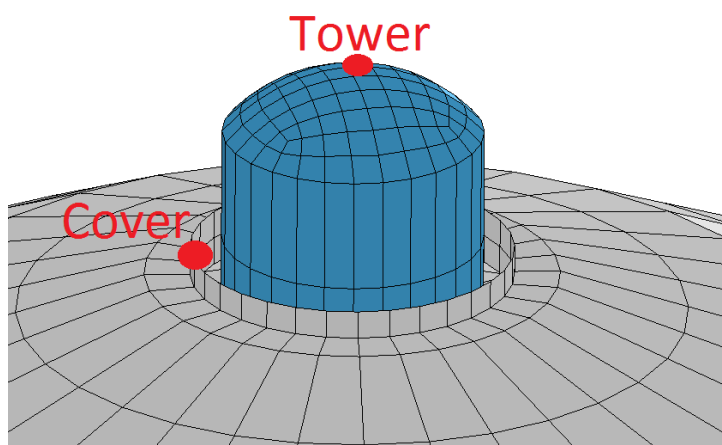


Figure 8.43: Spots for measuring accelerations in tank tower

To ensure that the possible motions are observed if they occur in any of the simulation methods, all the discussed spots are investigated for all of the three methods. It is assumed that the largest motions occur for the largest contact forces, and the investigated simulations are therefore all simulating impact at  $30^\circ$  angle.

### 8.6.1 Local initial velocity analysis

For the local initial velocity simulation, the nodes at the centre line are pinned and will therefore not move. The observed spots at the centre line are therefore moved a couple of meters against the outer hull. The observations show that only point B and the two points in the top of the tank are exposed to accelerations. As seen from figure 8.44, some large accelerations are found in point B. These are of magnitude up to approximately  $50 \text{ m/s}^2$  and they seem like very short impulses. The magnitude of these are nevertheless significantly lower than the accelerations observed in the previously discussed reports, which are of magnitude  $500 - 1500 \text{ m/s}^2$ . According to this, it is concluded that the accelerations obtained in the simplified initial velocity analyses in this thesis are not critical.

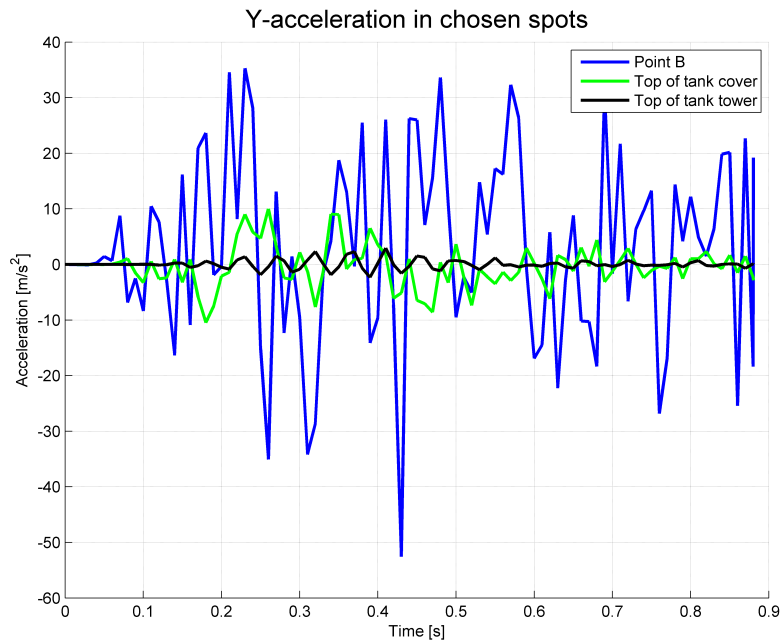


Figure 8.44: Acceleration curves for the given spots, local initial velocity analysis,  $30^\circ$

The velocities and deformations found in the given spots support the conclusion stating that the accelerations not are critical. As seen from figure 8.45 and 8.46, very small velocities and even smaller displacements are observed in the spots. A displacement of 3 mm can be regarded as neglectable.

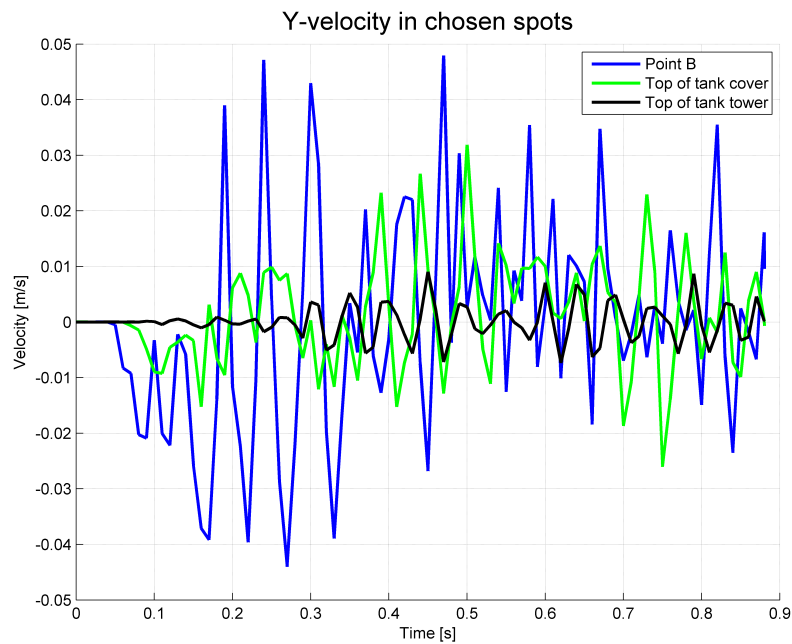


Figure 8.45: Velocity curves for the given spots, local initial velocity analysis,  $30^\circ$

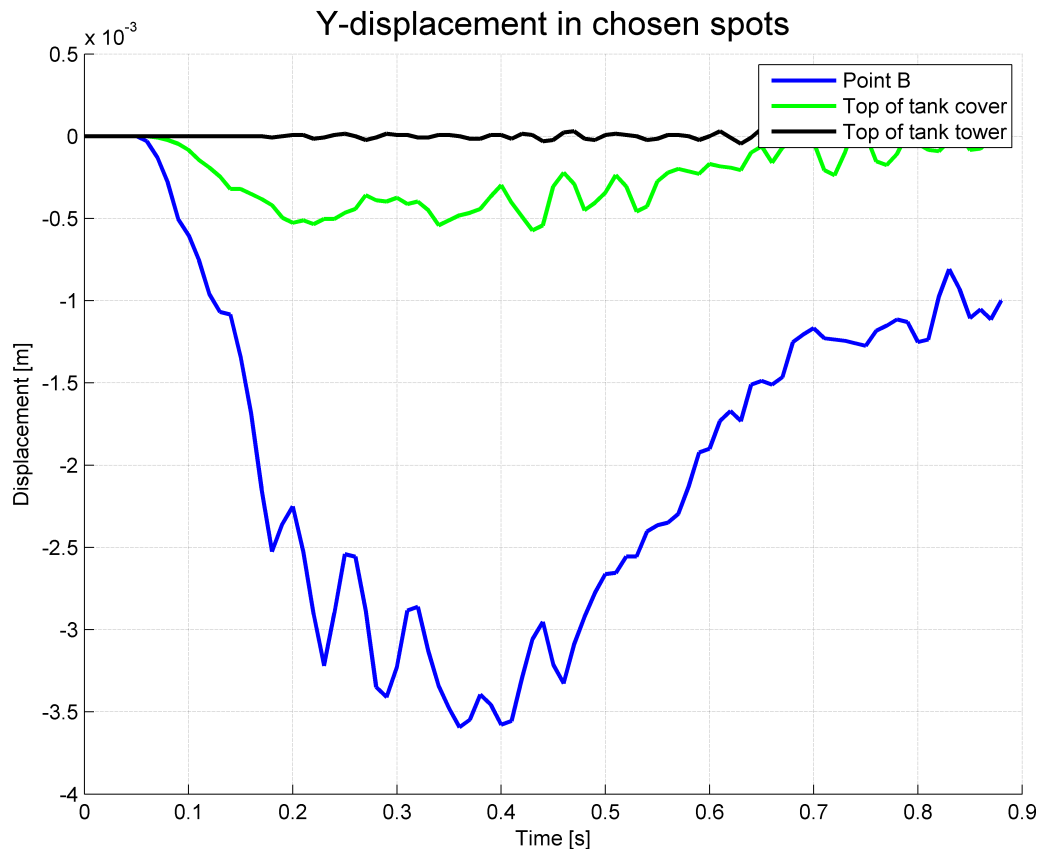


Figure 8.46: Deformation curves for the given spots, local initial velocity analysis, 30°

### 8.6.2 Local prescribed displacement analysis

In the same way as for the local initial velocity simulation, the nodes at the centre line are pinned for the local prescribed displacement analysis. Some accelerations are found in point A and C near the centre line, but these are of smaller magnitude than in point B. The accelerations in point B and the tank tower and cover are given in figure 8.47.

The accelerations which occur in this simulation method are larger than in the initial velocity method. The prescribed displacement method is used in the discussed reports where the extreme values of accelerations was found, and it is interesting to see that such accelerations do not occur in the analyses performed in this thesis. The impact point of the iceberg used in this thesis is at the corner, which means that the impact will be softer than if the impact point is the flat side of a box shaped iceberg. This contributes to lower vibrations in the hull, and therefore lower accelerations.

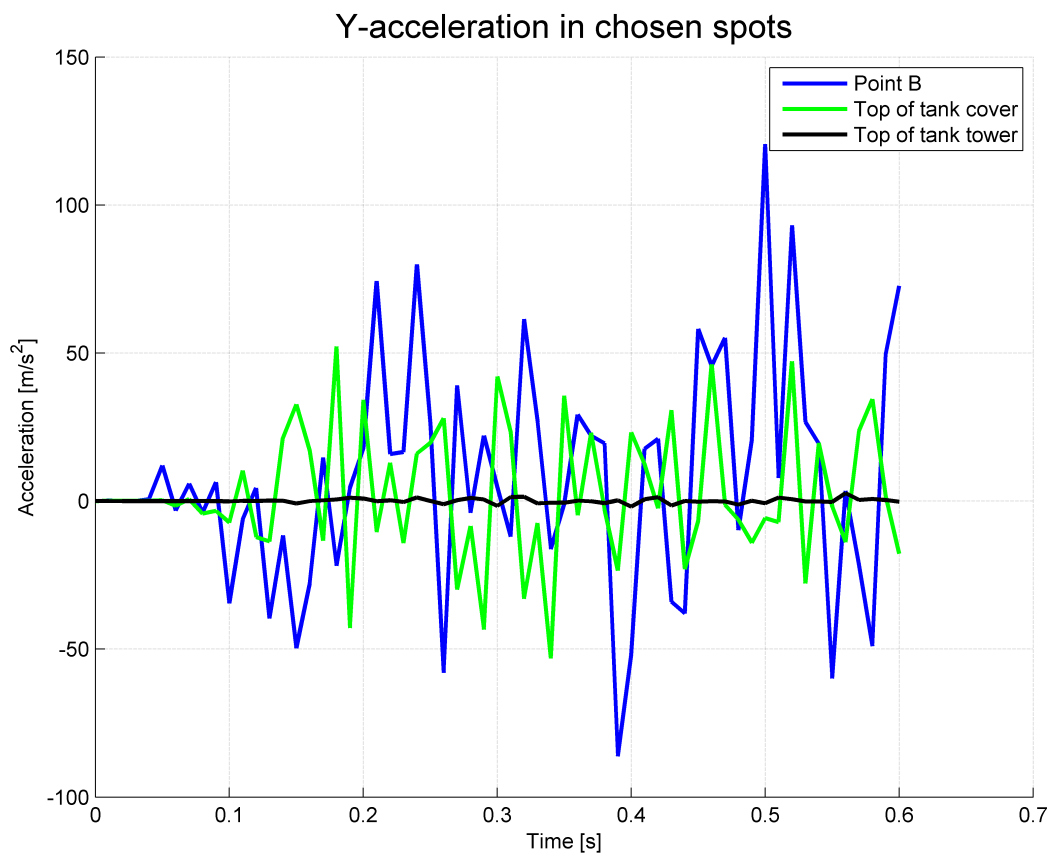


Figure 8.47: Acceleration curves for the given spots, local prescribed displacement analysis, 30°

The displacements at the discussed locations are given in figure 8.48. As seen from the y-axis of the figure the largest displacements are of magnitude 10 mm. The displacement at point B is larger than the points observed in the top of the tank and directed in negative y-direction due to the deformation of the hull which is very large for the prescribed displacement analysis. A displacement of 13 mm is nevertheless not critical. The relative displacement between the top of the tank tower and the tank cover is rather not critical.

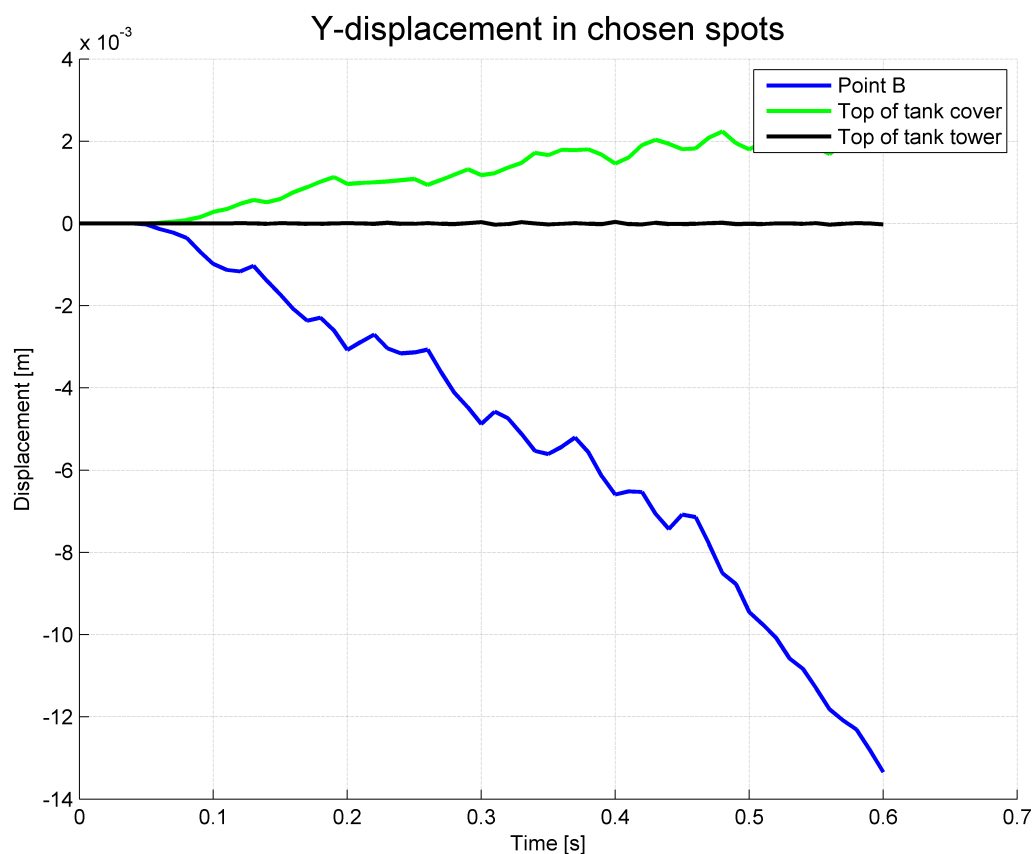


Figure 8.48: Deformation curves for the given spots, local prescribed displacement analysis,  $30^\circ$

### 8.6.3 Global model

For the global analysis the accelerations observed are smaller than for the local analyses. This is as expected since the global model will contribute to larger damping of the collision. Motions are only observed for point B and the two points in the top of the tank, and the accelerations are shown in figure 8.49.

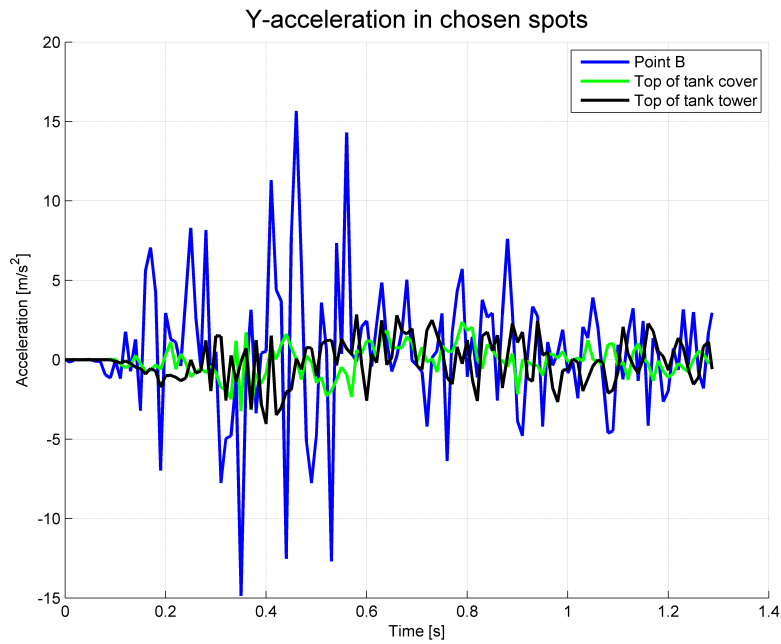


Figure 8.49: Acceleration curves for the given spots, global analysis, 30°

As previously described, it is interesting to investigate the relative motion between the tank cover and the tank tower. As seen from figure 8.50, the largest difference in motion for these two points is approximately 2 cm. The reason for the total displacement of approximately 16 cm is the deflection of the ship throughout the collision which appears since no boundary conditions are applied to the ship in this analysis.

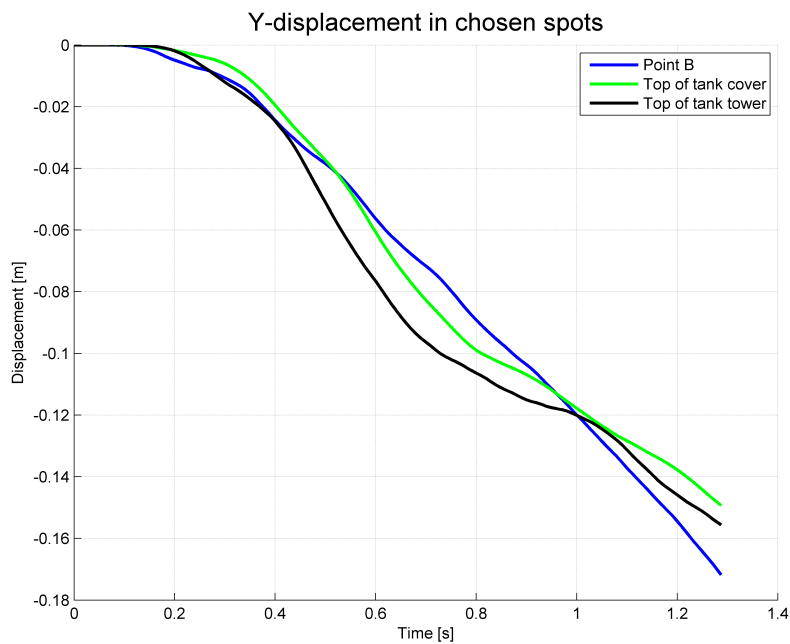


Figure 8.50: Deformation curves for the given spots, global analysis, 30°

### 8.6.4 Large iceberg

For the collision with the large iceberg both larger forces, deformations and energy levels are obtained. Larger vibrations in the hull are expected, and this will cause larger accelerations in the discussed points. The accelerations in these points are shown in figure 8.51. As shown in the figure, the accelerations for the large iceberg impact is lower than for the local prescribed displacement analysis with small iceberg. The damping in the global system contributes to smaller vibrations, and large acceleration seems not to be a problem in any of the analyses performed in this thesis.

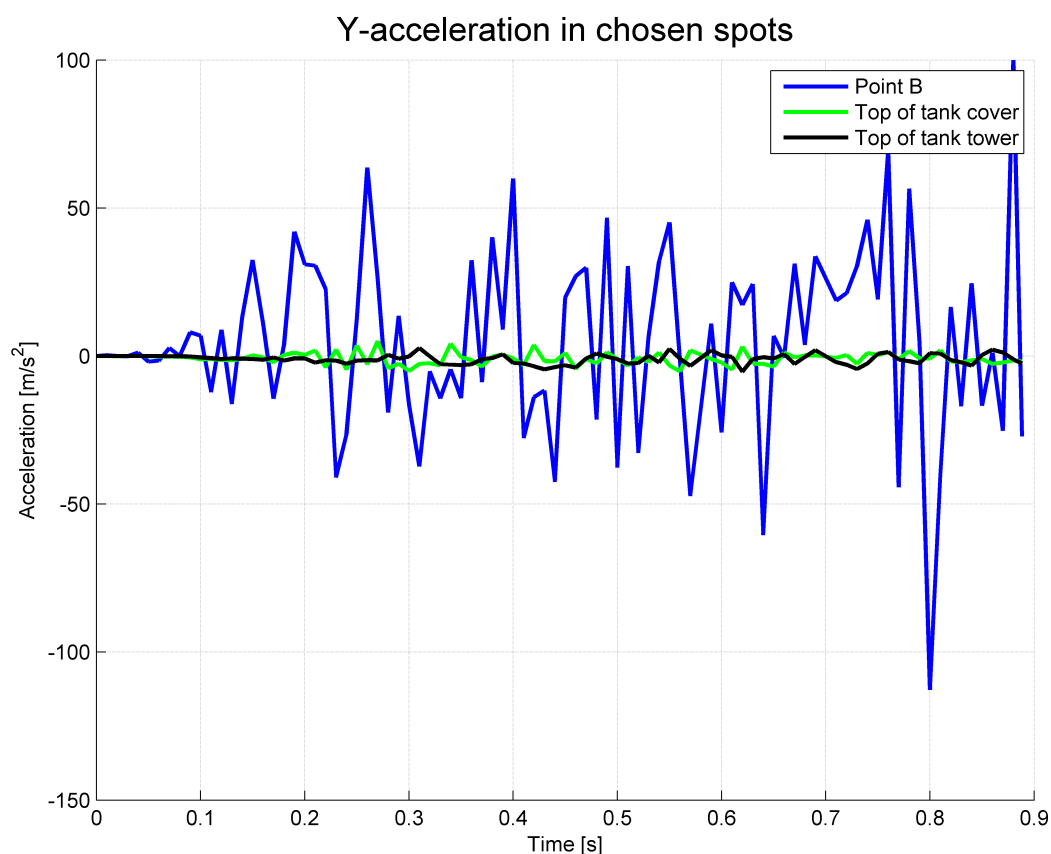


Figure 8.51: Acceleration curves for the given spots, global analysis, large iceberg, 30°

The displacement of the two spots in the top of the tank tower and cover needs to be controlled also for the large iceberg impact. The displacements are shown in figure 8.52.

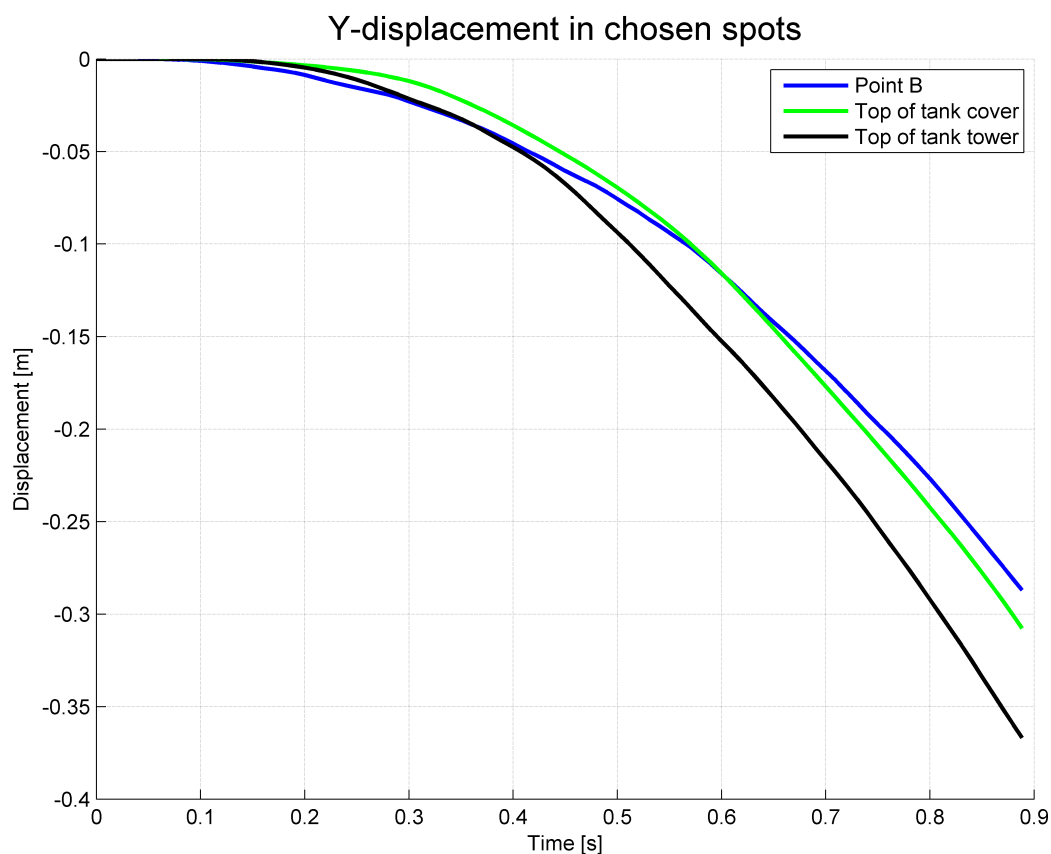


Figure 8.52: Deformation curves for the given spots, global analysis, large iceberg, 30°

The relative displacement obtained from the simulation is 5 cm. This is larger than for the previously described simulations, but still not critical. On the other hand, such relative displacement is remarkable, and only a limited further increase in this displacement can be allowed. The resultant displacement is checked, and this yields not larger relative displacement between these points.



### 8.7 External mechanics

When simplified methods for collision scenarios are used on simplified geometry, i.e. prescribed displacement or initial velocity analysis on local models, the expected dissipated energy can be calculated in terms of external mechanics. Based on Stronge’s impact mechanics a MATLAB code has been developed by Zhenhui Liu, [1], for such calculations. This code is based on different coordinate systems for the two colliding objects, and the relative motion of these have to be specified in addition to the geometry parameters.

The different input parameters used for this calculation are described in the MATLAB code in appendix C.

The calculation returns a value for the total energy the ship has to absorb. The results for the two different impact angles analysed in this thesis are given in figure 8.53. The contact force is also given as dotted green and blue curves in the figure. This is done to include the force development in order of the energy comparison to see if the intersection between Liu’s energy curves and the simulated energy curves can be related to the forces.

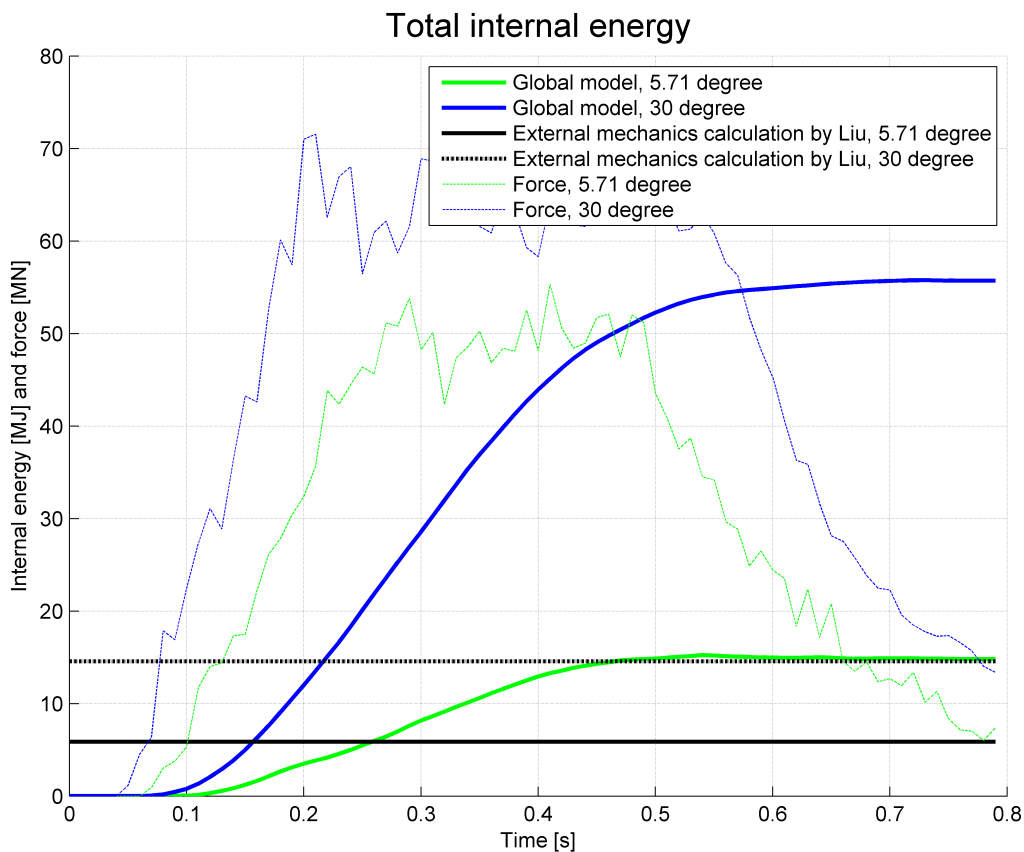


Figure 8.53: Comparison of energy values for numerical calculation and simulations

As seen from the figure, the match between the results obtained by the external mechanics code and the simulation results is poor. The MATLAB calculation for 30 ° impact angle matches the global model for 5.71° impact angle, but based on the code this is rather a

rare coincidence than an interesting result. The external mechanics code assumes the two colliding bodies to deform and get a common velocity after the collision. The ice material model is too hard to represent this scenario, and from the simulations it is seen that the iceberg is deflected from the ship after the collision. If the ice material had been modelled as a "softer" material it would probably give a more matching result with the external mechanics code. On the other hand, such simulation would not represent the physics in the problem.

The results from these calculations are based on e-mail correspondence with Zhenhui Liu where he has explained some of the different input parameters. The deviation between the absorbed energy obtained from these calculations and the observed energies from the global analyses is very large and further investigation of the MATLAB calculations should be carried out. Some of the parameters are estimated roughly based on similar geometry etc., but the deviations are nevertheless larger than what is reasonable. The MATLAB code yields conservative results, but especially for the large impact angle the results are over-conservative compared to the absorbed energy obtained from the global analysis.

## 8.8 Comparison with membrane type LNG carrier

In Stine Aas Myhres master thesis, [2], a membrane type LNG carrier is simulated during an iceberg collision. This ship is not ice strengthened, and a direct comparison of the results will therefore not be "fair", but it is interesting to investigate the effect of the increased strength in the ship. Another drawback with the comparison between the different ship types is that the model of the membrane type LNG carrier only includes a side model. This means that a side collision must be performed, and the results will again not be directly comparable.

The side model was originally modelled in mm. MATLAB is used for scaling all the node coordinates to dimensions in m, and all the properties are scaled manually. The collision point is chosen based on the collision points the Myhres master thesis. An analysis where the ship is rotated 30° is used to simulate the same contact point on the iceberg as for the local prescribed displacement analysis described in section 7. The 15 m iceberg used in this thesis is used for the comparison with the membrane type LNG carrier. The collision setup is shown in figure 8.54.

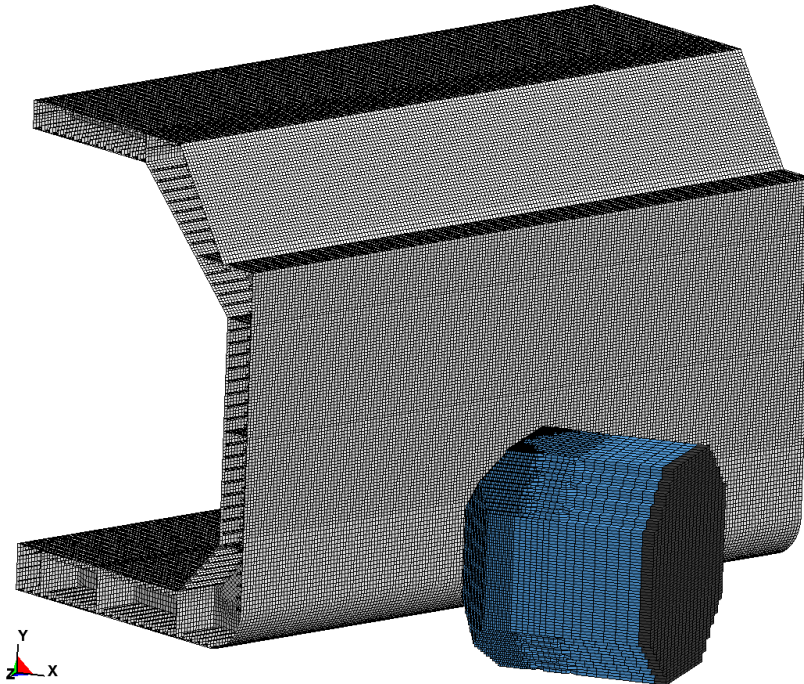


Figure 8.54: Collision setup for membrane type LNG carrier comparison

The energy absorption obtained in this analysis are shown in figure 8.55 together with the local prescribed displacement analysis at 30° impact angle for the spherical type LNG carrier.

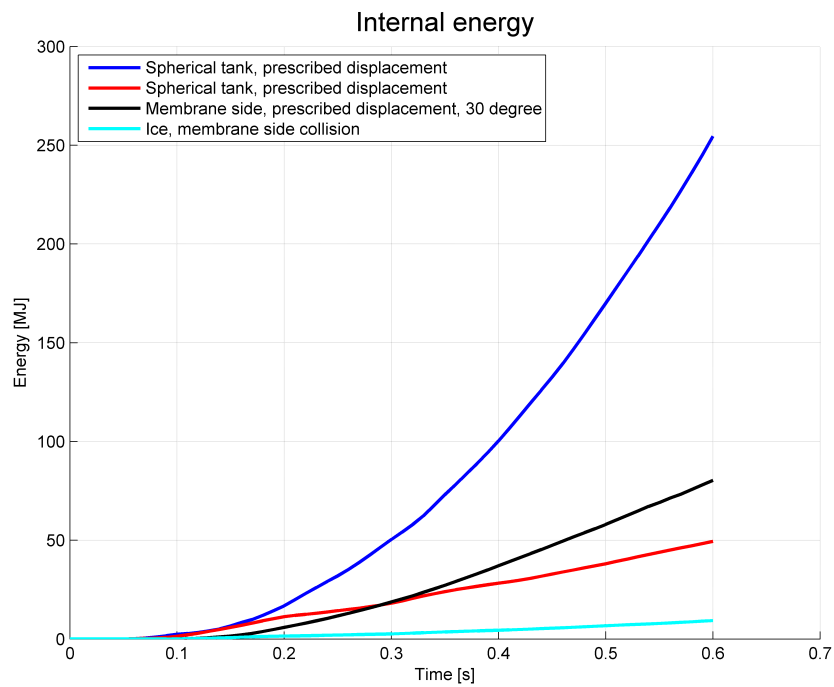


Figure 8.55: Internal energy in membrane type LNG carrier

A directly comparison of the values in the results will not lead to a correct representation of the situation. It is interesting to see that the crushing energy in the iceberg for the membrane tank analysis is low, which is expected due to the weaker side structure in the membrane tank. During the simulation it is also seen that the inner hull of the membrane side is exposed to large indentation. This has been discussed as a drawback of the membrane type LNG carrier, and may be investigated further by comparing it with a detailed FE model of the side structure of a spherical type LNG carrier. In such comparison, the membrane type LNGC should also be ice strengthened, since this is the most relevant situation for ships sailing in Arctic areas.

## 9 Conclusions and further work

### 9.1 Summary of results

The first part of the thesis work was to establish an ALE-model in LS-DYNA which could be used to simulate the surrounding water in the ship-iceberg collision scenario. After unsuccessfully testing different solutions to this problem, it was concluded that this work had to be postponed for further work. The modelling of the ship structure had to be preferred at this point in time. Despite the lack of useful results, this work was informative regarding use of LS-DYNA, and by correct use of the options for ALE-modelling discussed in section 5 the problems probably will be solved.

Based on the FE element model of the ship and iceberg both local and global analyses are performed. An enormous amount of results are obtained from the simulations, and the different approaches are compared based on contact force, indentation, internal energy and plastic strain. The aim of the thesis work is to verify the magnitude of the errors in the results obtained by use of simplified analysis approaches. The differences in obtained results between two different impact angles are also investigated.

The most common collision approach is an analysis where a prescribed displacement is given to the iceberg. In this approach pinned boundary conditions are applied to the local bow shoulder section. This approach is compared to a more resource demanding approach, where the iceberg is given an initial velocity. At  $5.71^\circ$  impact angle it is seen from the relationship between force and displacement that the two approaches yields similar results until an indentation of approximately 0.6 m. The same result is indicated by the absorbed energy. At  $30^\circ$  impact angle similar results for the two approaches are obtained until an indentation of approximately 0.8 m. While the energy absorption in the ship is approximately 100 % larger at  $30^\circ$  impact angle than at  $5.71^\circ$  impact angle, the energy absorbed by the ice has only increased by approximately 25 %. In other word, the ship absorbs a larger amount of the dissipated energy for large impact angles than for small impact angles. It is also seen that the impact at large angle is less sensitive to deflections than the impact at a small angle. The prescribed displacement approach yields as expected over-conservative results, but at large impact angles it seems as a more reasonable approach than for small impact angles.

The next comparison study performed is a comparison of the local initial velocity analysis and the global analysis. Here, a significant difference in the deformations is seen at  $5.71^\circ$  impact angle. A large difference is also seen in the energy absorption in the ship. The local model absorbs a significantly larger amount of energy than the corresponding global model, and this is due to the pinned boundary conditions of the local model. At  $30^\circ$  impact angle a large difference in indentation is seen, but the absorbed energy is similar for both the local and the global analysis. The indentation curve does not take the deformation pattern into account, and is therefore a bit misleading with respect to the energy absorption. Also this comparison indicates that the simplified approach yields better results at larger impact angles.

When the results from both impact angles for the global model are compared, it is seen that the deformations from the large impact angle are significantly larger than for the

small impact angle which is the same result as seen for all the other comparisons.

The results obtained from the large iceberg analyses are as expected showing significantly larger damage on the hull than the small iceberg simulations. At this impact also deformations on the inner hull are shown. These analyses were stopped before the iceberg had deflected from the ship side, and the results indicates that the deformations would have increased if the simulation had not been stopped. It is also interesting to see that the difference in the results between the local analysis and the global analysis are *smaller* for the analyses with the large iceberg than for the analyses with the small iceberg.

The critical plastic strains of each analysis are investigated. Large plastic strains are as expected obtained for all simulations except from the global analysis at  $5.71^\circ$  impact angle. At this angle the observed plastic strains are significantly lower, which indicates that this collision will not be critical to the ship structure. The other simulations shows large plastic strains of magnitude 30-35 % in the transverse frames. In these frames elements have started to collapse due to the large strain, but in the outer shell collapse of elements have not been observed for any of the simulations.

Accelerations and displacements at some spots which are not directly impacted by the collision are investigated. These motions seems not to be critical for any of the analyses, but, for the large iceberg collision, the relative motion between the tank tower and tank cover can not increase much further before this motion is critical.

The external mechanics MATLAB code developed by Liu has been used for external mechanics calculations. The results obtained from this code deviates a lot from the results obtained from the simulations in this thesis. No clear reason for this is found, and this should be further investigated.

As a last comparison, the membrane type LNG carrier tank side modelled by Stine Aas Myhre has been analysed. The results from this analysis are compared with the results from the spherical type LNG carrier, but this comparison will not yield usable results due to too large difference in both structural strength and impact scenario.

## 9.2 Concluding remarks

Based on the work carried out in this thesis and the results obtained from the analyses some conclusions can be made.

It is seen that the local prescribed displacement analysis yields over-conservative results for both impact angles simulated in this thesis. On the other hand, if only results from a short simulated time is the aim of the analysis, this approach can yield reasonable results. This requires that the prescribed displacement is modelled to equal a corresponding initial velocity. The results obtained from the prescribed displacement seems to be more reasonable for larger impact angles than for small impact angles. The boundary between "small" and "large" impact angles must be investigated, but a significant difference has been seen between the two angles investigated in this thesis,  $5.71^\circ$  and  $30^\circ$ .

When comparing the local initial velocity analysis with the global analysis it is seen that the local analysis yields conservative results with respect to indentation and energy ab-

sorption. As an example of the deviations between the three approaches, the indentation at  $t=0.4$  s for  $5.71^\circ$  impact angle can be compared. The local prescribed displacement analysis yields approximately an indentation of 0.7 m at this time step, while the local initial velocity analysis yields an indentation of 0.6 m. At this early time step it is seen that the deviation between the prescribed displacement method and the initial velocity method is small. When comparing these results with the result from the global analysis it is seen that the simplified approaches are conservative. In the global analysis an indentation of only 0.2 m is seen, and the indentations obtained from the two local approaches can be concluded to be over-conservative.

The energy levels obtained from the comparison between the local and global analyses limits the conclusion of over-conservatism to some extent. Based on the horizontal cuts of the deformation and the absorbed energy it seems like the deformation pattern in the global analyses differs from the ones in the local analyses. From the energy considerations it is seen that the local initial velocity analyses, especially at  $30^\circ$  impact angle yields reasonable results. At  $5.71^\circ$  impact angle the result is a bit conservative, but to a smaller extent than the indentation comparison indicated.

The simulations have based on this shown that the prescribed displacement approach, as long as the prescribed displacement is given to correspond an initial velocity, yields over-conservative results when long duration problems are simulated. In short duration problems, this method yields reasonable results when comparing it to the local initial velocity approach. The results are more reasonable for larger impact angles due to less deflection of the iceberg at these angles.

When comparing the local simulations with the global simulations, it is seen that the indentations are over-estimated in the local approaches. This means that the simplified methods yields conservative and to some extent even over-conservative results.

The analyses including the large iceberg shows large deformations in the ship structure. Indentation of the inner hull is initialised and from the energy curves it seems like larger indentions can be expected. A collision scenario with an iceberg of this size seems therefore to possibly cause a critical situation for the ship.

The investigated plastic strains shows no collapse of elements in the outer shell. The transverse frames absorbs a large amount of energy in the deformation, but no sign of leakage is seen. The simulations of the collision with the large iceberg can still give larger indentations, and it is therefore not possible to give a conclusion stating that no leakage will occur. For the small iceberg simulations it seems like the collision not will be critical with respect to leakage.

The investigated accelerations shows that these will not be critical. No extreme values are found in any of the observed spots.

### 9.3 Further work

Based on the work in this thesis and on the given conclusions some recommendations for further work can be given.

**ALE-modelling:**

For the ALE-modelling part an ALE-model which can be used in the ship-iceberg collision simulations should be established. This will probably be successful by use of the correct equation of state and the initial volume fraction command.

**Geometry modelling and meshing:**

Detailed geometry for a larger part of the ship will make it possible to analyse and compare results for different impact scenarios. These detailed parts should be modelled and meshed in different sections that can be included in the global model one by one to reduce computation time. If all details are modelled in the global model, the total amount of elements will be too large for reasonable computation time.

The mesh in the model used for this thesis has been modelled with undistorted four-node quad elements, but in sharp corners and other spots with advanced geometry, the elements are more distorted. These spots can be addressed and re-meshed to get more accurate results and to reduce the computation time.

**Iceberg:**

An irregular shaped iceberg is chosen in this thesis. This iceberg has been meshed by elements of various size to reduce the total number of elements. The smallest element sizes, which is modelled in the contact area, are still a little too large according to the ice material model. For a more accurate result the iceberg can therefore be re-meshed with smaller elements in the collision area.

To get a more realistic collision approach, the iceberg can be modelled based on real measurements of iceberg geometry. The meshing part of this iceberg will be very time consuming, and it is important to have a very dense mesh in the area where crushing is assumed to happen.

**Impact angle:**

To verify for which angle it can be assumed that the local prescribed displacement analysis yields reasonable results, impacts at a lot of different angles can be simulated and compared. This work is time consuming regarding computation time, but by use of existing models the time spent on the analysis setup is short.

**Results:**

The amount of results obtained from the simulations is enormous. The presented results only represent a selection of the obtained results, and further investigation of these can be done. Especially the results obtained from the external mechanics code can be further investigated and compared to the results from the simulations.

In the collision scenario with the large iceberg it was found that the difference between the simplified local approach and the global approach was small. It was expected that the boundary conditions would give a larger contribution to the results at these analyses than for the small iceberg analyses due to smaller deflection of the large iceberg. This seems not to be correct, and further investigation of this scenario can be done.



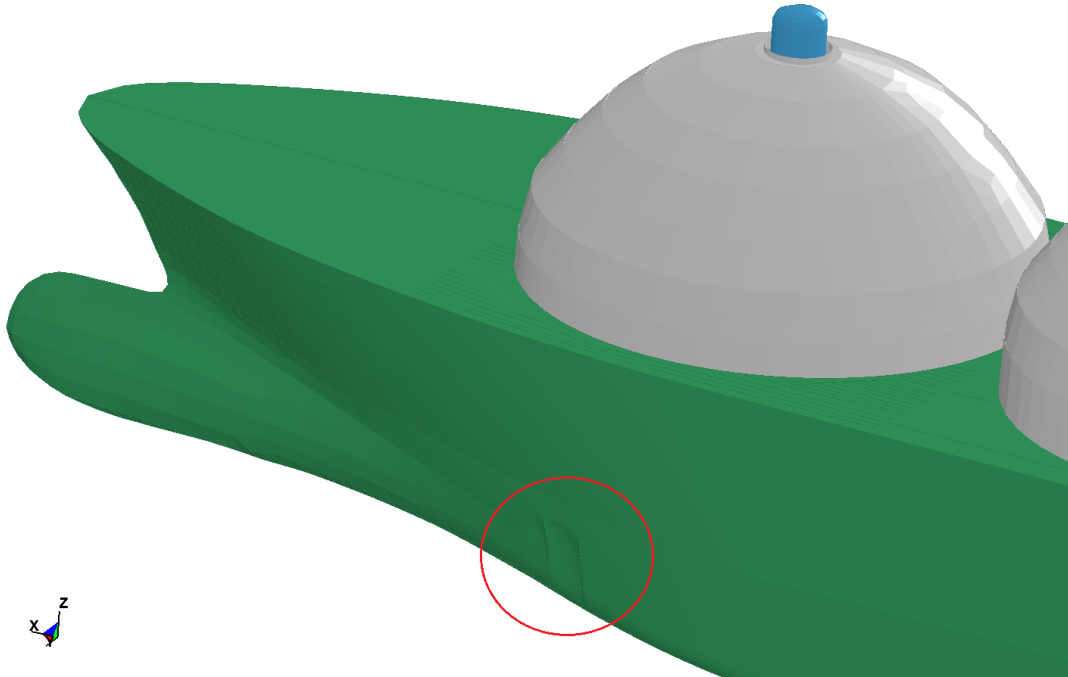
## References

- [1] Zhenhui Liu. *Analytical and numerical analysis of iceberg collisions with ship structures*. PhD thesis, NTNU, 2011.
- [2] Stine Aas Myhre. Analysis of accidental iceberg impacts with membrane tank LNG carriers. Master's thesis, NTNU, 2010.
- [3] Jie Wang. A study on technical development on LNG vessel. In *IEEE International Conference on Systems, Man and Cybernetics*, 2009. Compendex database.
- [4] R.E. Gagnon. Results of numerical simulations of growler impact tests. Technical report, Institute of Ocean Technology National Research Council of Canada St. John's, 2007.
- [5] Sang-Gab Lee and Hong-Anh Nguyen. LNGC collision response analysis with iceberg considering surrounding seawater. In *Proceedings of the twenty-first (2011) International Offshore and Polar Engineering Conference*, 2011.
- [6] Martin Storheim, Ekaterina Kim, Prof. Jørgen Amdahl, and Prof. Sören Ehlers. Iceberg shape sensitivity in ship impact assessment in view of existing material models. In *Proceedings of the 31st International Conference on Ocean, Offshore and Arctic Engineering, OMAE 2012*, 2012. To be published.
- [7] W. S. Kim (HHI), S. H. Shin (HHI), H. S. Urm (DNV), T. Hysing (DNV), L. Sannes (Moss Maritime), and J. S. Che (InnoQual). Safety of cargo containment system and support structure in spherical tank type LNG carrier under iceberg-ship collision. Technical report, Hyundai Heavy Industries Co., Ltd, Det Norske Veritas AS, Moss Maritime and InnoQual Co., Ltd, 2006.
- [8] Morten Mejlænder-Larsen and Thor Hysing. Technical report no. 2006-0672, ice collision scenario. Technical report, DNV, 2006.
- [9] Martin Storheim. Analysis of structural damage of tankers subjected to collision. Master's thesis, NTNU, 2008.
- [10] Jim Day. Guidelines for ALE modelling in LS-DYNA (draft). Technical report, LSTC, 2010.
- [11] John O. Hallquist. *LS-DYNA theory manual*, March 2006.
- [12] Torgeir Moan. *TMR4190 - Finite Element Modelling and Analysis of Marine Structures*. 2003.
- [13] Hagbart Skage Alsos. *Ship grounding - Analysis of ductile fracture, bottom damage and hull girder response*. PhD thesis, NTNU, 2008.
- [14] Moss Maritime. Cargo tank cool down and stress analysis. Technical Report 2819-R002, 2005.
- [15] Federico M. Mazzolani. *Aluminium alloy structures*. E & FN SPON, second edition edition, 1995.
- [16] Eurocode 9. *Design of aluminium structures*, 2000.

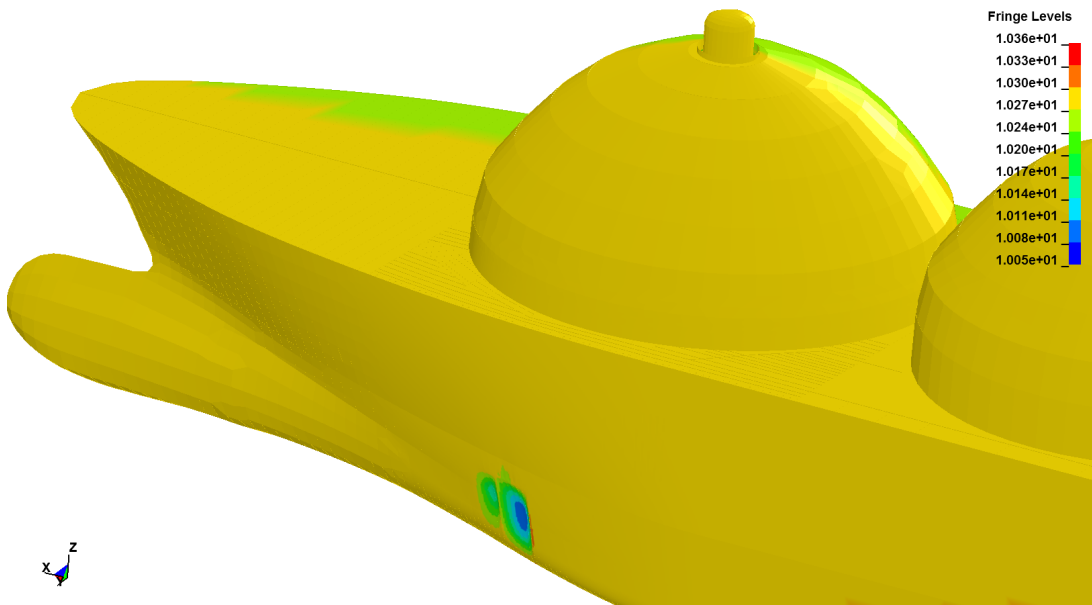
- [17] Andreas Berling. Analysis of accidental iceberg impacts with membrane LNG carriers. Master's thesis, NTNU, 2011.
- [18] Lin Hong and Jørgen Amdahl. *Simplified analysis and design of ships subjected to collision and grounding*. PhD thesis, NTNU, 2008.
- [19] Livermore Software Technology Corporation (LSTC). *LS-DYNA keyword user's manual, Volume 1, Version 971*, May 2007.
- [20] Alexandr I. Korotkin. Added masses of ship structures. Technical report, Krylov shipbuilding research institute, 2009.
- [21] International Standards Organisation. *Petroleum and natural gas industries - Arctic offshore industries*, ISO/CD 19906 edition, 2007.

# Appendices

## A Deformations of hull

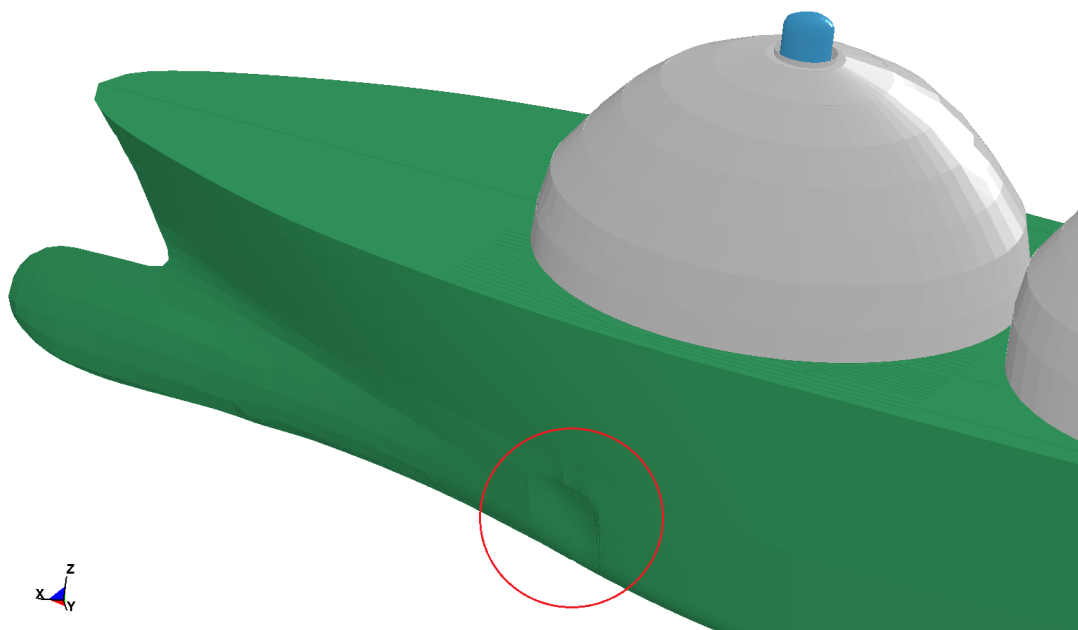


(a) Deformation in global analysis, 5.71° impact angle

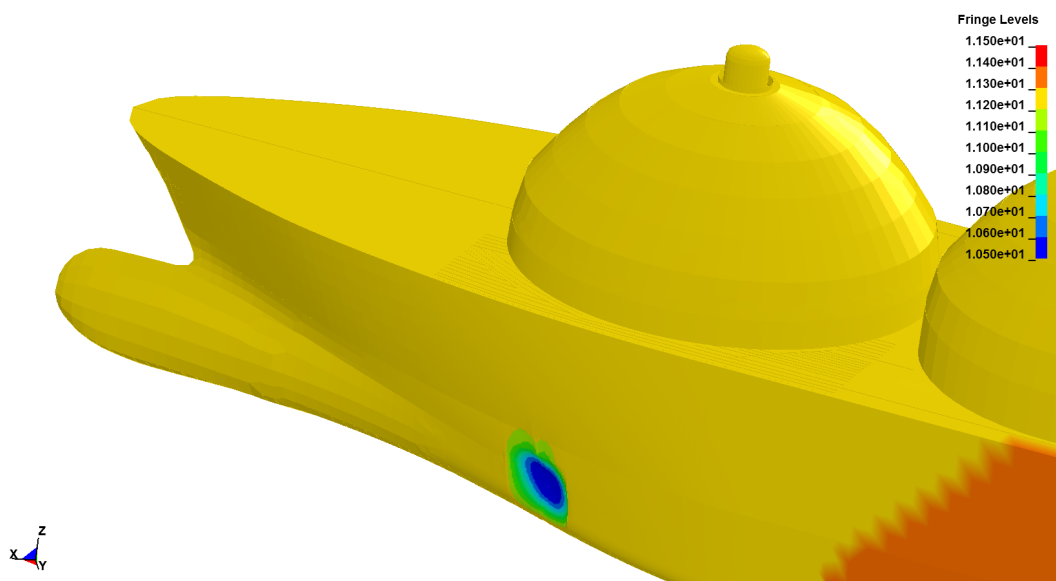


(b) Deformation in global analysis, fringe levels

Figure A.1: Deformation of hull for the global analysis, 5.71° impact angle

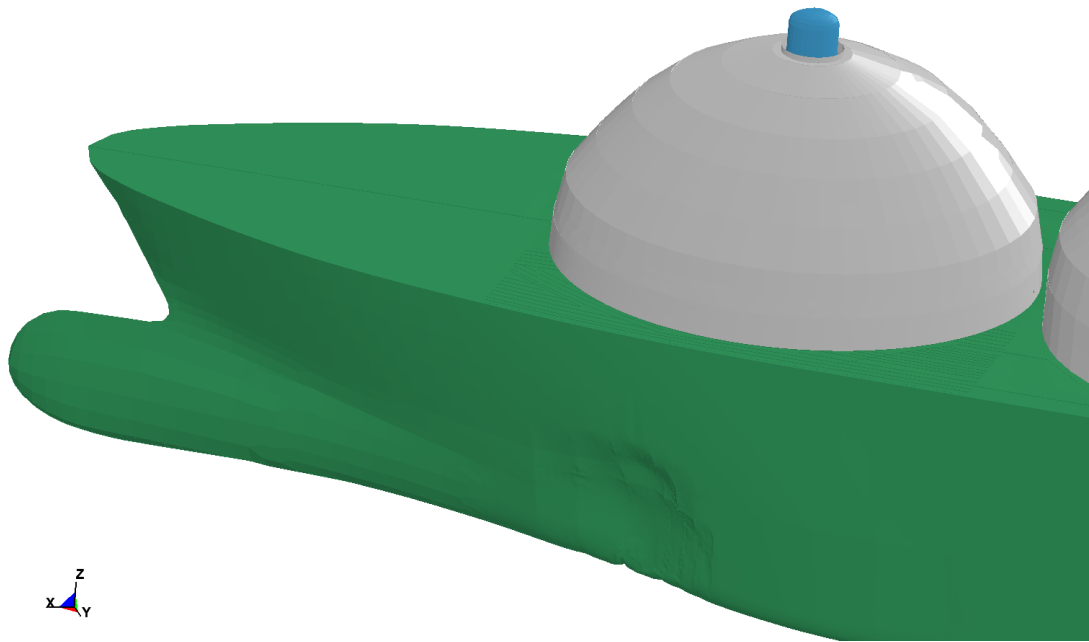


(a) Deformation in global analysis, 30° impact angle

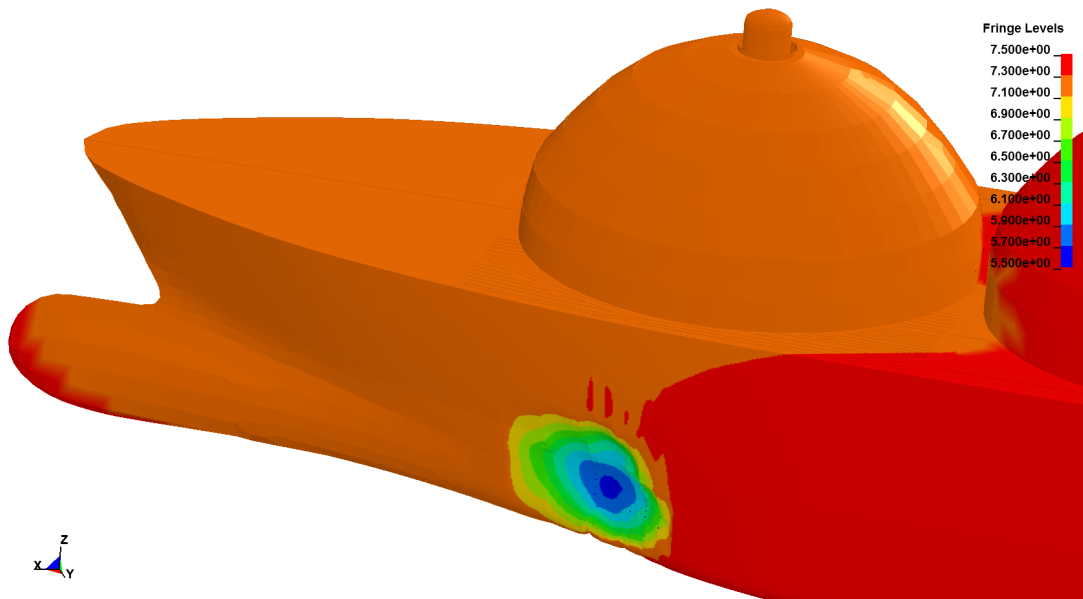


(b) Deformation in global analysis, fringe levels

Figure A.2: Deformation of hull for the global analysis, 30 ° impact angle



(a) Deformation in global analysis, large iceberg impact



(b) Deformation in global analysis, fringe levels

Figure A.3: Deformation of hull for the global analysis, colliding with the large iceberg

## B Plastic strains

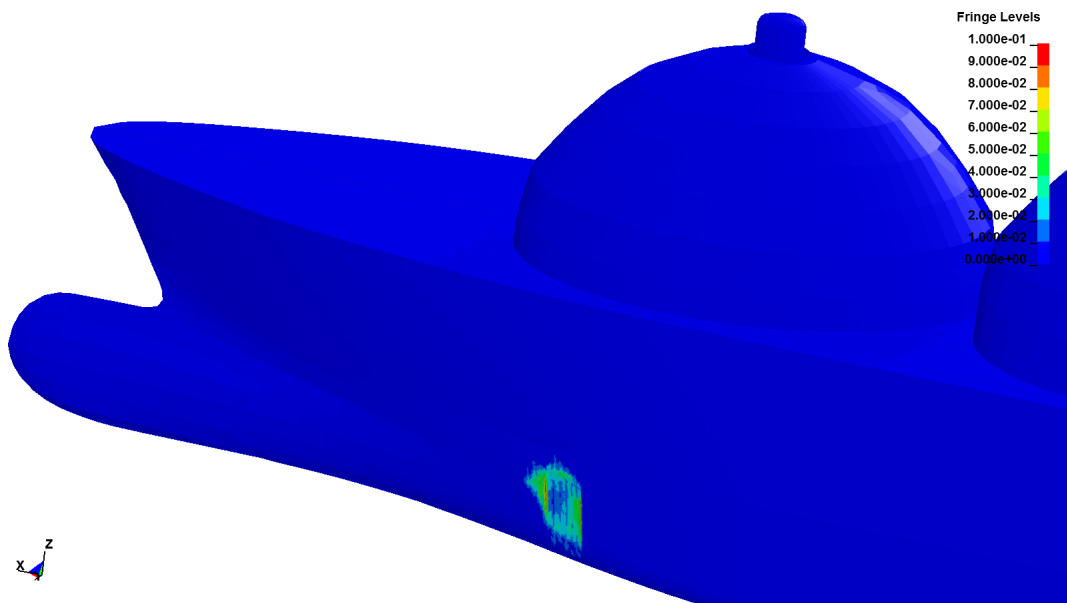


Figure B.1: Plastic strain for global model, 5.71 ° impact angle

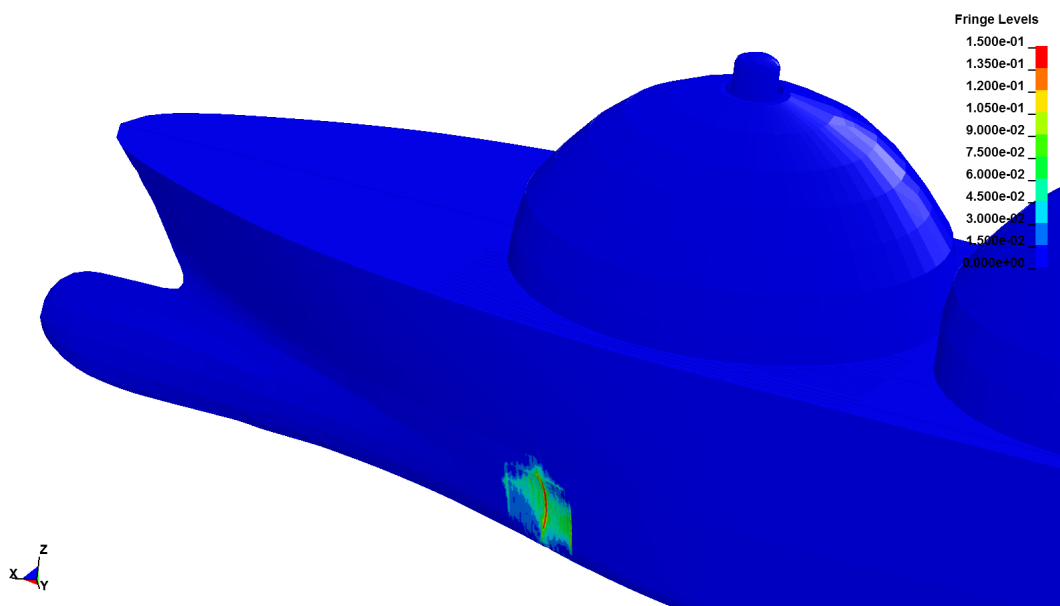


Figure B.2: Plastic strain for global model, 30 ° impact angle

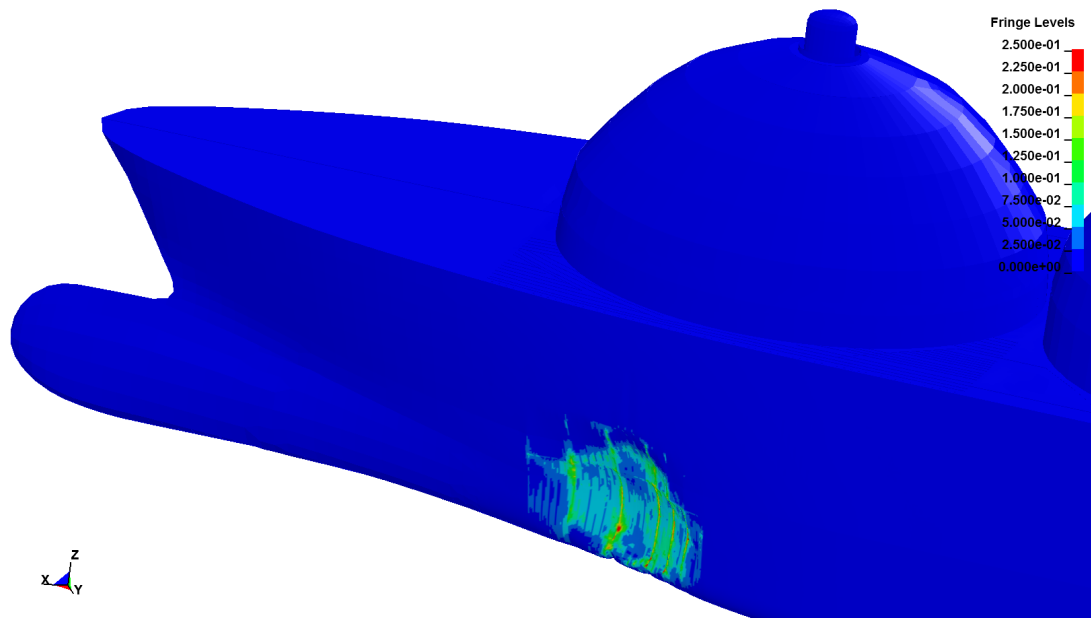


Figure B.3: Plastic strain for global model, large iceberg impact

## C MATLAB code for external mechanics calculation

```

1
2 %% The 3D collision mechanics based on Stronge's theory
3
4 % MATLAB code used for calculating external mechanics in collision
5 % scenarios, developed by Zhenhui Liu
6
7 %% Ship data
8 Ha=27.5; %Height (deck edge to keel)
9 La=300; %Loa
10 Lpp=283.5; %Lpp
11 Ba=52; %Breadth
12 Ta=11.00; %Draught
13 dw=1025; %Density of water
14 di=900; %Density of ice
15 Am = 531.3614; %Area of mid-frame
16 Awp = 11827.525; %Water plane area
17 Mass1=125000000; %Mass of ship
18 Mass2=2457000; %Mass of iceberg
19
20 %% Coefficients
21 Cwp=Awp/(La*Ba); %Water plane coefficient
22 Cm=Am/(Ba*Ta); %Mid-frame coefficient
23 Cb=(Mass1/dw)/(Lpp*Ba*Ta); %Coefficient of fineness
24
25 %% Added mass coefficients, ship
26 Amx=0.05;
27 Amy=1;
28 Amz=2/3*Ba*Cwp^2/(Ta*Cb*(1+Cwp));
29 Amrol=0.25;
30 Ampit=Ba/(Ta*(3-2*Cwp)*(3-Cwp));
31 Amyaw=0.21;
32
33 %% Added mass coefficients, iceberg
34 Bmx=0.8;
35 Bmy=0.8;
36 Bmz=0.8;
37 Bmrol=0.15;
38 Bmpit=0.15;
39 Bmyaw=0.15;
40
41 %% Mass matrix included added mass
42 mass1=[1+Amx 0 0; 0 1+Amy 0; 0 0 1+Amz]*Mass1;
43 mass2=[1+Bmx 0 0; 0 1+Bmy 0; 0 0 1+Bmz]*Mass2;
44 %% Gyration radius squared, ship
45 rxa = 73.39^2;
46 rya = 72.91^2;
47 rza = 20.70^2;
48 % rxa=(Cwp*Ba^2/(11.4*Cm)+Ha^2/12); %Generic formulas for calculating I/M
49 % rya=0.07*Cwp*La^2;
50 % rza=La^2/16;
51
52 %% Gyration radius squared, sphere
53 rxb = 5.40^2;
54 ryb = 4.41^2;

```



```

55 rzb = 4.18^2;
56 %rxb=2/5*R*R; %Generic formulas for calculating I/M
57 %ryb=2/5*R*R;
58 %rzb=2/5*R*R;
59
60 %% Inertia matrix
61 Itrx1=[(1+Amrol)*rxa 0 0;0 (1+Ampit)*rya 0; 0 0 (1+Amyaw)*rza]*Mass1;
62 Itrx2=[(1+Bmrol)*rxb 0 0;0 (1+Bmpit)*ryb 0; 0 0 (1+Bmyaw)*rzb]*Mass2;
63
64 %% Gravity center of ship under global system
65 shipg=[0 0 0]';
66
67 %% Angles used for calculation
68 alpha=0.377; %Angle between two ship's frame, see Liu's paper
69 gama=alpha; %water line angle
70 betap=0.295; %See Liu's paper
71
72 %% Coordinates for collision point, relative to CGship
73 cpg=[89.6 18.5 5.44]';
74 %cpg=[226.3 18.5 8]';
75
76 %% Centre of gravity, iceberg, relative to CGship
77 iceb=[94.7 22.7 -8.42]';
78
79 %% Velocity of ship and iceberg under global system
80 shipvg=[10.29 1.029 0]';
81 %shipvg=[8.91 5.144 0]';
82 icevb=[0 0 0]';
83
84 %% Calculate the relative direction vector from CG to collision point
85 rad1g=shipg-cpg; %Collision point to CG-ship
86 rad2b=cpg-iceb; %CGice to collision point
87
88 %% Transformation matrix between local and global system
89 l=sin(alpha)*cos(betap);
90 m=cos(alpha)*cos(betap);
91 n=-sin(betap);
92 Mab=[cos(gama) sin(gama) 0;
93 -sin(gama) cos(gama) 0;
94 0 0 1];
95 Mlg=[cos(alpha) -sin(alpha) 0;
96 -sin(alpha)*sin(betap) -cos(alpha)*sin(betap) -cos(betap);
97 l m n];
98 Mtr2=Mlg*Mab;
99
100 %% Calculate the rotated inertia matrix
101 Rtrx1=inv(Mlg*Itrx1*inv(Mlg));
102 Rtrx2=inv(Mtr2*Itrx2*inv(Mtr2));
103 mass1f=inv(Mlg*mass1*inv(Mlg));
104 mass2f=inv(Mtr2*mass2*inv(Mtr2));
105
106 %% Calculate the radius regarding to the inertia
107 rad1=Mlg*rad1g;
108 rad2=Mtr2*rad2b;
109
110 %% Calculate the relative velocity under local system
    
```

```

111 rvl=Mlg*shipvg-Mtr2*icevb;
112
113 %% Reversed mass matrix
114 m11=(mass1f(1,1)+rad1(2)^2*Rtrx1(3,3)-2*rad1(2)*rad1(3)*Rtrx1(2,3)+rad1(3)
      ^2*Rtrx1(2,2)) + (mass2f(1,1)+rad2(2)^2*Rtrx2(3,3)-2*rad2(2)*rad2(3)*
      Rtrx2(2,3)+rad2(3)^2*Rtrx2(2,2));
115 m12=(mass1f(1,2)+mass2f(1,2))+(rad1(1)*rad1(3)*Rtrx1(2,3)-rad1(3)^2*Rtrx1
      (2,1)-rad1(1)*rad1(2)*Rtrx1(3,3)+rad1(2)*rad1(3)*Rtrx1(3,1)) + (rad2(1)*
      rad2(3)*Rtrx2(2,3)-rad2(3)^2*Rtrx2(2,1)-rad2(1)*rad2(2)*Rtrx2(3,3)+rad2
      (2)*rad2(3)*Rtrx2(3,1));
116 m13=(mass1f(1,3)+mass2f(1,3))+(rad1(1)*rad1(2)*Rtrx1(3,2)-rad1(2)^2*Rtrx1
      (3,1)-rad1(1)*rad1(3)*Rtrx1(2,2)+rad1(2)*rad1(3)*Rtrx1(2,1)) + (rad2(1)*
      rad2(2)*Rtrx2(3,2)-rad2(2)^2*Rtrx2(3,1)-rad2(1)*rad2(3)*Rtrx2(2,2)+rad2
      (2)*rad2(3)*Rtrx2(2,1));
117 m22=(mass1f(2,2)+rad1(1)^2*Rtrx1(3,3)-2*rad1(1)*rad1(3)*Rtrx1(1,3)+rad1(3)
      ^2*Rtrx1(1,1)) + (mass2f(2,2)+rad2(1)^2*Rtrx2(3,3)-2*rad2(1)*rad2(3)*
      Rtrx2(1,3)+rad2(3)^2*Rtrx2(1,1));
118 m23=(mass1f(2,3)+mass2f(2,3))+(rad1(3)*rad1(1)*Rtrx1(1,2)-rad1(3)*rad1(2)*
      Rtrx1(1,1)-rad1(1)^2*Rtrx1(3,2)+rad1(1)*rad1(2)*Rtrx1(3,1)) + (rad2(3)*
      rad2(1)*Rtrx2(1,2)-rad2(3)*rad2(2)*Rtrx2(1,1)-rad2(1)^2*Rtrx2(3,2)+rad2
      (1)*rad2(2)*Rtrx2(3,1));
119 m33=(mass1f(3,3)+rad1(1)^2*Rtrx1(2,2)-2*rad1(1)*rad1(2)*Rtrx1(1,2)+rad1(2)
      ^2*Rtrx1(1,1)) + (mass2f(3,3)+rad2(1)^2*Rtrx2(2,2)-2*rad2(1)*rad2(2)*
      Rtrx2(1,2)+rad2(2)^2*Rtrx2(1,1));
120 m21=m12;
121 m31=m13;
122 m32=m23;
123 m=[m11,m12,m13;m12,m22,m23;m13,m23,m33];
124 syms dv1 dv2 dv3 dp1 dp2 dp3
125 rm=inv(m);
126
127 % Introducing the friction
128 % Dry friction colliding bodies can be representd by the Amontons-Coulomb
129 % law of sliding friction (Johnson, 1985).
130 % calculate the extreme case for stick together get the critical value miu
131 e=0; % restitution factor
132 % dv1=-rvl(1);
133 % dv2=-rvl(2);
134 % dv3=-rvl(3)*(1+e);
135 dp1=subs(rm(1,1)*dv1+rm(1,2)*dv2+rm(1,3)*dv3,{dv1,dv2,dv3},{-rvl(1),-rvl(2)
      ,-rvl(3)*(1+e)});
136 dp2=subs(rm(2,1)*dv1+rm(2,2)*dv2+rm(2,3)*dv3,{dv1,dv2,dv3},{-rvl(1),-rvl(2)
      ,-rvl(3)*(1+e)});
137 dp3=subs(rm(3,1)*dv1+rm(3,2)*dv2+rm(3,3)*dv3,{dv1,dv2,dv3},{-rvl(1),-rvl(2)
      ,-rvl(3)*(1+e)});
138 miu=sign(dp1)*sqrt(dp1^2+dp2^2)/dp3;
139 miu2=dp2/dp1;%n2/n1
140
141 miu0=0.15; %the input real friction
142
143 %% Friction matrix
144 flag1=1;
145 sm1=m11+m12*miu2+m13*sqrt(1+miu2*miu2)/miu;
146 sm2=m21/miu2+m22+m23*sqrt(1+miu2*miu2)/miu/miu2;
147 sm3=m31*miu/sqrt(1+miu2*miu2)+m32*miu*miu2/sqrt(1+miu2*miu2)+m33;
148 if miu0==0

```

```

149     flag1=2;
150     dv3=rvl(3)*(1+e);
151     dp3=dv3/m33;
152     dv1=m13*dp3;
153     dv2=m23*dp3;
154     sm1=Inf;
155     sm2=Inf;
156     sm3=m33;
157     dp1=0;
158     dp2=0;
159 else
160     if abs(miu)>=miu0 % sliding case
161         dv3=rvl(3)*(1+e);
162         fai=atan(miu2);
163         if dp2==0
164             fai=0/180*pi;
165         end
166         flag1=2;
167         sm1=m11+m12*miu2+m13*sqrt(1+miu2*miu2)/miu0;
168         sm2=m21/miu2+m22+m23*sqrt(1+miu2*miu2)/miu0/miu2;
169         sm3=m31*miu0/sqrt(1+miu2*miu2)+m32*miu0*miu2/sqrt(1+miu2*miu2)+m33;
170         AA=[miu0*cos(fai)*1e06 -rm(1,1) -rm(1,2);
171             miu0*sin(fai)*1e06 -rm(2,1) -rm(2,2);
172             1e06 -rm(3,1) -rm(3,2)];
173         BB=[rm(1,3)*dv3 rm(2,3)*dv3 rm(3,3)*dv3]';
174         CC=AA\BB;
175         dp3=CC(1,1)*1e06;
176         dv1=CC(2,1);
177         dv2=CC(3,1);
178         dp1=miu0*cos(fai)*dp3;
179         dp2=miu0*sin(fai)*dp3;
180     end
181 end
182
183 dpp=sqrt(dp1^2+dp2^2+dp3^2);
184 E1=abs(1/sm1/2*dv1*(dv1+2*rvl(1)));
185 E2=abs(1/sm2/2*dv2*(dv2+2*rvl(2)));
186
187 if miu2==0
188     E2=0;
189 end
190
191 E3=abs(1/sm3/2*dv3*(dv3+2*rvl(3)));
192 dvv=[dv1;dv2;dv3];
193 tt=E1+E3+E2;
194
195 %% Total dissipated energy, given in [J]
196 disp('Total dissipated energy in [J]:')
197 disp(tt)
    
```

# D Spreadsheet used for weight calculations

	A	B	C	D	E	F	G	H	I	J	K	L	M	N	O	P	Q	R	S	T	U
		Global model	Volume	x	y	z	m <sup>2</sup> x	m <sup>2</sup> y	m <sup>2</sup> z	Tenheit											
2																					
3	BHD_23000	4.585E+05	58.410	122.100	23.000	20.620	5.999E+07	1.055E+07	9.455E+06	7850	Tank2_eq	6.487E+04	24.480	168.300	0.000	24.770	1.092E+07	0.000E+00	1.607E+06	2650	
4	Bulkheads	1.624E+06	206.900	114.000	0.000	15.670	1.832E+08	0.000E+00	2.545E+07	7850	Tank 2_eq_std	1.297E+05	48.980	99.000	0.000	24.770	1.284E+07	0.000E+00	3.214E+06	2650	
5	Bulkheads_std	7.968E+05	101.500	78.990	0.000	16.120	6.294E+07	0.000E+00	1.284E+07	7850	Tank 2_eq_std	6.540E+05	246.800	168.300	0.000	25.670	1.101E+08	0.000E+00	1.679E+07	2650	
6	Deck 16200_std	8.753E+05	111.500	92.880	0.000	22.500	8.125E+07	0.000E+00	1.969E+07	7850	Tank2_shell_C_std	1.308E+06	499.700	99.000	0.000	25.670	1.295E+08	0.000E+00	3.358E+07	2650	
7	Deck 22500	6.954E+04	8.400	32.840	0.000	2.801	2.165E+06	0.000E+00	1.847E+05	7850	Tank2_shirt	8.030E+04	30.300	168.300	0.000	21.980	1.351E+07	0.000E+00	1.765E+06	2650	
8	Deck 2800_std	1.023E+05	13.090	116.400	0.000	5.431	1.191E+07	0.000E+00	5.555E+05	7850	Tank2_shirt_C	1.606E+05	60.610	99.000	0.000	21.980	1.590E+07	0.000E+00	3.590E+06	2650	
9	Deck 3300_std	9.889E+05	125.300	115.700	0.000	9.898	1.138E+08	0.000E+00	9.736E+06	7850	Tank2_lower_C_std	4.100E+04	15.470	168.300	0.000	28.450	6.900E+06	0.000E+00	1.166E+06	2650	
10	Deck 9900_std	9.489E+05	120.800	145.400	0.000	4.693	1.379E+08	0.000E+00	4.450E+06	7850	Tank2_lower_C_std	1.829E+07	1.829E+07	213.780	0.000	23.900	3.910E+09	0.000E+00	4.371E+08	2650	
11	Deck main_std	2.602E+05	3.389E+02	153.000	14.540	10.360	4.099E+08	3.810E+07	2.215E+07	7850	Tank1	1.950E+07	1.950E+07	167.700	0.000	24.840	3.270E+09	0.000E+00	4.844E+08	2650	
12	Frames_iner	2.481E+06	3.160E+02	149.900	-14.700	10.670	3.712E+08	-3.646E+07	2.647E+07	7850	Tank2	1.950E+07	1.950E+07	121.600	0.000	24.840	2.372E+09	0.000E+00	4.844E+08	2650	
13	Frames_iner_std	5.388E+05	68.380	153.700	1.084	2.243	8.200E+07	5.819E+05	1.204E+06	7850	Tank4	1.950E+07	1.950E+07	75.540	0.000	24.840	1.273E+09	0.000E+00	4.844E+08	2650	
14	Long 12650	3.657E+05	46.590	151.900	0.000	3.735	5.555E+07	0.000E+00	1.966E+06	7850	Sum	2.476E+08	4.520E+03				3.962E+10	4.722E+06	3.306E+09		
15	Long 19800	6.659E+04	8.477	43.400	0.000	16.200	2.888E+06	0.000E+00	1.078E+06	7850	Front tank										
16	Long 23000	6.228E+05	79.340	146.700	-22.400	20.590	9.137E+07	-1.395E+07	1.282E+07	7850	BHD_23000_temp	2.149E+05	27.380	215.300	20.860	20.140	4.828E+07	4.484E+06	4.329E+06	7850	
17	Long 5300	2.068E+05	26.340	136.500	0.000	3.375	2.822E+07	0.000E+00	6.978E+05	7850	BHD_23000_stiff	3.644E+03	0.464	214.500	22.490	36.420	7.818E+05	8.195E+04	9.672E+04	7850	
18	Long 5300_std	1.652E+05	21.040	159.100	0.000	6.014	2.628E+07	0.000E+00	9.939E+05	7850	Deck_main_bridgects	1.600E+04	2.038	216.600	16.490	15.900	3.545E+06	2.638E+05	2.244E+05	7850	
19	Long 8100	2.805E+04	3.573	42.070	0.000	3.150	1.180E+06	0.000E+00	8.835E+04	7850	Deck_stiff_16200	6.996E+03	0.815	217.300	21.380	22.280	1.396E+06	1.368E+05	1.423E+05	7850	
20	Long 8100_std	1.287E+06	163.900	126.700	22.080	20.450	1.639E+08	2.841E+07	2.631E+07	7850	Deck_stiff_22500	2.522E+04	5.213	206.600	16.160	9.671	5.211E+06	4.076E+05	2.499E+05	7850	
21	Outer_shell	1.287E+06	163.900	126.700	-22.080	20.480	1.639E+08	-2.825E+07	2.631E+07	7850	Deck_stiff_bottom	4.569E+04	5.821	214.100	9.412	5.014	9.282E+06	4.301E+05	2.291E+05	7850	
22	Outer_shell_std	6.396E+07	184.900	133.700	14.590	3.693	8.679E+09	9.331E+08	2.304E+08	345900	Deck_stiff_main	1.923E+04	2.450	214.600	17.350	27.230	4.127E+06	4.564E+05	5.371E+05	7850	
23	Outer_shell_Below_WL	6.396E+07	184.900	133.800	-14.500	3.692	8.685E+09	-9.274E+08	2.304E+08	345900	Deck_stiff_main_sme	1.923E+04	1.659	213.800	17.350	27.300	2.782E+06	2.260E+05	3.555E+05	7850	
24	Outer_shell_Below_WL_std	7.518E+05	95.770	132.500	0.000	17.350	9.961E+07	0.000E+00	1.304E+07	7850	Side_WB_tank_stiff	1.057E+04	1.346	197.700	16.640	18.700	5.448E+07	4.640E+06	2.179E+06	7850	
25	Skirt_support	5.094E+05	64.890	139.400	0.000	9.452	7.101E+07	0.000E+00	4.815E+06	7850	Tank1_cover	2.514E+05	32.020	214.500	3.385	18.690	5.392E+07	8.508E+05	4.689E+06	7850	
26	Tank2_cover	8.659E+05	110.300	168.300	0.000	38.370	1.457E+08	0.000E+00	3.322E+07	7850	Tank1_cover_std										
27	Tank2_cover_C	1.732E+06	220.600	99.000	0.000	38.370	1.714E+08	0.000E+00	6.645E+07	7850	Tank1_equator	6.487E+04	24.480	214.500	0.000	24.470	1.392E+07	0.000E+00	1.587E+06	2650	
28	Tank3_shirt	1.579E+06	201.200	122.100	0.000	14.890	1.928E+08	0.000E+00	2.344E+07	7850	Tank1_shell	6.270E+05	236.600	214.500	0.000	24.740	1.345E+08	0.000E+00	1.512E+07	2650	
29	Tank3_shirt_std	5.772E+05	73.530	37.420	0.000	41.860	2.160E+07	0.000E+00	2.418E+07	7850	Tank1_shell_std	3.972E+04	14.990	214.500	0.000	27.590	8.321E+06	0.000E+00	1.096E+06	2650	
30	Wheelhouse										Tank1_lower_std										
31	Wheelhouse_std										Sum	2.381E+06	4.861E+02				5.103E+08	1.364E+07	6.102E+07		
32											Centre of gravity										
33											Front tank	214.345	5.729	25.633	135.767	0.019	13.351	136.515	0.073	13.468	
34											Total mass	250011326.300	250011.3263								

## E MATLAB codes used for post-processing

### nodecount.m

```
1
2 %% Counts the number of nodes in the ncforc file. Only adjusted to fit
3 %% files where only the master side is written
4
5 function nnodes = nodecount(file)
6
7 %Initialize
8 %file='ncforc';
9 fid = fopen(file, 'r');
10 if fid < 0
11     error(['Could not open ', file, ' for input']);
12 end
13
14
15 t=1; %time step counter
16
17
18 % Lines to be skipped
19 head=14;
20 for i=1:head
21     l=fgets(fid);
22 end
23
24
25 %% read data to check number of sections
26 nnodes = 0;
27 temp=1;
28 while temp >= 1
29     l=fgets(fid);
30     l=fgets(fid);
31     if length(l)==2
32         %temp=0;
33         break
34     elseif length(l)==1
35         break
36     else
37         temp=sscanf( l(3:10), '%i' );
38         nodenumber=temp;
39     end
40     nnodes = nnodes+1;
41 end
42
43 disp(sprintf('Number of elements in file %s : %i', file, nnodes));
44
45 return
```

**read\_ncforc.m**

```
1
2 %% Code developed for reading the output file ncforc from LS-DYNA analyses
3 % Based on a code developed by Ph.D. candidate Martin Storheim
4
5 function [node, nforce, timestep] = read_ncforc(file, nnodes)
6
7 %Load file
8 fid = fopen(file, 'r');
9 if fid < 0
10     error(['Could not open ', file, ' for input']);
11 end
12
13
14 t=1; %time step counter
15
16
17 % Lines to be skipped
18 head=8;
19 for i=1:head
20     l=fgets(fid);
21 end
22
23
24 %% Read actual data
25 % nforce(nodeID, timestep, variable)
26 % Variable name:
27 % 1 : time
28 % 2 : x-force
29 % 3 : y-force
30 % 4 : z-force
31 % 5 : pressure
32 % 6 : x-coord
33 % 7 : y-coord
34 % 8 : z-coord
35     node=zeros(nnodes,1);
36     t=1;
37 while t >= 1
38     for k=1:4
39         l=fgets(fid);
40     end
41     % Check if line is empty
42     if l == -1 %terminate if end of file
43         % disp('No more lines to read - last timestep completed');
44         tt=t;
45         t=0;
46         break
47     end
48     time=sscanf(l(12:22), '%f ');
49     l=fgets(fid);
50     l=fgets(fid);
51     l=fgets(fid);
52
53     for i=1:nnodes
54         % Read line
```

```
55     l=fgets(fid);
56
57     %read time step
58     node(i,1)=sscanf(l(3:10), '%f ');
59     nforce(i,t,1)=time;
60     nforce(i,t,2)=sscanf(l(18:30), '%f ');
61     nforce(i,t,3)=sscanf(l(32:44), '%f ');
62     nforce(i,t,4)=sscanf(l(46:58), '%f ');
63     nforce(i,t,5)=sscanf(l(60:72), '%f ');
64     l=fgets(fid);
65     nforce(i,t,6)=sscanf(l(18:30), '%f ');
66     nforce(i,t,7)=sscanf(l(32:44), '%f ');
67     nforce(i,t,8)=sscanf(l(46:58), '%f ');
68
69     end
70
71     % Break again to get out of while loop
72     if t==0
73         break
74     end
75 % %   disp(sprintf('Time step reading started for time = %f',time));
76     t=t+1;
77
78
79 end
80
81     disp(sprintf('Nodal contact force data is read for %i time steps',tt
82                 -1));
83
84     fclose(fid);
85
86     for i=1:(tt-1)
87         timestep(i)=nforce(1,i,1);
88     end
89
90
91 return
```

**read\_matsum.m**

```
1
2 %% Code developed for reading the output file matsum from LS-DYNA analyses
3 % Based on a code developed by Ph.D. candidate Martin Storheim
4
5 function [section , sect , matnumber , nsections , tt] = read_matsum(file)
6
7 %Load file
8 fid = fopen(file , 'r');
9 if fid < 0
10     error(['Could not open ', file , ' for input']);
11 end
12
13
14 t=1; %time step counter
15
16
17 % Lines to be skipped
18 head=5;
19 for i=1:head
20     l=fgets(fid);
21 end
22
23
24 %% read data to check number of sections
25 counter = 0;
26 temp=1;
27 while temp >= 1
28     l=fgets(fid);
29     temp=sscanf( l(6:9) , '%i' );
30     if size(temp)==0
31         disp(sprintf('Number of sections in file %s : %i', file , counter));
32         temp=0;
33     else
34         cnt=temp;
35     end
36     if temp ~= 0
37         matnumber(counter+1,1) = temp;
38     end
39     counter=counter+1;
40 end
41 nsections=counter-1;
42
43
44 % Lines to be skipped
45 head=3;
46 for i=1:head
47     l=fgets(fid);
48 end
49
50 %% Read actual data
51 % sect(sectionID , timestep , variable)
52 % Variable name:
53 % 1 : time
54 % 2 : internal energy
```



```
55 % 3 : kinetic energy
56 % 4 : eroded internal energy
57 % 5 : eroded kinetic energy
58 % 6 : x-moment
59 % 7 : y-moment
60 % 8 : z-moment
61 % 9 : x-rbv
62 % 10 : y-rbv
63 % 11 : z-rbv
64 % 12 : hgeng
65
66     t=1;
67 while t>=1
68     l=fgets(fid);
69     if l==-1 %terminate if end of file
70 %         disp('No more lines to read - last timestep completed');
71         tt=t;
72         t=0;
73         break
74     end
75 %read time step
76     time=sscanf(l(9:20), '%f ');
77     for i=1:nsections
78         % Read line
79         l=fgets(fid);
80         % Check if line is empty
81         if l==-1 %terminate if end of file
82 %             disp('No more lines to read - last timestep completed');
83             tt=t;
84             t=0;
85             break
86         end
87
88         section(i,1)=sscanf(l(8:12), '%f ');
89         sect(i,t,1)=time;
90         sect(i,t,2)=sscanf(l(33:44), '%f ');
91         sect(i,t,3)=sscanf(l(57:68), '%f ');
92         sect(i,t,4)=sscanf(l(85:96), '%f ');
93         sect(i,t,5)=sscanf(l(113:124), '%f ');
94         l=fgets(fid);
95         sect(i,t,6)=sscanf(l(9:20), '%f ');
96         sect(i,t,7)=sscanf(l(33:44), '%f ');
97         sect(i,t,8)=sscanf(l(57:68), '%f ');
98         l=fgets(fid);
99         sect(i,t,9)=sscanf(l(9:20), '%f ');
100        sect(i,t,10)=sscanf(l(33:44), '%f ');
101        sect(i,t,11)=sscanf(l(57:68), '%f ');
102        l=fgets(fid);
103        sect(i,t,12)=sscanf(l(33:44), '%f ');
104        l=fgets(fid);
105        l=fgets(fid);
106    end
107 % Break again to get out of while loop
108    if t==0
109        break
110    end
```

```
111     t=t+1;
112
113     l=fgets(fid);
114     l=fgets(fid);
115
116 end
117
118     disp(sprintf('Material data is read for %i time steps',tt-1));
119
120 return
```

**forcecalc.m**

```

1
2 %% Function for calculating contact area, force and pressure in addition
3 % to the ISO-curve used as comparison
4
5 function [ConAr, Force, time_maxforce, Pressure, ISO_19906, A] = forcecalc(
6     timestep, nforce, nnodes)
7 %% Force per timestep
8 Force = zeros(length(timestep),1);
9 for i=1:length(timestep)
10     for j=1:nnodes
11         Force(i,1) = Force(i,1) + sqrt(nforce(j,i,2)^2 + nforce(j,i,3)^2 +
12             nforce(j,i,4)^2);
13     end
14 end
15 time_maxforce=0;
16 counter=0;
17 for i=1:length(Force)
18     if Force(i,1) >= counter
19         counter = Force(i,1);
20         time_maxforce=i;
21     end
22 end
23
24
25 %% calculates total contact area
26
27 ConAr = zeros(length(timestep),1);
28 for i=1:length(timestep)
29     for j=1:nnodes
30         if nforce(j,i,5)<=0
31             ConAr(i,1)=ConAr(i,1)+0;
32         else
33             ConAr(i,1) = ConAr(i,1) + ( (sqrt(nforce(j,i,2)^2 + nforce(j,i,3)^2
34                 + nforce(j,i,4)^2)) / nforce(j,i,5));
35         end
36     end
37 end
38 %% Calculates pressure on contact area given by the force
39 Pressure = zeros(length(timestep),1);
40 for i=1:length(timestep)
41     for j=1:nnodes
42         Pressure(i,1) = Force(i,1)/ConAr(i,1);
43     end
44 end
45
46 A = 1:0.1:22;
47 for i=1:length(A)
48     if A(1,i) <= 10
49         ISO_19906(i,1)=(7.4*A(i)^(-0.7));
50     else
51         ISO_19906(i,1)=1.48;

```

```
52     end
53 end
54
55 return
```

---

## energycalc.m

```

1
2 %% Function for calculating the energies from the output file matsum
3 % Only created for non-rigid iceberg. Must be modified to include
4 % rigid icebergs
5
6 function [E_tot_ship, E_int_ship, E_kin_ship, E_tot_ice, E_int_ice,
    E_kin_ice, E_tot_ice_total, E_int_ice_total, E_kin_ice_total, E_tot,
    E_kin_tot, E_int_tot, E_eroded_ice_int, E_eroded_ice_kin]=energycalc(tt,
    section, sect)
7
8 E_tot_ship=zeros(tt-1,1);
9 E_int_ship=zeros(tt-1,1);
10 E_kin_ship=zeros(tt-1,1);
11 E_tot_ice_total=zeros(tt-1,1);
12 E_int_ice_total=zeros(tt-1,1);
13 E_kin_ice_total=zeros(tt-1,1);
14 E_tot_ice=zeros(tt-1,1);
15 E_int_ice=zeros(tt-1,1);
16 E_kin_ice=zeros(tt-1,1);
17 E_eroded_ice_int=zeros(tt-1,1);
18 E_eroded_ice_kin=zeros(tt-1,1);
19
20 E_tot=zeros(tt-1,1);
21 E_int_tot=zeros(tt-1,1);
22 E_kin_tot=zeros(tt-1,1);
23
24 for i=1:length(section)-1
25     for j = 1:tt-1
26         E_tot_ship(j,1) = E_tot_ship(j,1) + sect(i,j,2) + sect(i,j,3);
27         E_int_ship(j,1) = E_int_ship(j,1) + sect(i,j,2);
28         E_kin_ship(j,1) = E_kin_ship(j,1) + sect(i,j,3);
29     end
30 end
31
32 %% Must be changed when icebergs with rigid parts are included
33 ice=length(section);
34
35 for j=1:tt-1
36     E_tot_ice_total(j,1) = E_tot_ice_total(j,1) + sect(ice,j,2) + sect(ice,
        j,3) + sect(ice,j,4) + sect(ice,j,5);
37     E_int_ice_total(j,1) = E_int_ice_total(j,1) + sect(ice,j,2) + sect(ice,
        j,4);
38     E_kin_ice_total(j,1) = E_kin_ice_total(j,1) + sect(ice,j,3) + sect(ice,
        j,5);
39     E_eroded_ice_int(j,1) = E_eroded_ice_int(j,1) + sect(ice,j,4);
40     E_eroded_ice_kin(j,1) = E_eroded_ice_kin(j,1) + sect(ice,j,5);
41     E_tot_ice(j,1) = E_tot_ice(j,1) + sect(ice,j,2) + sect(ice,j,3);
42     E_int_ice(j,1) = E_int_ice(j,1) + sect(ice,j,2);
43     E_kin_ice(j,1) = E_kin_ice(j,1) + sect(ice,j,3);
44 end
45
46 for j=1:tt-1
47     E_kin_tot(j,1) = E_kin_tot(j,1) + E_kin_ice(j,1) + E_kin_ship(j,1) +
        E_eroded_ice_kin(j,1);

```

```
48     E_int_tot(j,1) = E_int_tot(j,1) + E_int_ice(j,1) + E_int_ship(j,1) +  
         E_eroded_ice_int(j,1);  
49     E_tot(j,1) = E_tot(j,1) + E_tot_ice_total(j,1) + E_tot_ship(j,1);  
50 end  
51  
52 return
```

**nodedisplacement.m**

```
1
2 %% Function created to calculate the node displacement for the two
   described methods
3
4 function [displacement , displ_maxrow , displ_maxcol , maxcounter ,
   maxdisplacement] = nodedisplacement (timestep , nforce , nnodes)
5
6 %% tracks node displacement
7 displacement=zeros (nnodes , length (timestep));
8 for h=1:nnodes
9     for i=2:length (timestep)
10        displacement (h,i) = sqrt ((nforce (h,i,6)-(nforce (h,1,6)))^2 + (
           nforce (h,i,7)-(nforce (h,1,7)))^2 + (nforce (h,i,8)-(nforce (h,1,8)
           ))^2);
11    end
12 end
13
14
15 %% Tracks the node with the largest displacement
16 maxcounter = 0;
17 for i=1:nnodes
18     for j=1:length (timestep)
19         if displacement (i,j) >= maxcounter
20             maxcounter = displacement (i,j);
21             displ_maxrow=i;
22             displ_maxcol=j;
23         end
24     end
25 end
26
27 %% Tracks the node with largest displacement at each timestep , and creates
   a matrix consisting of the largest displacement at each timestep
28
29 maxdisplacement=zeros (length (timestep) ,1);
30 for i=1:length (timestep)
31     maxcount = 0;
32     for j=1:nnodes
33         if displacement (j,i)>=maxcount
34             maxcount=displacement (j,i);
35             maxdisplacement (i,1)=maxcount;
36         end
37     end
38 end
39
40
41 return
```

## F Input files for LS-DYNA

The input files used for the simulations in LS-DYNA are not public, and in agreement with Professor Jørgen Amdahl and Ph.D. candidate Martin Storheim, representing Moss Maritime, these input files are stored on file storage servers at Department of Marine Technology, NTNU.

The following input files are stored on this server:

- Local model, initial velocity analysis, 5.71° impact angle.  
Filename: Initial\_velocity\_571.key
- Local model, prescribed displacement analysis, 5.71° impact angle.  
Filename: Prescribed\_displacement\_571.key
- Local model, initial velocity analysis, 30° impact angle.  
Filename: Initial\_velocity\_30.key
- Local model, prescribed displacement analysis, 30° impact angle.  
Filename: Prescribed\_displacement\_30.key
- Local model, initial velocity analysis, 30° impact angle, large iceberg.  
Filename: Initial\_velocity\_large\_iceberg.key
- Global model, initial velocity, 5.71° impact angle.  
Filename: Global\_model\_initial\_velocity\_571.key
- Global model, initial velocity, 30° impact angle.  
Filename: Global\_model\_initial\_velocity\_30.key
- Global model, initial velocity, 30° impact angle, large iceberg.  
Filename: Global\_model\_large\_iceberg\_30.key
  
- Bow shoulder and front tank model  
Filename: Bow\_shoulders\_area.key
- Global ship model  
Filename: Global\_model\_ship.key
- Small iceberg  
Filename: Small\_iceberg.key
- Rigid iceberg  
Filename: Rigid\_iceberg.key
- Large iceberg  
Filename: Large\_iceberg.key

In addition to these files, MSc. Patran databases for the modelled geometries are uploaded to this file server in addition to all result files from LS-DYNA and MATLAB.



